Approaches to Non-Perturbative Problems in Hadron Physics

Joseph P. Day

Dissertation

zur Erlangung des Doktorgrades der Naturwissenschaften
verfasst am Institut für Physik, FB Theoretische Physik,
an der Karl-Franzens-Universität Graz

Betreuer:

Univ.-Prof. Dr. Willibald Plessas

Graz, 2013

Dedicated to

Ana

Abstract

This thesis focuses on two complementary approaches to low-energy quantum chromodynamics (QCD). Specifically, they are a relativistic constituent-quark model and the treatment of QCD in anti-de-Sitter (AdS) space. Beyond the set-up of these models for the description of a series of hadron properties, we furthermore discuss and employ two alternative tools for treating hadrons as few-quark systems, namely, a stochastic variational method and an integral-equation approach that we have adapted to work with infinitely rising confinement interactions.

First, we develop a relativistic constituent quark model that can describe all known baryons of flavors up, down, strange, charm, and bottom in a universal manner. Its dynamics rely on a linear confinement and a hyperfine interaction deduced from an effective Lagrangian that takes into account the spontaneous breaking of chiral symmetry of low-energy QCD. The model reproduces the whole baryon spectroscopy in good agreement with phenomenology. It is also successfully applied to electromagnetic, axial, and gravitational nucleon form factors. These observables are produced in a relativistically invariant manner using the point form of Poincaré-invariant quantum mechanics.

Second, in the AdS approach we step out from the QCD action in five-dimensional space and use a holographic mapping to arrive at light-front QCD in ordinary (3+1)-dimensional space. In this way we produce the spectroscopy of light-flavored mesons and baryons with the correct Regge trajectories. In addition, we apply the AdS/QCD model to calculate the nucleon electromagnetic form factors within the so-called soft-wall model and find reasonable momentum dependences. While the two approaches give different insights into the properties of QCD at low energies, they both pave the way for further applications in hadronic physics.

Declaration

The work in this thesis is based on research primarily carried out in the Department of Theoretical Physics, at the University of Graz, in Austria. No part of this thesis has been submitted elsewhere for any other degree or qualification and it is all my own work unless referenced otherwise in the text.

The research in this thesis was carried out in collaboration with Stanley J. Brodsky, Ki-Seok Choi, Matin Mojaza, Zoltan Papp, and Willibald Plessas. It is based on the following works (appearing in reverse chronological order):

- J. P. Day and W. Plessas, *in preparation*
- J. P. Day and Z. Papp, *in preparation*
- J. P. Day and S. J. Brodsky, *in preparation*
- [1] J. P. Day, K. -S. Choi, and W. Plessas, *Spectroscopy of Baryons as Relativistic Three-Quark Systems,* Few Body Syst. 54, 329 (2013).
- [2] J. P. Day, W. Plessas, and K. -S. Choi, *Unified Model for Light- and Heavy-Flavor Baryon Resonances,* in Proceedings of the Bled Workshop on "Hadronic Resonances" 2012, p.5. (Bled Workshops in Physics. Vol. 13, No. 1, 2012)
- [3] J. P. Day, K. -S. Choi, and W. Plessas,*Relativistic Quark-Model Spectroscopy of Light and Heavy Baryons,* PoS(QNP 2012), 078.
- [4] J. P. Day, W. Plessas, and K. -S. Choi, *Universal Constituent-Quark Model for Baryons,* arXiv:1205.6918 [hep-ph].

- [5] J. P. Day and Z. Papp, *Treatment of Broken Symmetry in the Faddeev Approach to the Strange Baryon Spectra,* Phys. Rev. D **85**, 114042 (2012) [arXiv:1202.4488 [hep-ph]].

- [6] J. P. Day, K. -S. Choi, and W. Plessas, *Spectroscopy of Heavy Baryons,* in Proceedings of the Bled Workshop on "Understanding Hadronic Spectra" 2011, p.25. (Bled Workshops in Physics. Vol. 12, No. 1, 2011)

- [7] J. P. Day, K. -S. Choi, and W. Plessas, *Effective Quark-Quark Interaction in Heavy Baryons,* arXiv:1108.3450 [hep-ph].

Financial Support: The work in this thesis was supported by the Austrian Science Fund, FWF, through the Doctoral Program on Hadrons in Vacuum, Nuclei, and Stars (FWF DK W1203-N16).

Contents

Chapter 1

Introduction

Going back as far as 80 years ago one primary task of physicists has been to explain the building blocks of nature known as the elementary particles. Over the times more and more of these particles were found in experiments and in fact most turned out to be not elementary, but composed of more fundamental particles. This concerns the strongly interacting hadrons, which, in the so-called valence-quark picture, are believed to be constituted of quarks and antiquarks (in the case of mesons) or three quarks in the case of baryons. In a first approach this seems like a straightforward problem but as always nature is not so simple. One problem is the case of hadron spectroscopy. Naively one would assume that the mass of a bound state of quarks and/or antiquarks would be approximately the sum of the masses of the constituent quarks plus some binding energy. Evidence from experiment tells us this is not the case especially for the lightest hadrons.

1.1 The Problem of Strong Coupling

It is now commonly assumed that the theory for the strong interaction between quarks and antiquarks is quantum chromodynamics (QCD), proposed in the early 1970's [8, 9]. QCD is a non-Abelian gauge theory, where the Lagrangian is given as

$$\mathcal{L}_{\mathrm{QCD}} = \sum_n \bar{\psi}_n \left(i\gamma^\mu D_\mu - m_n \right) \psi_n - \tfrac{1}{4} G^a_{\mu\nu} G^{a\,\mu\nu}. \tag{1.1.1}$$

It couples quark fields ψ_n, of mass m with gluon fields A^a_μ. The sum over the quark fields n runs from 1 to 6, commonly referred to as up, down, strange, charm, and bot-

tom flavors. Here the covariant derivative is defined as $D_\mu = \partial_\mu - i\alpha_s A^a_\mu T^a$ and $G^a_{\mu\nu} = \partial_\mu A^a_\nu - \partial_\nu A^a_\mu + \alpha_s c^{abc} A^b_\mu A^c_\nu$ is the gluon field strength tensor. $\left[T^a, T^b\right] = ic^{abc}T^c$ where a, b, c are $SU(3)_C$ color indices, and α_s is the strong coupling constant. While the proposal and later experimental justification of this theory in the perturbative regime was a resounding success, it was soon realized that a very deep problem arose. Unlike quantum electrodynamics (QED) the field-theoretical predecessor to QCD, the strong coupling constant α_s is running and turns out to be quite large at low energies, typical of hadronic ground and resonant states. This makes the usual method of perturbation theory unapplicable in this domain. In an insight worthy of the 2004 Nobel Prize it was found that, as one increases the energy scale, by which one probes the hadron, the QCD coupling constant becomes very small and the constituents behave asymptotically as if they are free [10, 11]. This phenomenon is known as asymptotic freedom. This notion has allowed very accurate

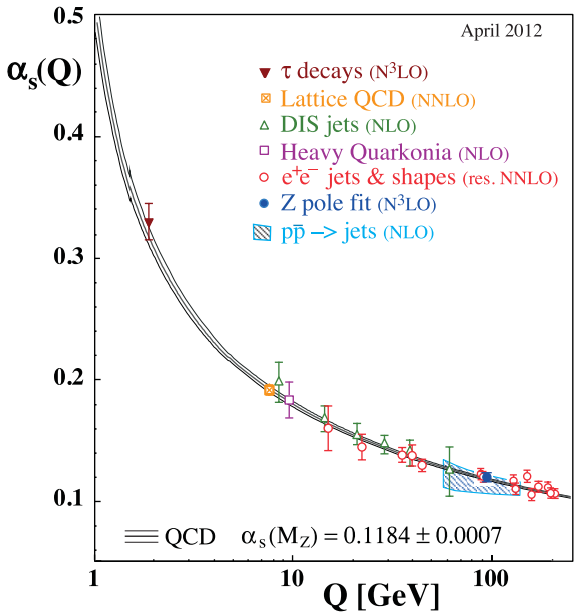

Figure 1.1: Experimental results which show the strength of the strong coupling constant α_s as a function of energy with which the hadron is probed [12].

calculations in the high-energy regime via perturbation theory. The problem that is puzzling physicists now for more than 40 years, is how to calculate anything sensible in the low-energy, hence strong-coupling regime. Up until now we have seen several different approaches to attacking the non-perturbative regime of hadron physics. Approaches such as lattice QCD consist of brute-force computer calculations using the QCD Lagrangian

with some assumptions as a starting point. In addition there is an abundance of other models and effective theories. While far from being comprehensive some examples are, chiral perturbation theory [13], Dyson-Schwinger equations [14,15], QCD sum rules [16], light-front holography [17], and relativistic constituent-quark models (RCQM) [18].

The work in this thesis will rely most heavily on flavor-dependent RCQM's as well as some additional insights from light-front holography (AdS/QCD).

Chapter 2

Relativity and Quantum Mechanics

In this chapter we will present the physical and mathematical grounds that the models and calculations in the subsequent chapters will be laid upon. The motivation is to construct a model for baryons to be described as three-quark relativistic bound states. This is undertaken along a relativistic constituent-quark model (RCQM), constructed with a Hamiltonian for three spin-1/2 quarks. In order for such a quantum mechanical model to satisfy relativistic invariance, it must satisfy the symmetry conditions of Poincaré invariance.

2.1 Relativistic Quantum Mechanics

In this section we outline the requirements for our relativistic quantum-mechanical theory following the motivations of Dirac [19] and Weinberg [20].

2.1.1 Quantum Mechanics

Physical states are represented by rays in a Hilbert space. If $\mathbf{\Phi}$ and $\mathbf{\Psi}$ are state vectors in this complex vector space then so is $\xi\mathbf{\Phi} + \eta\mathbf{\Psi}$, where ξ and η are arbitrary complex numbers. The Hilbert space has a norm: for any pair of vectors there is a complex number $\langle\mathbf{\Phi}|\mathbf{\Psi}\rangle$, such that

$$\langle\mathbf{\Phi}|\mathbf{\Psi}\rangle = \langle\mathbf{\Psi}|\mathbf{\Phi}\rangle^* \,, \tag{2.1.1}$$

$$\langle\mathbf{\Phi}|\xi_1\mathbf{\Psi_1} + \xi_2\mathbf{\Psi_2}\rangle = \xi_1\langle\mathbf{\Phi}|\mathbf{\Psi_1}\rangle + \xi_2\langle\mathbf{\Phi}|\mathbf{\Psi_2}\rangle \,, \tag{2.1.2}$$

$$\langle \eta_1 \mathbf{\Phi}_1 + \eta_2 \mathbf{\Phi}_2 | \mathbf{\Psi} \rangle = \eta_1^* \langle \mathbf{\Phi}_1 | \mathbf{\Psi} \rangle + \eta_2^* \langle \mathbf{\Phi}_2 | \mathbf{\Psi} \rangle \,, \tag{2.1.3}$$

$$\langle \mathbf{\Psi} | \mathbf{\Psi} \rangle \geq 0 \,. \tag{2.1.4}$$

Observables are represented by Hermitian operators. These are mappings $\mathbf{\Psi} \to A\mathbf{\Psi}$ of a Hilbert space into itself. These mappings are linear such that

$$A(\xi \mathbf{\Psi} + \eta \mathbf{\Phi}) = \xi A \mathbf{\Psi} + \eta A \mathbf{\Phi} \,, \tag{2.1.5}$$

where A satisfies the condition $A^\dagger = A$. Here, A is any linear operator and its adjoint is defined as

$$\langle \mathbf{\Phi} | A^\dagger \mathbf{\Psi} \rangle = \langle A\mathbf{\Phi} | \mathbf{\Psi} \rangle = \langle \mathbf{\Psi} | A \mathbf{\Phi} \rangle^* \,. \tag{2.1.6}$$

A state represented by a ray $\mathcal{R}$ has a definite value λ for the observable represented by an operator A, if vectors $\mathbf{\Psi}$ belonging to this ray are eigenvectors of A with eigenvalue λ:

$$A\mathbf{\Psi} = \lambda \mathbf{\Psi} \quad \text{for} \quad \mathbf{\Psi} \text{ in } \mathcal{R} \,. \tag{2.1.7}$$

If A is Hermitian then λ is real and eigenvectors with different λ's are orthogonal.

If a system is in a state represented by a ray $\mathcal{R}$ and an experiment is performed to test whether it is in any one of the different states represented by mutually orthogonal rays $\mathcal{R}_1, \mathcal{R}_2, \ldots$ then the probability of finding it in the state represented by $\mathcal{R}_n$ is

$$P(\mathcal{R} \to \mathcal{R}_n) = |\langle \mathbf{\Psi} | \mathbf{\Psi}_n \rangle|^2 \,, \tag{2.1.8}$$

where $\mathbf{\Psi}$ and $\mathbf{\Psi}_n$ are any vectors belonging to the rays $\mathcal{R}$ and $\mathcal{R}_n$, respectively. If the state vectors $\mathbf{\Psi}_n$ form a complete set then the sum of probabilities will result in unity

$$\sum_n P(\mathcal{R} \to \mathcal{R}_n) = 1 \,. \tag{2.1.9}$$

2.1.2 Quantum Lorentz Transformations

Now that we have solidified what we require for our theory from a quantum mechanics perspective we can move forward with how to marry this to special relativity. Einstein's principle of relativity is different from Galileo's principle of relativity by the transformation connecting coordinate systems in different inertial frames. If x^μ are the coordinates

in one inertial frame (with x^i being the usual Cartesian coordinates and $x^0 = t$[‡]), then the coordinate x'^μ must satisfy

$$g_{\mu\nu} dx'^\mu dx'^\nu = g_{\mu\nu} dx^\mu dx^\nu \,, \tag{2.1.10}$$

or equivalently

$$g_{\mu\nu} \frac{\partial x'^\mu}{\partial x^\rho} \frac{\partial x'^\nu}{\partial x^\sigma} = g_{\rho\sigma} \,, \tag{2.1.11}$$

where $g_{\mu\nu}$ is the Minkowski metric with diagonal elements, $g_{11} = g_{22} = g_{33} = +1$ and $g_{00} = -1$. Any coordinate transformation $x^\mu \to x'^\mu$ that satisfies Eq. (2.1.11) is linear

$$x'^\mu = \Lambda^\mu{}_\nu x^\nu + a^\mu \,, \tag{2.1.12}$$

where a^μ are arbitrary constants and $\Lambda^\mu{}_\nu$ is a constant matrix satisfying the condition

$$g_{\mu\nu} \Lambda^\mu{}_\rho \Lambda^\nu{}_\sigma = g_{\rho\sigma} \,. \tag{2.1.13}$$

The transformations $\Lambda^\nu{}_\mu$ form the so called Lorentz group. They are a subset of the larger Poincaré group that is fundamental to defining relativistic quantum mechanics.

2.1.3 Poincaré Algebra

In the case of any Lie symmetry group much of the information is contained in properties of the group elements near the identity. In the case of the Lorentz group, the identity is the transformation $\Lambda^\mu{}_\nu$ and $a^\mu = 0$. We want to study the transformations near the identity

$$\Lambda^\mu{}_\nu = \delta^\mu{}_\nu + \omega^\mu{}_\nu \tag{2.1.14}$$

and

$$a^\mu = \epsilon^\mu, \tag{2.1.15}$$

where $\omega^\mu{}_\nu$ and ϵ^μ are taken to be infinitesimal. In this case the Lorentz condition from Eq. 2.1.13 is

$$\begin{aligned} g_{\rho\sigma} &= g_{\mu\nu}(\delta^\mu{}_\rho + \omega^\mu{}_\rho)(\delta^\nu{}_\sigma + \omega^\nu{}_\sigma) && (2.1.16) \\ &= g_{\sigma\rho} + \omega_{\sigma\rho} + \omega_{\rho\sigma} + \mathcal{O}(\omega^2) \,. && (2.1.17) \end{aligned}$$

[‡]Throughout this thesis unless otherwise specified we use natural units with $\hbar = c = 1$.

Keeping only first-order terms we see that the implementation of the Lorentz condition reduces simply to the antisymmetrization of $\omega_{\mu\nu}$

$$\omega_{\mu\nu} = -\omega_{\nu\mu} \, . \tag{2.1.18}$$

In four dimensions an antisymmetric second-rank tensor has 6 independent components. Including the four components we get from ϵ^μ we see that this group, called Poincaré group (or inhomogenous Lorentz group) is described by 6+4=10 parameters.

We introduce a unitary linear transformation on the vectors in the physical Hilbert space

$$\mathbf{\Psi} \to U(\Lambda, a)\mathbf{\Psi} \, , \tag{2.1.19}$$

where the operators U satisfy the composition rule

$$U(\bar{\Lambda}, \bar{a})U(\Lambda, a) = U(\bar{\Lambda}\Lambda, \bar{\Lambda}a + \bar{a}) \, . \tag{2.1.20}$$

We see that since $U(1, 0)$ carry any ray into itself it must be proportional to the unit operator and by correctly choosing the phase can be made equal to the unit operator. For the case of the infinitesimal Lorentz transformation, $U(1 + \omega, \epsilon)$ must be equal to unity plus terms linear in $\omega_{\rho\sigma}$ and ϵ_ρ.

$$U(1 + \omega, \epsilon) = 1 + \frac{1}{2} i\omega_{\rho\sigma} J^{\rho\sigma} - i\epsilon_\rho P^\rho + \cdots \, . \tag{2.1.21}$$

Here, $J^{\rho\sigma}$ and P^ρ are operators independent of the infinitesimal transformations ω and ϵ. In order for $U(1 + \omega, \epsilon)$ to satisfy unitarity, $J^{\rho\sigma}$ and P^ρ must be Hermitian

$$J^{\rho\sigma\dagger} = J^{\rho\sigma} \qquad , \qquad P^{\rho\dagger} = P^\rho \, . \tag{2.1.22}$$

In addition we know that $\omega_{\rho\sigma}$ is antisymmetric, telling us that its coefficient $J^{\rho\sigma}$ be also

$$J^{\rho\sigma} = -J^{\sigma\rho} \, . \tag{2.1.23}$$

We are now interested in the Lorentz transformation properties of $J^{\rho\sigma}$ and P^ρ. Let us consider the product

$$U(\Lambda, a)U(1 + \omega, \epsilon)U^{-1}(\Lambda, a) \, , \tag{2.1.24}$$

where $\Lambda^\mu{}_\nu$ and a^μ are now parameters of a new transformation unrelated to ω and ϵ. From our composition rule defined in Eq. (2.1.20) the product of $U(\Lambda^{-1}, -\Lambda^{-1}a)U(\Lambda, a)$ is equal

to $U(1,0)$ which tells us that $U(\Lambda^{-1}, -\Lambda^{-1}a)$ is the inverse of $U(\Lambda, a)$. It follows that

$$U(\Lambda,a)U(1+\omega,\epsilon)U^{-1}(\Lambda,a) = U(\Lambda(1+\omega)\Lambda^{-1}, \Lambda\epsilon - \Lambda\omega\Lambda^{-1}a) \,. \tag{2.1.25}$$

Again to first order in ω and ϵ we get

$$U(\Lambda,a)[\frac{1}{2}\omega_{\rho\sigma}J^{\rho\sigma} - \epsilon_\rho P^\rho]U^{-1}(\Lambda,a) = \tag{2.1.26}$$
$$\frac{1}{2}(\Lambda\omega\Lambda^{-1})_{\mu\nu}J^{\mu\nu} - (\Lambda\epsilon - \Lambda\omega\Lambda^{-1}a)_\mu P^\mu \,.$$

Equating the coefficients of $\omega_{\rho\sigma}$ and ϵ_ρ on both sides we get

$$U(\Lambda,a)J^{\rho\sigma}U^{-1}(\Lambda,a) = \Lambda_\mu{}^\rho\Lambda_\nu{}^\sigma(J^{\mu\nu} - a^\mu P^\nu + a^\nu P^\mu) \tag{2.1.27}$$

$$U(\Lambda,a)P^\rho U^{-1}(\Lambda,a) = \Lambda_\mu{}^\rho P^\mu \,. \tag{2.1.28}$$

These transformation rules tell us a lot about the physics of the system. First it is evident from the transformation properties that $J^{\mu\nu}$ is a tensor and P^μ is a vector. For pure translations (with $\Lambda^\mu{}_\nu = \delta^\mu{}_\nu$), we see that P^ρ is translation invariant but $J^{\rho\sigma}$ is not. In fact we see that the space-space components of $J^{\rho\sigma}$ under a spatial translation is just the usual change of the angular momentum under a change of the origin relative to which the angular momentum is calculated.

Applying Eqns. (2.1.27) and (2.1.28) to an infinitesimal transformation $\Lambda^\mu{}_\nu = \delta^\mu{}_\nu + \omega^\mu{}_\nu$ and $a^\mu = \epsilon^\mu$, with infinitesimals $\omega^\mu{}_\nu$ and ϵ^μ unrelated to the previous ω and ϵ, then using Eq. (2.1.21) and keeping only the first-order terms in $\omega^\mu{}_\nu$ and ϵ^μ Eqns. (2.1.27) and (2.1.28) become

$$i[\frac{1}{2}\omega_{\mu\nu}J^{\mu\nu} - \epsilon_\mu P^\mu, J^{\rho\sigma}] = \omega_\mu{}^\rho J^{\mu\sigma} - \omega_\nu{}^\sigma J^{\rho\nu} - \epsilon^\rho P^\sigma + \epsilon^\sigma P^\rho \,, \tag{2.1.29}$$

$$i[\frac{1}{2}\omega_{\mu\nu}J^{\mu\nu} - \epsilon_\mu P^\mu, P^\rho] = \omega_\mu{}^\rho P^\mu \,. \tag{2.1.30}$$

Equating the coeffiecients of $\omega_{\mu\nu}$ and ϵ_μ we find the commutation rules known as the Lie algebra of the Poincaré group

$$i[J^{\mu\nu}, J^{\rho\sigma}] = g^{\nu\rho}J^{\mu\sigma} - g^{\mu\rho}J^{\nu\sigma} - g^{\sigma\mu}J^{\rho\nu} + g^{\sigma\nu}J^{\rho\mu} \,, \tag{2.1.31}$$

$$i[P^\mu, J^{\rho\sigma}] = g^{\mu\rho}P^\sigma - g^{\mu\sigma}P^\rho \,, \tag{2.1.32}$$

$$[P^\mu, P^\rho] = 0 \,. \tag{2.1.33}$$

Based on the commutation relations shown here, the identification of J^{23}, J^{31}, and J^{12} as the angular momentum generators is forced upon us. However the commutation relations do not allow us to distinguish between P^μ and $-P^\mu$ so the sign of the $\epsilon_\rho P^\rho$ term in Eq. (2.1.21) is a matter of convention. In quantum mechanics operators that are conserved in time commute with the energy operator $H = P^0$. The Poincaré algebra tells us that the conserved quantities are the momentum three-vector and the angular momentum three-vector

$$\mathbf{P} = \{P^1, P^2, P^3\}\,, \tag{2.1.34}$$

$$\mathbf{J} = \{J^{23}, J^{31}, J^{12}\}\,, \tag{2.1.35}$$

respectively. The remaining generators

$$\mathbf{K} = \{J^{01}, J^{02}, J^{03}\} \tag{2.1.36}$$

form the boost three-vector. These are not conserved and hence the eigenvalues of $\mathbf{K}$ are not used to label physical states. Explicitly the commutation relations of the Poincaré algebra can be written out as

$$[J_i, J_j] = i\epsilon_{ijk}J_k\,, \tag{2.1.37}$$

$$[J_i, K_j] = i\epsilon_{ijk}K_k\,, \tag{2.1.38}$$

$$[K_i, K_j] = -i\epsilon_{ijk}J_k\,, \tag{2.1.39}$$

$$[J_i, P_j] = i\epsilon_{ijk}P_k\,, \tag{2.1.40}$$

$$[K_i, P_j] = -iP^0\delta_{ij} = -iH\delta_{ij}\,, \tag{2.1.41}$$

$$[J_i, H] = [P_i, H] = [H, H] = 0\,, \tag{2.1.42}$$

$$[K_i, H] = -iP_i\,. \tag{2.1.43}$$

where i, j, k run from 1 to 3 and ϵ_{ijk} is the totally antisymmetric Levi-Civita tensor with $\epsilon_{123} = +1$. We have now reached the main point. These commutation relations are the fundamental requirement for a system of relativistic quantum mechanics.

2.2 The Bakamjian-Thomas Construction

We have shown the requirements for a system of relativistic quantum mechanics, however, our previous analysis was only for interaction-free systems. To build up a model of

interacting quarks we are naturally led to the problem of a system with interactions. It is an important and non-trivial point to construct a theory with interactions that still fulfills the Poincaré algebra. The way forward was first shown by Bakamjian and Thomas [21]. To outline the problem let us look at the commutation relation

$$[K_i, P_j] = iH\delta_{ij} \, . \tag{2.2.44}$$

In the interaction-free case considered above H does not have an interaction term. Now if we add an interaction term, it becomes

$$H = H_0 + V \, . \tag{2.2.45}$$

In non-relativistic quantum mechanics this does not pose any problem. In RQM we now run into the problem that adding an arbitrary interaction term to the Hamiltonian doesn't allow the Poincaré algebra to close. In order to compensate for the V on the right-hand side of Eq. (2.2.44) we must also add an interaction term to the left-hand side. We now have three choices:

- add interactions only to K_i (instant form),
- add interactions only to P_j (point form),
- add interactions to both K_i and P_j (front form).

These cases refer to Dirac's forms of relativistic dynamics [22]. In principle one can parametrize space-time in a infinite number of ways by introducing some generalized coordinates $\tilde{x}(x)$, but in practice one should exclude all forms that can access one another by a simple Lorentz transformation. This limits the number of different forms and obviously excludes forms related by rotation angles. Dirac's showed that there are basically three different forms that cannot be mapped onto each other by a Lorentz transformation; they are commonly referred to as the instant form, point form, and front form. The hypersphere on which each form is initialized is different. As a consequence they can be seen as an indication of how time is parameterized in the theory. In case of the instant form the initial surface is a plane for constant time $x^0 = 0$. In case of the point form we have the initial surface $x^2 = \tau^2$, where τ is a constant i.e. a hyperboloid that has the forward light

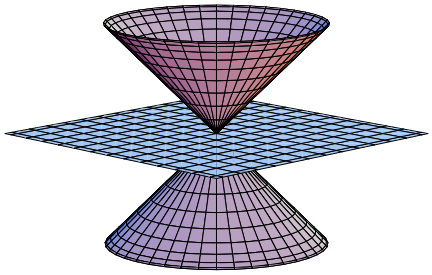

Figure 2.1: The space-like hypersurface of Minkowski-space $x^0 = 0$, which is invariant under the instant-form kinematic group of spatial translations and rotations.

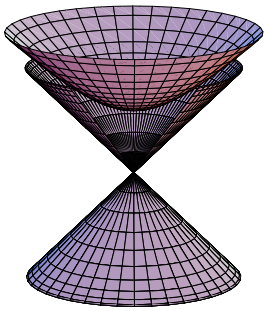

Figure 2.2: The forward light cone hyperboloid $x^2 = \tau^2$ representing the invariant surface of the point form.

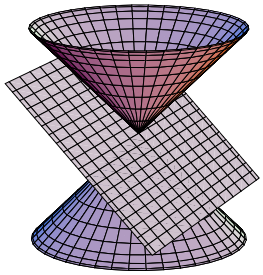

Figure 2.3: The light-like hypersurface $\tau = x^0 + x^3 = 0$ representing the invariant surface of the front form.

cone as an asymptote. In case of the front form the initial surface $\tau = x^0 + x^3$ is a plane tangent to the light cone.

Whatever we choose we must be careful that the other commutators are satisfied, for example

$$[P^\mu, P^\nu] = 0 \tag{2.2.46}$$

and

$$[K_i, K_j] = -i\epsilon_{ijk} J_k \ . \tag{2.2.47}$$

In order to add interactions and fulfill the requirements of the Poincaré algebra we must look at the Casimir operators of the Poincaré group. In this case there are two of them, the mass-operator squared

$$M^2 = P^\mu P_\mu = H^2 - \vec{P}^2 \tag{2.2.48}$$

and the Pauli-Lubanski operator

$$W^\mu = \frac{1}{2}\epsilon^{\mu\alpha\beta\gamma} P_\alpha J_{\beta\gamma} \ , \tag{2.2.49}$$

where $\epsilon^{\mu\alpha\beta\gamma}$ is the completely anti-symmetric Levi-Civita tensor in four dimensions. Let us first look at the mass operator. If we say M^2 represents the mass of the system then we must imply the additional condition that $M^2 \geq 0$ such that

$$M = +\sqrt{H^2 - \vec{P}^2} \ . \tag{2.2.50}$$

Following Bakamjian and Thomas we deconstruct the full mass operator M into a free part M_{free} and a part with interactions M_{int}. The linear composition of the full mass operator is therefore

$$M = M_{\text{free}} + M_{\text{int}} \ . \tag{2.2.51}$$

It is imperative that the full mass operator fullfills the Poincaré algebra. In this way one can add interactions to the system and maintain a fully relativistic theory. Below it is outlined, how the Bakamjian-Thomas construction looks in the point form.

In the point form all interactions are contained in the space-time translations P_j, while the other six generator $J^{\mu\nu}$ are kinematical (interaction-free). We define the set of 10 interaction-free generators in terms of auxiliary operators

$$\{M_{\text{free}}, \vec{V}_{\text{free}}, \vec{K}_{\text{free}}, \vec{J}_{\text{free}}\} \tag{2.2.52}$$

$$M_{\text{free}} = +\sqrt{H_{\text{free}}^2 - \vec{P}_{\text{free}}^2} \tag{2.2.53}$$

$$V_{\text{free}}^{\mu} = \frac{P_{\text{free}}^{\mu}}{M_{\text{free}}} \tag{2.2.54}$$

The next step is to introduce the full mass operator

$$M = M_{\text{free}} + M_{\text{int}} \ , \tag{2.2.55}$$

where M_{int} must now fulfill the commutation relations

$$[\vec{V}_{\text{free}}, M_{\text{int}}] = [\vec{K}_{\text{free}}, M_{\text{int}}] = [\vec{J}_{\text{free}}, M_{\text{int}}] = 0 \ . \tag{2.2.56}$$

The Poincaré algebra will now be fulfilled for an interaction theory with the set

$$\{M, \vec{V}_{\text{free}}, \vec{K}_{\text{free}}, \vec{J}_{\text{free}}\} \tag{2.2.57}$$

in the same way, as it was fulfilled in the free case of $\{M_{\text{free}}, \vec{V}_{\text{free}}, \vec{K}_{\text{free}}, \vec{J}_{\text{free}}\}$. From here one can now reconstruct the original set of operators, first encountered in the usual point form Poincaré group, namely

$$\{H, \vec{P}, \vec{K}_{\text{free}}, \vec{J}_{\text{free}}\} \ . \tag{2.2.58}$$

Then it is evident that in the point form all components of the four-momentum are interaction-dependent

$$P^{\mu} = M V_{\text{free}}^{\mu} \ , \tag{2.2.59}$$

while the six other independent generators $J^{\mu\nu}$ remain free. This characterizes the Bakamjian-Thomas construction in the point form. Analogous constructions for the instant and front form are also possible and follow similar lines of reasoning. Details can be found in the works by Choi [23], Biernat [24], and in the classic review article by Keister and Polyzou [25].

Chapter 3

The Relativistic Constituent-Quark Model

We first look at the description of hadrons through a historical lens beginning with the work of Gell-Mann and Zweig in the 1960's. Next we discuss various attempts to describe hadron spectroscopy and note achievements and shortcomings. The culmination of the chapter is the result of the Graz group via the flavor-dependent relativistic constituent-quark model (RCQM) [18].

3.1 The Quark Model

Beginning with Gell-Mann's eightfold way in 1961 a revolution in particle physics began. Gell-Mann used this precursor to the quark model to predict the existence of an as yet unseen particle, the triply strange Ω^-. This consisted of arranging the known particles in various geometrical arrangements according to their known properties; details can be found in Appendix B. Indeed a few years later in 1964 experiments at Brookhaven National Lab showed experimental agreement not only with the existence of the Ω^- particle but also it's mass [26]. This great success only begged the question of why do the particles fall into such patterns? Surely there must be some greater underlying principle. This led to the idea of the quark model proposed independently by Gell-Mann [27] and Zweig [28, 29] in 1964. The proposition was that baryons were not fundamental, instead they were made up of three spin 1/2 particles. The mesons were considered to be made up to two spin 1/2 particles. It is an interesting historical note that although Gell-Mann proposed the quark model he did not in the beginning, believe in their existence as real particles, only

as theoretical constructs. This situation changed in 1969 when experiments at SLAC motivated by Feynman's parton model [30, 31] and theoretical work by Bjorken [32, 33], showed conclusively that the proton indeed had an inner structure [34, 35]. Gell-Mann's quark model only required three flavors of quark up, down, and strange. However in the "November Revolution" of 1974 a bound state of a fourth-flavor charm quark was discovered at Brookhaven National Laboratory and SLAC by detecting the J/Ψ meson [36, 37]. The fifth-flavor bottom quark was discovered in 1977 [38] and the top quark was experimentally verified as recently as 1995 [39]. At present date our understanding is that there are at least six flavors of quarks; up, down, strange, charm, bottom, and top. Since the proposals of Gell-Mann and Zweig we have seen various quark models with increasing levels of sophistication. What follows is a brief summary of a few of the historically relevant iterations.

3.1.1 Flavor SU(6) Model

The flavor $SU(6)$ model is built upon the hypothesis that the up, down, and strange quarks are eigenvalues of the internal symmetry group $SU(3)_F$. This internal symmetry is extended to $SU(6)$ in order to include spin $SU(2)_S$, which is vital to provide the proper splitting between the spin 1/2 and 3/2 baryons. So the total symmetry group is $SU(6) \supset SU(3)_F \otimes SU(2)_S$. This symmetry is broken so that the mass terms in the theory depend only on diagonalizable operators. The result is the Gürsey-Radicati mass formula [40]. For mesons

$$\mu = \mu_0^2 + \alpha S(S+1) + \gamma\left[T(T+1) - \frac{1}{4}Y^2\right], \tag{3.1.1}$$

and for baryons

$$M = M_0 + aS(S+1) + bY + c\left[T(T+1) - \frac{1}{4}Y^2\right], \tag{3.1.2}$$

where Y is the hypercharge, T the isospin, and S the spin of the hadrons. For mesons μ_0, α, and γ are free parameters that are fit to the spectra. Respectively, for baryons M_0, a, b, and c are free parameters. Let us look at an example for baryons. By choosing

$$M_0 = 1065.5 \quad , \quad a = 67.5 \quad , \quad b = -193 \quad , \text{and} \quad c = 32.5$$

with all values in MeV, we can fit the lowest lying states very well as shown in Table 3.1. This can be extended with the assumption that the quarks also have degrees of freedom

Baryon	Theory [MeV]	Experiment [MeV]
$N(\frac{1}{2}^+)$	939	939
$\Lambda(\frac{1}{2}^+)$	1116	1116
$\Sigma(\frac{1}{2}^+)$	1181	1189
$\Xi(\frac{1}{2}^+)$	1325	1318
$\Delta(\frac{3}{2}^+)$	1239	1230-1234
$\Sigma(\frac{3}{2}^+)$	1384	1385
$\Xi(\frac{3}{2}^+)$	1528	1533
$\Omega(\frac{3}{2}^+)$	1672	1672

Table 3.1: Results for the lowest lying baryon states given by the Gursey-Radicati mass formula, Eq. (3.1.2), with the parameters specified in the text.

due to angular momentum. This gives us $SU(6) \otimes O(3)$ symmetry group and corresponding mass formulas. This leads to a proliferation of parameters which is displeasing. In addition, if we want to add more flavors to our theory, i.e. charm and bottom, the symmetry group becomes even more extended and the theory becomes less predictive. Furthermore, excited states are not well described.

3.1.2 The Skyrmion Model

The Skyrme Model was proposed in 1962 by Skyrme [41]. The baryon number is considered as a topological quantum number. To illustrate the theory let us consider a pion. Spin and isospin are isomorphic. The regular representation of isospin for the pion has three isospin unit vectors

$$|\pi^0\rangle \quad , \quad \frac{1}{\sqrt{2}}(|\pi^+\rangle + |\pi^-\rangle) \quad , \quad \frac{1}{\sqrt{2}i}(|\pi^+\rangle - |\pi^-\rangle) \tag{3.1.3}$$

which are isomorphic to angular momentum. This gives us an interpretation of the pions as vectors in three-dimensional space, the same as we would for angular momentum in physical space. If we couple the direction of the isospin vector $\mathbf{t}$ to the position vector $\mathbf{x}$ by demanding $\mathbf{t} = \frac{\mathbf{x}}{|\mathbf{x}|}$ in isospin space we obtain a pion field consisting purely of π^0

along the z axis and a mixture of π^0, π^+, and π^- with regard to rotations. A schematic picture is shown in Fig. 3.1. This construction is known as the hedgehog solution, due to the isospin vectors pointing outwards resembling a hedgehog. These hedgehogs are

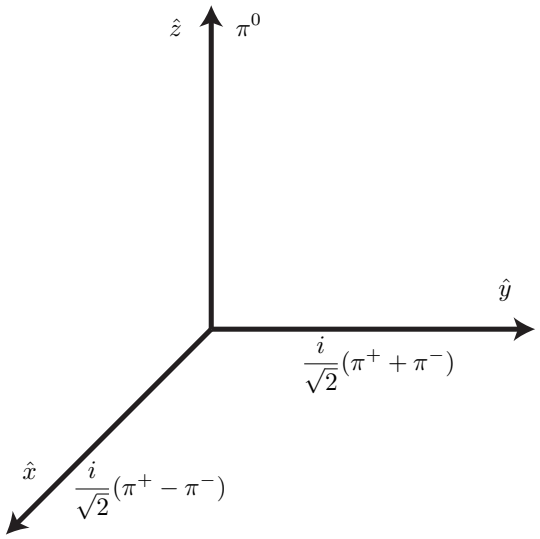

Figure 3.1: Schematic form of the hedgehog solution.

stable because it would require infinite energy to reverse the orientation of the pion field, meaning one would have to change $\pi(\mathbf{x})$ in an infinite spatial domain $\mathbf{x} \to \infty$. So we see that in this model a topological quantum number is defined that specifies how often $\pi(|\mathbf{x}|)$ covers all isospin values for $|\mathbf{x}| \to \infty$. Baryons are identified with the different states that have topological quantum number 1. This conjecture was again produced in 1983 by Witten [42]. Some results from the model proposed by Adkins, Nappi, and Witten [43] are shown below.

3.1.3 M.I.T. Bag Model

The M.I.T. Bag Model [44], is the first model we consider that was built after the establishment of QCD and in particular its property of asymptotic freedom [10, 11]; which showed beyond doubt that QCD was the correct theory of the strong interactions. The idea of the bag model was not only to describe hadron spectra but also to effectively model confinement which is to say that there are no colored particles seen in nature. This tells us quarks cannot exist freely in nature, only inside hadrons. The M.I.T. Bag Model

Quantity	Prediction	Experiment
M_N	input	939 [MeV]
M_Δ	input	1232 [MeV]
F_π	129 [MeV]	186 [MeV]
$\langle r^2\rangle^{1/2}_{l=0}$	0.59 [fm]	0.72 [fm]
$\langle r^2\rangle^{1/2}_{M,l=0}$	0.92 [fm]	0.81 [fm]
μ_p	1.87	2.79
μ_n	-1.31	-1.91
$\lvert\frac{\mu_p}{\mu_n}\rvert$	1.43	1.46
g_A	0.61	1.23
$g_{\pi NN}$	8.9	13.5
$g_{\pi N\Delta}$	13.2	20.3
$\mu_{N\Delta}$	2.3	3.3

Table 3.2: Some results from the Skyrme model as calculated by Adkins, Nappi, and Witten in Ref. [43].

simulated confinement by saying quarks could freely propagate within a certain region of space (inside the bag) while implementing a hard boundary wall in which the confined quarks could not escape. This model was a considerable step forward in understanding confinement, however, it lead to several problems as well. The rigid boundary conditions can lead to spurious motions, for example the oscillations of all quarks with respect to the bag, furthermore it is not Lorentz invariant, which, we know, for hadrons is a fundamental ingredient. There is a rich literature regarding this model. The interested reader is directed to Ref. [45] to name only one source. In addition, extensive results and predictions can be found in the original work [44].

3.2 The Relativistic Constituent-Quark Model

The final class of models that we will look at are known as quark models. In this thesis many of the core results will emerge from contemporary versions of this class of model. Usually they are based on a Hamiltonian

$$\hat{H} = \hat{T} + \hat{V} \tag{3.2.4}$$

such that the kinetic energy operator can be either non-relativisitic or relativistic. In this thesis we will concern ourselves only with fully relativistic models that fulfill the Poincaré algebra. In addition different types of hyperfine interactions can be included in the potential. We will look first at the Bhaduri, Cohler, Nogami (BCN) one-gluon exchange model (OGE) which was first formulated in a non-relativistic way [46]; however, we will investigate the relativistic version as presented in [47]. Finally, the flavor-dependent relativistic constituent-quark model of the Graz group is presented [18].

3.3 The General Quark-Model Hamiltonian

In the (RCQM) for baryons we have a Hamiltonian such as

$$H = H_{\text{free}} + \sum_{i<j}^{3} V_{ij} \,, \tag{3.3.5}$$

where H_{free} is a relativistic kinetic-energy operator given as

$$H_{\text{free}} = \sum_{i=1}^{3} \sqrt{m_i^2 + \mathbf{k}_i^2} \,, \tag{3.3.6}$$

where m_i represents the constituent-quark masses and $\mathbf{k}_i$ their three-momenta in the center-of-momentum frame. It is important to use a relativistic kinetic-energy operator so that one can set up a Poincaré invariant mass operator.

Here we will focus on the potential.

$$V_{ij} = V_{\text{conf}}(\vec{r}_{ij}) + V_{\text{hf}}(\vec{r}_{ij}) \,. \tag{3.3.7}$$

$V_{\text{conf}}(\vec{r}_{ij})$ confines the three quarks to a finite volume and $V_{\text{hf}}(\vec{r}_{ij})$ is the hyperfine interaction.

3.4 One-Gluon-Exchange RCQM

3.4.1 OGE Confinement

In the OGE model confinement is described by a Cornell-type potential

$$V_{\text{conf}}(\vec{r}_{ij}) = V_0 + C r_{ij} - \frac{2b}{3r_{ij}} \tag{3.4.8}$$

The parameter V_0 sets the scale of the potential giving the nucleon ground state. The other two free parameters are C and b determine the strengths of the linear and Coulomb term respectively.

3.4.2 OGE Hyperfine Interaction

The one-gluon-exchange hyperfine interaction is considered only with regard to the spin-spin interaction and is given as follows

$$V_{\rm hf}(r_{ij}) = \frac{\alpha_s}{9m_i m_j}\Lambda^2 \frac{e^{\Lambda r_{ij}}}{r_{ij}} \vec{\sigma}_i \cdot \vec{\sigma}_j \ . \tag{3.4.9}$$

Here m_i and m_j are the constituent-quark masses and $\vec{\sigma}_i$ their spin operators, α_s is the effective strong coupling constant and Λ is a cut-off parameter. The numerical values of the parameters as determined in Ref. [47] are given in Tab. 3.3.

$m_u = m_d$ [MeV]	m_s [MeV]	α_s	Λ [fm^{-1}]	C [fm^{-2}]	V_0 [MeV]	b
337	600	0.59	2.7	3.12	-409	0.57

Table 3.3: Parameters of the relativistic version of the BCN OGE constituent-quark model.

3.5 Goldstone-Boson-Exchange RCQM

3.5.1 GBE Confinement

Here the confinement potential is taken as

$$V_{\rm conf}(r_{ij}) = V_0 + C r_{ij} \ , \tag{3.5.10}$$

Where $C = 2.33$ fm^{-2} is a constant with a strength of about the string tension of QCD. V_0 is a constant needed to fix the nucleon ground state to 939 MeV.

3.5.2 GBE Hyperfine Interaction

The hyperfine potential has the form

$$V_{\rm hf} = V_\chi^{\rm octet} + V^{\rm singlet} \ , \tag{3.5.11}$$

where V^{octet} refers to the exchange of the pseudoscalar octet mesons π, K, and η_8. V^{singlet} to the exchange of the pseudoscalar singlet meson η_0. In any case only the spin-spin part is included, since this is the most dominant force component for baryon spectroscopy and tensor as well as spin orbit forces can be neglected[‡]. The spin-spin potentials are given by [18]

$$V_\chi^{\text{octet}}(\vec{r}_{ij}) = \left[V_\pi(\vec{r}_{ij}) \sum_{a=1}^{3} \lambda_i^a \lambda_j^a + V_K(\vec{r}_{ij}) \sum_{a=4}^{7} \lambda_i^a \lambda_j^a + V_{\eta_8}(\vec{r}_{ij}) \lambda_i^8 \lambda_j^8\right] \vec{\sigma}_i \cdot \vec{\sigma}_j \tag{3.5.12}$$

and

$$V^{\text{singlet}}(\vec{r}_{ij}) = \left(V_{\eta_0}(\vec{r}_{ij}) \lambda_i^0 \lambda_j^0\right) \vec{\sigma}_i \cdot \vec{\sigma}_j \tag{3.5.13}$$

The particular form of the meson-exchange potentials contains a Yukawa-type cut off and is expressed by

$$V_\gamma(\vec{r}_{ij}) = \frac{g_\gamma^2}{2\pi} \frac{1}{12 m_i m_j} \left[m_\gamma^2 \frac{e^{-m_\gamma r_{ij}}}{r_{ij}} - \Lambda_\gamma^2 \frac{e^{-\Lambda_\gamma r_{ij}}}{r_{ij}}\right] \tag{3.5.14}$$

for $\gamma = \pi, K, \eta_8$, and η_0. The prescription for the cut-off is

$$\Lambda_\gamma = \Lambda_0 + \kappa \mu_\gamma \tag{3.5.15}$$

where μ_γ is the mass of the exchanged meson. The various pre-fixed and fit parameters of the GBE RCQM are summarized in Tab. 3.4.

3.6 Results for Spectroscopy

Spectral results for both the GBE and OGE RCQM's are given in Tab. 3.5.

In general a good description of the experimental data is achieved for baryon ground and resonant states below $\approx$ 2 GeV. This is especially true for the GBE RCQM which also succeeds in reproducing the right level orderings of resonances both in the N and Λ

[‡] In Ref. [48] an extended GBE RCQM was constructed that includes all possible force components from pseudoscalar-, vector-, and scalar-meson exchanges. It produces a very similar baryon spectrum.

Quark masses [MeV]		Exchange meson masses [MeV]			
m_u, m_d	m_s	μ_π	μ_K	μ_η	μ_{η_0}
340	500	139	494	547	958
Additional Parameters					
$\frac{g_8^2}{4\pi}$	$(g_0/g_8)^2$	Λ_0 [fm^{-1}]	κ	V_0 [MeV]	C [fm^{-2}]
0.67	1.34	2.87	0.81	−416	2.33

Table 3.4: Parameters of the GBE RCQM.

spectra. On the contrary the OGE RCQM fails to reproduce the correct level orderings of the $N(1440)$ and $N(1535)$ resonances. By comparing the Λ spectrum we learn that it is crucial for the quark-quark interaction to be flavor-dependent, in order to simultaneously produce the right level orderings in the N and Λ spectra. That the GBE hyperfine interaction is responsible for the level orderings becomes evident by stepping out from the case of confinement only and gradually increasing the coupling constant $g_8^2/4\pi$.Plots showing the level crossing as a function of hyperfine interaction strength are shown in Fig. 3.2 (reproduced from Ref. [18]).

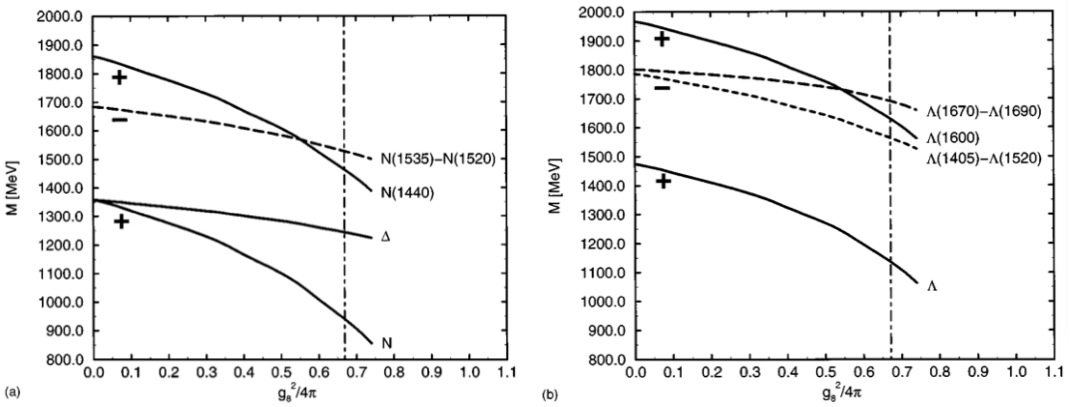

Figure 3.2: The N and Λ baryon spectra as the hyperfine interaction is turned on.

3.7 Stochastic Variational Method

The spectra in this thesis have been calculated by using two different methods. The first we will discuss is the Stochastic Variational Method (SVM). The second is a modified Faddeev integral-equation method which we will devote a deeper discussion to in the following chapter.

The SVM represents a powerful tool to solve the eigenvalue problem of a given interacting mass operator. Its application to RCQM's has been covered extensively in the following works [23, 49–51]. However, for completeness we will concisely summarize it here. First proposed by Kukulin and Krasnopolsky [52] and later extended by Suzuki and Varga [81] the SVM essentially exploits with its test functions all the flexibility allowed by a given mass operator. Suitable basis functions for three-quark bound states can be constructed stepping out from correlated Gaussians and considering all spin and flavor degrees of freedom. They can be expressed in terms of Jacobi coordinates $\mathbf{x} = (\mathbf{x}_1, \ldots, \mathbf{x}_{N-1})$. The three-particle basis functions then become

$$\psi_{(LS)JM_JTM_T}(\mathbf{x}, A) = \mathcal{S} \cdot \{e^{-\frac{1}{2}\tilde{\mathbf{x}}A\mathbf{x}}[\Theta_{LM_L}(\tilde{\mathbf{x}})\chi_S]_{JM_J}\phi_{TM_T}\} \,. \tag{3.7.16}$$

Here J is the intrinsic baryon spin and M_J is its z-projection. The function χ describes the spin part and ϕ describes the flavor part of the full basis function. $\Theta_{LM_L}(\tilde{\mathbf{x}})$ is the angular part of the the relative wave function. The Jacobi coordinates are represented as $\mathbf{x}$, while $\tilde{\mathbf{x}}$ are their transpose. A is a symmetric positive-definite square $(N-1)\times(N-1)$ dimensional matrix. $\mathcal{S}$ is an operator that ensures the symmetry of the wave function with respect to the interchange of identical particles.

Because of Fermi statistics the baryon wave function should be antisymmetric overall because baryons are fermions. The baryon wave function is composed of several parts

$$\Psi = \psi_{(\text{space})}\psi_{(\text{spin})}\psi_{(\text{flavor})}\psi_{(\text{color})} \,. \tag{3.7.17}$$

The color state being a colorless singlet must always be antisymmetric

$$\psi_{(\text{color})} = \frac{1}{\sqrt{6}}(rgb - rbg + gbr - grb + brg - bgr) \,, \tag{3.7.18}$$

where r, g, and b are the color charges red, green, and blue respectively. This means that we can essentially ignore the color part, because it is spoken for, and our task is to make

sure that the total of the other parts is symmetric:

$$\psi_{(\text{space})}\psi_{(\text{spin})}\psi_{(\text{flavor})} \quad \rightarrow \quad \text{symmetric} \, . \tag{3.7.19}$$

We are interested in finding the discrete eigenvalues and eigenstates of the general mass operator $\hat{M}$ or equvalently Hamiltonian $\hat{H}$ for the three-quark system. The Hamiltonian must be time-independent, Hermitian, and bounded from below. Its eigenvalue problem reads

$$\hat{H}\Psi_n = E_n\Psi_n \quad , \quad n = 1, 2, \cdots , \, . \tag{3.7.20}$$

The eigenenergies E_n are real and we assume a non-degenerate ground state. The SVM gives an approximate determination of the baryon energy states beginning with the ground state via the Rayleigh-Ritz principle

$$E \equiv \frac{\langle\Psi|\,\hat{H}\,|\Psi\rangle}{\langle\Psi|\Psi\rangle} \geq E_1 \, . \tag{3.7.21}$$

In the Hilbert space $\mathcal{H}$, Ψ can be expanded into a combination of basis functions that span this Hilbert space. We want to minimize the energy functional with respect to the set of variational parameters A. We calculate

$$\langle\Psi(A)|\,H\,|\Psi(A)\rangle = E(A)\langle\Psi(A)|\Psi(A)\rangle \, , \tag{3.7.22}$$

where $\Psi(A)$ is an arbitrary function in the Hilbert space normalized to 1, i.e. $\langle\Psi(A)|\Psi(A)\rangle = 1$. The goal is to choose an optimized A that will give us the best approximation of the ground-state energy and possibly the (first) resonances. In order to calculate the eigenstates of the Hamiltonian including the excited states we apply the generalized Ritz theorem. Let us take at first the parameter set A to include only N linear parameters c_i. So $A = \{c_i, i = 1, 2, \cdots N\}$, where c_i are the coefficients of the N linearly independent basis functions ψ_i. Hence we expand the variational wave functions as

$$\Psi(A) = \sum_{i=1}^{N} c_i\psi \tag{3.7.23}$$

The test functions ψ_i do not neccesarily span the complete Hilbert space. As a consequence the $\Psi(A)$ corresponds only to approximates value of the true eigenvalues E of the Hamiltonian. We can insert Eq. (3.7.23) into the principle eigenvalue equation (3.7.20) giving us

$$\sum_{i=1}^{N}\sum_{j=1}^{N} c_i c_j^* \langle\psi_j|\,H\,|\psi_i\rangle = E_N \sum_{i=1}^{N}\sum_{j=1}^{N} c_i c_j^* \langle\psi_j|\psi_i\rangle \, . \tag{3.7.24}$$

Now our generalized matrix eigenvalue problem is reduced to an N-dimensional state space spanned by $\{\psi_i,\ i = 1, 2, \cdots N\}$ resulting in

$$\sum_{i=1}^{N} c_i H_{ji} = E_N \sum_{i=1}^{N} c_i B_{ji} \ , \tag{3.7.25}$$

where H_{ji} and B_{ji} are specifically

$$H_{ji} = \langle \psi_j | \, H \, | \psi_i \rangle \quad , \quad B_{ji} = \langle \psi_j | \psi_i \rangle \ , \tag{3.7.26}$$

which are simply the matrix elements of the $N \times N$ matrices $\mathbf{H}$ and $\mathbf{B}$. By extending N to higher and higher order the upper bound provided by the SVM gets closer and closer the the *true* value of the ground state.

The variational eigenfunctions for the N ground plus excited states are written as

$$\Psi_k = \sum_{i=1}^{N} c_{i,k} \psi_i, \qquad (k = 1, \cdots N), \tag{3.7.27}$$

where the corresponding variational parameters are expressed as $c_{i,k}$. The normalization of the states is

$$\sum_{j,i=1}^{N} c^*_{j,k} B_{ji} c_{i,k} = 1 \ . \tag{3.7.28}$$

Following the work of Suzuki and Varga [81] we will seek to optimize our basis in order to decrease the error of our upper energy bound calculation. We will try a refined ansatz where the basis functions depend in addition on a set of nonlinear variational parameters α_i which may contain discrete quantum numbers as well as continuous parameters arising from the spatial wave function.

$$\Psi(A) = \sum_{i=1}^{N} c_i \psi(\alpha_i) \tag{3.7.29}$$

where $\{(c_i, \alpha_i), i = 1, 2, \ldots N\}$ now contains both linear and nonlinear variational parameters.

In order to arrive at not only the most important basis states for a particular problem but also the pertinent selection of parameters via random selection, we outline a procedure that has proven successful in previous work regarding baryon spectroscopy in RCQM's [23, 49–51]. The methodology consists of a trial and error procedure in conjunction with an admittance test.

Beginning with a single basis state we generate a number of random parameter sets α_i^{rand} then calculate the matrix elements of the Hamiltonian $\langle\Psi(\alpha_i^{\text{rand}})|\, H\, |\Psi(\alpha_i^{\text{rand}})\rangle$ for all corresponding basis states. Next we chose the particular basis state that has the property

$$\langle\Psi(\alpha_1)|\, H\, |\Psi(\alpha_1)\rangle = \min_i \langle\Psi(\alpha_i^{\text{rand}})|\, H\, |\Psi(\alpha_i^{\text{rand}})\rangle \ . \tag{3.7.30}$$

In this way we add new basis states step by step.

Assuming we have already N basis states with the corresponding N eigenenergies $E_{N,n}$ for the generalized eigenvalue problem we select the next $N+1$ basis state by the following procedure

- Generate a number of random parameter sets α_i^{rand}
- Add the corresponding basis states separately to the basis and solve the resulting $N+1$ dimensional eigenvalue problems yielding in each case $N+1$ eigenvalues $E_{N+1,n}(\alpha_i^{\text{rand}})$
- Finally select as a new basis state $\psi(\alpha_j^{\text{rand}})$

$$E_{N+1,1}(\alpha_j^{\text{rand}}) = \min_i E_{N+1,1}(\alpha_i^{\text{rand}}) \tag{3.7.31}$$

The idea is to minimize the upper bound for the ground-state energy. It has been shown that using a stochastic choice of basis parameters will lead to a path-independent convergence of energy eigenvalues. This is an important point because it allows us to be sure that we avoid falling into local minima, which can often happen in numerical methods. It was shown by Wagenbrunn [49] that once $N \approx 40$ there is very good convergence of the upper bound. This tells us that even with a small amount of computer power we can converge upon the true ground state of the baryon within a few MeV. Table 3.5 shows the light and strange baryon spectra as calculated with the SVM for both the GBE and OGE RCQM's.

Baryon	J^P	GBE	OGE	Experiment
N(939)	$\frac{1}{2}^+$	939	939	938-940
N(1440)	$\frac{1}{2}^+$	1459	1577	1420-1470
N(1520)	$\frac{3}{2}^-$	1519	1521	1515-1525
N(1535)	$\frac{1}{2}^-$	1519	1521	1525-1545
N(1650)	$\frac{1}{2}^-$	1647	1690	1645-1670
N(1675)	$\frac{5}{2}^-$	1647	1690	1670-1680
N(1700)	$\frac{3}{2}^-$	1647	1690	1650-1750
N(1710)	$\frac{1}{2}^+$	1776	1859	1680-1740
Δ(1232)	$\frac{3}{2}^+$	1240	1231	1231-1233
Δ(1600)	$\frac{3}{2}^+$	1718	1854	1550-1700
Δ(1620)	$\frac{1}{2}^-$	1642	1621	1600-1660
Δ(1700)	$\frac{3}{2}^-$	1642	1621	1670-1750
Λ(1116)	$\frac{1}{2}^+$	1136	1113	1116
Λ(1405)	$\frac{1}{2}^-$	1556	1628	1401-1410
Λ(1520)	$\frac{3}{2}^-$	1556	1628	1519-1521
Λ(1600)	$\frac{1}{2}^+$	1625	1747	1560-1700
Λ(1670)	$\frac{1}{2}^-$	1682	1734	1660-1680
Λ(1690)	$\frac{3}{2}^-$	1682	1734	1685-1695
Λ(1800)	$\frac{1}{2}^-$	1778	1844	1720-1850
Λ(1810)	$\frac{1}{2}^+$	1799	1957	1750-1850
Λ(1830)	$\frac{5}{2}^-$	1778	1844	1810-1830
Σ(1193)	$\frac{1}{2}^+$	1180	1213	1189-1197
Σ(1385)	$\frac{3}{2}^+$	1389	1373	1383-1387
Σ[1560]	$\frac{1}{2}^-$	1677	1732	1546-1576
Σ[1620]	$\frac{1}{2}^-$	1736	1829	1594-1643
Σ(1660)	$\frac{1}{2}^+$	1616	1845	1630-1690
Σ(1670)	$\frac{3}{2}^-$	1677	1732	1665-1685
Σ[1690]	$\frac{3}{2}^+$	1865	1991	1670-1727
Σ(1750)	$\frac{1}{2}^-$	1759	1784	1730-1800
Σ(1775)	$\frac{5}{2}^-$	1736	1829	1770-1780
Σ(1880)	$\frac{1}{2}^+$	1911	2049	1806-2025
Σ[1940]	$\frac{3}{2}^-$	1736	1829	1900-1950
Σ	$\frac{3}{2}^-$	1759	1784	-
Ξ(1318)	$\frac{1}{2}^+$	1348	1346	1315-1321
Ξ(1530)	$\frac{3}{2}^+$	1528	1516	1532-1535
Ξ[1690]	$\frac{1}{2}^+$	1805	1975	1680-1700
Ξ(1820)	$\frac{3}{2}^-$	1792	1894	1818-1828
Ξ[1950]	$\frac{5}{2}^-$	1881	1993	1935-1965
Ω	$\frac{3}{2}^+$	1656	1661	1673.45±0.29

Table 3.5: Light- and strange-baryon spectra for GBE and OGE RCQM's as calculated via the SVM. All values are given in MeV.

Chapter 4

The Faddeev Approach

In addition to the SVM illustrated in the previous chapter we can also calculate the baryon spectra using the Faddeev integral-equation approach. This method was pioneered by Faddeev in the early 1960's when he proposed a way to circumvent that the Lippmann-Schwinger equation does not necessarily have a unique solution for the three-body problem [54].

Large portions of this chapter are based on the article [5]. In the RCQM's in $SU(3)_F$ most of the strange baryons are made of light and strange quarks. In these models the quarks are considered to be identical particles. The interaction is derived from the exchange of particles, like the exchange of Goldstone bosons. The constituent quarks of different flavors have masses, which can be quite different.

In this chapter we demonstrate the performance of the Faddeev approach for RCQM's with different constituent-quark masses. In $SU(2)_F$ the u and d quark masses are taken identical and the isospin symmetry is correct. Beyond that the strange quark mass is considered, as a heavier particle, as seen in nature.

The relativistically invariant mass spectra are obtained by a Faddeev integral-equation method, adapted to treating long-range interactions, such as the quark confinement. In the Faddeev approach the wave function is broken into three components. If some pair of particles is symmetric, then the corresponding Faddeev components have the same functional form. This allows one to reduce the number of components. Here we treat the two-light-and-one-strange or two-strange-and-one-light quark systems in a two-component Faddeev model. One component is responsible for the light-light or strange-strange pair, while the

other one for the light-strange pair. This way we retain the $SU(3)_F$ limit as the interactions are derived from this symmetry, but due to the explicit symmetry breaking of the system, the masses of the constituent quarks are different, hence we do not impose any explicit symmetry between light and strange quarks.

In Section 4.1 below we outline the Faddeev approach to three-quark systems with a confining long-range potential. In Section 4.2 we discuss the consequences of the permutation symmetry of the particles on the formalism. Then in Section 4.3 we describe the application of the method to the GBE RCQM. In Section 4.4 we present the results of our calculations as obtained along the Faddeev approach.

4.1 Faddeev Approach to Three-Quark Problems

We consider a three-particle Hamiltonian

$$H = H_{\text{free}} + v_1 + v_2 + v_3, \tag{4.1.1}$$

where H_{free} is the kinetic-energy operator and v_α, with $\alpha = 1, 2, 3$, are the mutual interactions of the quarks[‡]. We represent it through the usual configuration-space Jacobi coordinates: e.g. $\vec{x}_1$ is the coordinate between particles 2 and 3 and $\vec{y}_1$ is the coordinate between the center of mass of the pair $(2, 3)$ and particle 1.

The kinetic energy operator is given in the relativistic form

$$H_{\text{free}} = \sum_{i=1}^{3} \sqrt{k_i^2 + m_i^2}, \tag{4.1.2}$$

where m_i are the quark masses and $\mathbf{k}_i$ are the three-momenta of the quarks in the rest frame, where the total three-momentum $\mathbf{P} = \sum_{i=1}^{3} \mathbf{k}_i = 0$.

The quark-quark interaction is a long-range confining potential. In order that we can apply the Faddeev procedure along the method presented in Refs. [59, 82, 83] we split the quark-quark potential into confining and non-confining parts

$$v_\alpha = v_\alpha^{(c)} + v_\alpha^{(s)}, \tag{4.1.3}$$

[‡]This is the same as Eq. (3.3.5) with $\sum_{i<j}^{3} V_{ij}$ written out explicitly.

where superscripts c and s stand for confining and short-range, respectively. Then the Schrödinger equation takes the form

$$H|\Psi\rangle = (H^{(c)} + v_1^{(s)} + v_2^{(s)} + v_3^{(s)})|\Psi\rangle = E|\Psi\rangle \,, \tag{4.1.4}$$

with

$$H^{(c)} = H_{\text{free}} + v_1^{(c)} + v_2^{(c)} + v_3^{(c)}. \tag{4.1.5}$$

We introduce

$$G^{(c)}(E) = (E - H^{(c)})^{-1}, \tag{4.1.6}$$

and by rearranging (4.1.4), we have

$$\begin{aligned} |\Psi\rangle \quad &= G^{(c)}(E)(v_1^{(s)} + v_2^{(s)} + v_3^{(s)})|\Psi\rangle \\ &= G^{(c)}(E)v_1^{(s)}|\Psi\rangle + G^{(c)}(E)v_2^{(s)}|\Psi\rangle + G^{(c)}(E)v_3^{(s)}|\Psi\rangle. \end{aligned} \tag{4.1.7}$$

So, the three-particle wave function $|\Psi\rangle$ naturally splits into three components

$$|\Psi\rangle = |\psi_1\rangle + |\psi_2\rangle + |\psi_3\rangle \,, \tag{4.1.8}$$

where

$$|\psi_\alpha\rangle = G^{(c)}(E)v_\alpha^{(s)}|\Psi\rangle, \quad \alpha = 1, 2, 3, \tag{4.1.9}$$

are the so-called Faddeev components. They satisfy the following set of equations (Faddeev equations),

$$\begin{aligned} (E - H^{(c)} - v_1^{(s)})|\psi_1\rangle &= v_1^{(s)}(|\psi_2\rangle + |\psi_3\rangle) \\ (E - H^{(c)} - v_2^{(s)})|\psi_2\rangle &= v_2^{(s)}(|\psi_1\rangle + |\psi_3\rangle) \\ (E - H^{(c)} - v_3^{(s)})|\psi_3\rangle &= v_3^{(s)}(|\psi_1\rangle + |\psi_2\rangle) \,. \end{aligned} \tag{4.1.10}$$

Indeed, by adding up these equations and considering (4.1.7) we recover the Schrödinger equation. With the help of channel Green's operators

$$G_\alpha^{(c)}(E) = (E - H^{(c)} - v_\alpha^{(s)})^{-1}, \tag{4.1.11}$$

we can rewrite Eqs. (4.1.10) into integral equations,

$$\begin{aligned} |\psi_1\rangle &= G_1^{(c)}(E)\, v_1^{(s)}(|\psi_2\rangle + |\psi_3\rangle) \\ |\psi_2\rangle &= G_2^{(c)}(E)\, v_2^{(s)}(|\psi_1\rangle + |\psi_3\rangle) \\ |\psi_3\rangle &= G_3^{(c)}(E)\, v_3^{(s)}(|\psi_1\rangle + |\psi_2\rangle) \,. \end{aligned} \tag{4.1.12}$$

Even for such a simple system like a three-quark system the wave function Ψ can be rather complicated. The quark-quark potential for various angular momentum channels may have strong attractive and repulsive components. This leads to a strong quark-quark correlation in each of the possible subsystems of the three-quark system, which leads to a complicated wave function. The Faddeev components possess a simpler structure. For example, in Eq. (4.1.9), the short range potential $v_1^{(s)}$ acting on $|\Psi\rangle$, suppresses those asymptotic structures when particles 2 and 3 are far away. Consequently, $|\psi_1\rangle$ contains only one kind of physical situation when particle 1 is far away and particles 2 and 3 are in strong correlation. A similar statement is valid for $|\psi_2\rangle$ and $|\psi_3\rangle$. So, with the Faddeev decomposition we achieve a splitting of the wave function into parts such that each component possesses only one kind of asymptotic behavior and represents one kind of two-quark correlations.

We need to introduce the appropriate orbital angular momentum basis. The orbital angular momentum associated with coordinates x_α and y_α are denoted by l_α and λ_α, respectively, and they are coupled to the total orbital angular momentum L. The spin of particles β and γ, S_β and S_γ, respectively, are coupled to s_α, which is with the spin of particle α, S_α, coupled to the total spin S. Similarly, the isospin of particles β and γ, t_β and t_γ, respectively, are coupled to τ_α, which is with the isospin of particle α, t_α, coupled to the total isospin T. The angular momentum L and spin S are coupled to total angular momentum J. So, we adopted LS coupling, which is appropriate if the quark-quark interaction does not have tensor terms.

4.2 Faddeev Equations with Identical Particles

A further advantage of the Faddeev method is that the identity of particles greatly simplifies the equations (see, e.g. Ref. [62–64]). If particles β and γ, are identical the wave function Ψ must be symmetric with respect to exchange of these particles. We denote $\mathcal{P}_\alpha$ the operator that exchanges particles β and γ. Then

$$\mathcal{P}_\alpha|\Psi\rangle = p_\alpha|\Psi\rangle \tag{4.2.13}$$

where

$$p_\alpha = (-1)^{l_\alpha+s_\alpha-S_\beta-S_\gamma+\tau_\alpha-t_\beta-t_\gamma}\,, \tag{4.2.14}$$

if particles carry spin and isospin. The Faddeev component for β is defined by

$$|\psi_\beta\rangle = G^{(c)} v_\beta^{(s)} |\Psi\rangle. \tag{4.2.15}$$

By applying $\mathcal{P}_\alpha$ we have

$$\mathcal{P}_\alpha |\psi_\beta\rangle = \mathcal{P}_\alpha G^{(c)} v_\beta^{(s)} |\Psi\rangle = G^{(c)} \mathcal{P}_\alpha v_\beta^{(s)} \mathcal{P}_\alpha p_\alpha |\Psi\rangle. \tag{4.2.16}$$

Considering that $v_\beta^{(s)}$ is the interaction between particles α and γ and the operator P_α exchanges particles β and γ, we get

$$\mathcal{P}_\alpha v_\beta^{(s)} \mathcal{P}_\alpha = v_\gamma^{(s)}, \tag{4.2.17}$$

and Eq. (4.2.16) becomes

$$p_\alpha \mathcal{P}_\alpha |\psi_\beta\rangle = G^{(c)} v_\gamma^{(s)} |\Psi\rangle. \tag{4.2.18}$$

The right-hand side of this equation is the defining relation for $|\psi_\gamma\rangle$. So, we can conclude that

$$|\psi_\gamma\rangle = p_\alpha \mathcal{P}_\alpha |\psi_\beta\rangle, \tag{4.2.19}$$

and in a similar manner

$$|\psi_\beta\rangle = p_\alpha \mathcal{P}_\alpha |\psi_\gamma\rangle. \tag{4.2.20}$$

Since $\mathcal{P}_\alpha v_\alpha^{(s)} \mathcal{P}_\alpha = v_\alpha^{(s)}$, we get

$$\mathcal{P}_\alpha |\psi_\alpha\rangle = G^{(c)} \mathcal{P}_\alpha v_\alpha^{(s)} \mathcal{P}_\alpha p_\alpha |\Psi\rangle = p_\alpha |\psi_\alpha\rangle. \tag{4.2.21}$$

So, if particles β and γ are identical, then the angular channels for $|\psi_\alpha\rangle$ have to be selected such that $p_\alpha = 1$ for bosons and $p_\alpha = -1$ for fermions. On the other hand, the Faddeev equation for $|\psi_\alpha\rangle$ is given by

$$|\psi_\alpha\rangle = G_\alpha^{(c)} v_\alpha^{(s)} (|\psi_\beta\rangle + |\psi_\gamma\rangle) = (1 + p_\alpha \mathcal{P}_\alpha) G_\alpha^{(c)} v_\alpha^{(s)} |\psi_\beta\rangle. \tag{4.2.22}$$

We should notice that $1 + p_\alpha \mathcal{P}_\alpha$ is just twice the symmetrizing or anti-symmetrizing operator. If we select the angular basis for $|\psi_\alpha\rangle$ such that it ensures the correct symmetry or anti-symmetry the value of $1 + p_\alpha \mathcal{P}_\alpha$ is just 2.

Putting everything together and assuming that particles 2 and 3 are identical the three-component Faddeev equations simplify to

$$\begin{pmatrix} |\psi_1\rangle \\ |\psi_2\rangle \end{pmatrix} = \begin{pmatrix} 0 & 2G_1^{(c)} v_1^{(s)} \\ G_2^{(c)} v_2^{(s)} & G_2^{(c)} v_2^{(s)} p_1 \mathcal{P}_1 \end{pmatrix} \begin{pmatrix} |\psi_1\rangle \\ |\psi_2\rangle \end{pmatrix}. \tag{4.2.23}$$

If all three particles are identical, Eq. (4.2.23) gets further reduced to one single equation

$$|\psi_1\rangle = 2G_1^{(c)}v_1^{(s)}\mathcal{P}_{123}|\psi_1\rangle, \tag{4.2.24}$$

where $\mathcal{P}_{123} = \mathcal{P}_{12}\mathcal{P}_{23}$ is the operator for cyclic permutation of all three particles $\mathcal{P}_{123}|\psi_1\rangle = |\psi_2\rangle$.

The solution of the Faddeev equations for confining potentials has been presented in Refs. [82, 83]. We found that the simpler and faster method of Ref. [82] and the more elaborated method of Ref. [83] provides results which are in a very good agreement with each other. Therefore, in this paper we adopted the simpler method. These methods entails a separable approximation of the short-range parts of the quark-quark potentials on the three-body basis. Our basis is defined as before

$$\langle x_\alpha y_\alpha|n\nu\rangle_\alpha = \{\langle x_\alpha|n\rangle\langle y_\alpha|\nu\rangle\}, \tag{4.2.25}$$

where $\langle x|n\rangle$ are the Coulomb-Sturmian functions. The curly bracket stands for angular momentum coupling and for simplicity we have suppressed the angular momentum, the spin and isospin indexes. In this method we need to evaluate numerically the matrix elements ${}_1\langle n\nu|v_1^{(s)}|n'\nu'\rangle_2$, ${}_2\langle n\nu|v_2^{(s)}|n'\nu'\rangle_1$ and ${}_2\langle n\nu|v_2^{(s)}|n'\nu'\rangle_3$, which can be done in configuration space-representation. The Coulomb-Sturmian functions also have a nice analytic form in momentum space, which facilitates the evaluation of matrix elements of the Green's operator $G_\alpha^{(c)}$ as presented in Ref. [82].

4.3 GBE RCQM

We employ the GBE RCQM with the quark-quark interactions

$$v_\alpha = V_\alpha^{\rm conf} + V_\alpha^{\rm hf}\,, \tag{4.3.26}$$

where the confinement potential has the linear form

$$V_\alpha^{\rm conf} = V_0 + Cx_\alpha\,. \tag{4.3.27}$$

The hyperfine potential consists of the pseudoscalar meson exchanges for the octet

$$\begin{aligned} V_\alpha^{\rm hf}(\vec{x}_\alpha) &= \sum_{F=1}^{3} V_\pi(\vec{x}_\alpha)\lambda_\beta^F\lambda_\gamma^F\vec{\sigma}_\beta\cdot\vec{\sigma}_\gamma \\ &+\sum_{F=4}^{7} V_K(\vec{x}_\alpha)\lambda_\beta^F\lambda_\gamma^F\vec{\sigma}_\beta\cdot\vec{\sigma}_\gamma \\ &+V_{\eta_8}(\vec{x}_\alpha)\lambda_\beta^8\lambda_\gamma^8\vec{\sigma}_\beta\cdot\vec{\sigma}_\gamma, \end{aligned} \tag{4.3.28}$$

and for the singlet

$$V_\alpha^{\rm hf}(\vec{x}_\alpha) = \frac{2}{3}V_{\eta_0}(\vec{x}_\alpha)\vec{\sigma}_\beta\cdot\vec{\sigma}_\gamma, \tag{4.3.29}$$

where $\vec{\sigma}$ and λ^F are the quark spin and flavor matrices, respectively.

So, in angular momentum basis we get a flavor dependent quark-quark interaction for light quarks

$$V_\alpha^{\text{u(d)-u(d)}} = \left\{p_\alpha^{u(d)-u(d)}V_\pi T_\alpha + \frac{1}{3}V_{\eta_8} + \frac{2}{3}V_{\eta_0}\right\}\Sigma_\alpha, \tag{4.3.30}$$

for the light and strange quarks

$$V_\alpha^{\text{u(d)-s}} = \left\{2p_\alpha^{u(d)-s}V_K - \frac{2}{3}V_{\eta_8} + \frac{2}{3}V_{\eta_0}\right\}\Sigma_\alpha, \tag{4.3.31}$$

and for the strange quarks

$$V_\alpha^{\text{s-s}} = \left\{\frac{4}{3}V_{\eta_8} + \frac{2}{3}V_{\eta_0}\right\}\Sigma_\alpha. \tag{4.3.32}$$

The spins of the quarks are evidently $1/2$, particles and the isospin of the light quarks is $1/2$, while the isospin of the strange quark equals 0. For the symmetry coefficients we have

$$p_\alpha^{u(d)-u(d)} = (-1)^{l_\alpha+s_\alpha+\tau_\alpha-2} \tag{4.3.33}$$

and

$$p_\alpha^{u(d)-s} = (-1)^{l_\alpha+s_\alpha-1}, \tag{4.3.34}$$

and the T_α and Σ_α isospin-isospin and spin-spin factors are given by

$$T_\alpha = 2\tau_\alpha(\tau_\alpha+1) - 3 \tag{4.3.35}$$

and

$$\Sigma_\alpha = 2s_\alpha(s_\alpha+1) - 3, \tag{4.3.36}$$

respectively.

It is natural to incorporate $V^{\rm conf}$ into $v^{(c)}$ and $V^{\rm hf}$ into $v^{(s)}$. In Refs. [59, 82, 83] we showed that in order to avoid the appearance of spurious solutions the splitting of the quark-quark potential to $v^{(c)}$ and $v^{(s)}$ should be performed such that in the region of physical interest the resolvent $G^{(c)}$ does not have poles. To ensure this, we add a repulsive Gaussian term to $V^{\rm conf}$, which we subtract from $V^{\rm hf}$

$$v^{(c)} = V^{\rm conf} + a_0 e^{-(r/r_0)^2} \tag{4.3.37}$$

and

$$v^{(s)} = V^{\rm hf} - a_0 e^{-(r/r_0)^2} \ . \tag{4.3.38}$$

The parameters of the auxiliary potential have been taken as $a_0 = 3$ fm^{-1} and $r_0 = 1$ fm. By this choice of the parameter values any bound states of $H^{(c)}$ are avoided below ≈ 2 GeV. The values of a_0 and r_0 also influence the rate of convergence, but not the final results. The other parameters of the calculations are the same as for the light baryons, of Ref. [83]. The full parameter set for both OGE and GBE RCQM's can be found in sections 3.4 and 3.5 respectively.

4.4 Results from the Faddeev Approach for RCQM's

The results of our calculations of ground and resonant states with the GBE and OGE RCQM's along the Faddeev approach for the baryons with flavors u, d, and s are given in Table 4.1. For comparison, we present the results of the calculation along the SVM of Ref. [58]. The results from both types of calculations agree quite well, generally within a few percent. The spectra of the GBE RCQM are also shown in Figs. 4.1, 4.2, and 4.3 in comparison to experiment.

We have now presented the general structure of the Faddeev method for two RCQM's that consist of hyperfine interaction plus a linearly rising confinement potential. Here we consider the light quarks as identical and treat them in the framework of isospin symmetry. The light and strange quarks are also identical in the chiral symmetric limit of the theory. However, this symmetry is explicitly broken in nature hence the exchange bosons and quarks acquire mass. Additionally the masses of the strange and light quarks acquire different constituent masses via dynamical and explicit symmetry breaking. This mixture

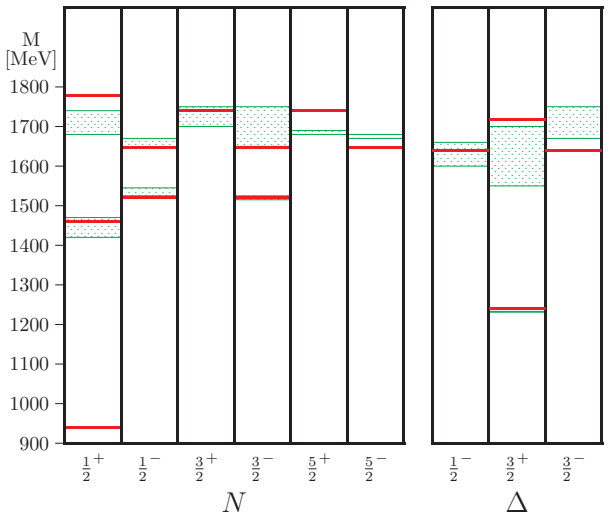

Figure 4.1: Spectra of N and Δ baryons of the GBE RCQM as calculated along the Faddeev approach (red lines); in comparison to experimental data as reported by the Particle Data Group [65] with uncertainties (green boxes).

of exact and broken symmetry can be treated nicely in the two-component version of the Faddeev method. In our method the particles 2 and 3 are identical and the exchange symmetry is exact. The symmetry between particles 1 and 2 or 3 is broken. The fact that it is an exact symmetry in the chiral limit is ensured by the potential form of Eq. (B), and in particular of Eq. (4.3.31). This treatment of broken symmetry will be very useful in the case of heavy baryon models where the masses of the charm and bottom constituent quarks will be $\approx 5m_u$ and $\approx 15m_u$ respectively. It is clear with regards to mass these cannot be treated identically in any reasonable approximation.

Baryon	J^P	Faddeev		SVM		Experiment
		GBE	OGE	GBE	OGE	
N(939)	$\frac{1}{2}^+$	939	940	939	939	938-940
N(1440)	$\frac{1}{2}^+$	1459	1578	1459	1577	1420-1470
N(1520)	$\frac{3}{2}^-$	1520	1521	1519	1521	1515-1525
N(1535)	$\frac{1}{2}^-$	1520	1521	1519	1521	1525-1545
N(1650)	$\frac{1}{2}^-$	1646	1686	1647	1690	1645-1670
N(1675)	$\frac{5}{2}^-$	1646	1686	1647	1690	1670-1680
N(1700)	$\frac{3}{2}^-$	1646	1686	1647	1690	1650-1750
N(1710)	$\frac{1}{2}^+$	1779	1862	1776	1859	1680-1740
Δ(1232)	$\frac{3}{2}^+$	1240	1229	1240	1231	1231-1233
Δ(1600)	$\frac{3}{2}^+$	1718	1852	1718	1854	1550-1700
Δ(1620)	$\frac{1}{2}^-$	1640	1618	1642	1621	1600-1660
Δ(1700)	$\frac{3}{2}^-$	1640	1618	1642	1621	1670-1750
Λ(1116)	$\frac{1}{2}^+$	1133	1127	1136	1113	1116
Λ(1405)	$\frac{1}{2}^-$	1561	1639	1556	1628	1401-1410
Λ(1520)	$\frac{3}{2}^-$	1561	1639	1556	1628	1519-1521
Λ(1600)	$\frac{1}{2}^+$	1607	1749	1625	1747	1560-1700
Λ(1670)	$\frac{1}{2}^-$	1672	1723	1682	1734	1660-1680
Λ(1690)	$\frac{3}{2}^-$	1672	1723	1682	1734	1685-1695
Λ(1800)	$\frac{1}{2}^-$	1777	1844	1778	1844	1720-1850
Λ(1810)	$\frac{1}{2}^+$	1799	1950	1799	1957	1750-1850
Λ(1830)	$\frac{5}{2}^-$	1777	1844	1778	1844	1810-1830
Σ(1193)	$\frac{1}{2}^+$	1163	1200	1180	1213	1189-1197
Σ(1385)		1391	1376	1389	1373	1383-1387
Σ[1560]	$\frac{1}{2}^-$	1666	1718	1677	1732	1546-1576
Σ[1620]	$\frac{1}{2}^-$	1734	1827	1736	1829	1594-1643
Σ(1660)	$\frac{1}{2}^+$	1605	1823	1616	1845	1630-1690
Σ(1670)	$\frac{3}{2}^-$	1666	1718	1677	1732	1665-1685
Σ[1690]	$\frac{3}{2}^+$	1864	1986	1865	1991	1670-1727
Σ(1750)	$\frac{1}{2}^-$	1753	1783	1759	1784	1730-1800
Σ(1775)	$\frac{5}{2}^-$	1734	1827	1736	1829	1770-1780
Σ(1880)	$\frac{1}{2}^+$	1891	2012	1911	2049	1806-2025
Σ[1940]	$\frac{3}{2}^-$	1734	1827	1736	1829	1900-1950
Σ	$\frac{3}{2}^-$	1753	1783	1759	1784	-
Ξ(1318)	$\frac{1}{2}^+$	1345	1346	1348	1346	1315-1321
Ξ(1530)	$\frac{3}{2}^+$	1526	1516	1528	1516	1532-1535
Ξ[1690]	$\frac{1}{2}^+$	1797	1966	1805	1975	1680-1700
Ξ(1820)	$\frac{3}{2}^-$	1787	1886	1792	1894	1818-1828
Ξ[1950]	$\frac{5}{2}^-$	1875	1988	1881	1993	1935-1965
Ω	$\frac{3}{2}^+$	1657	1659	1656	1661	1672.45±0.29

Table 4.1: Comparison of $SU(3)_F$ baryon spectra as calculated from the Faddeev approach with those of the SVM for both the GBE potential and the OGE RCQM's. All values are given in MeV.

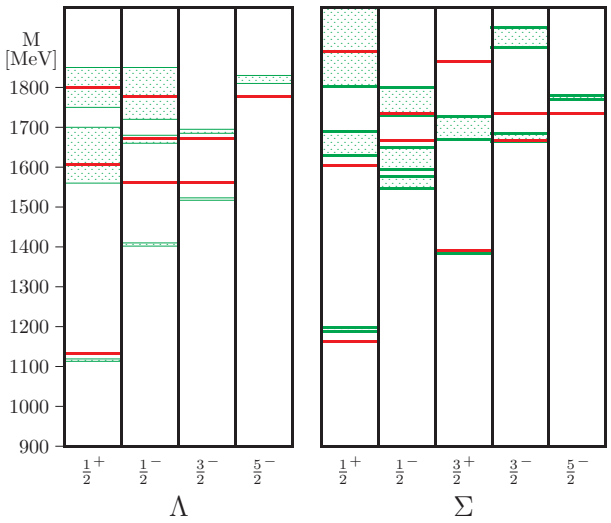

Figure 4.2: The same as in Fig. 4.1 for Λ and Σ baryons.

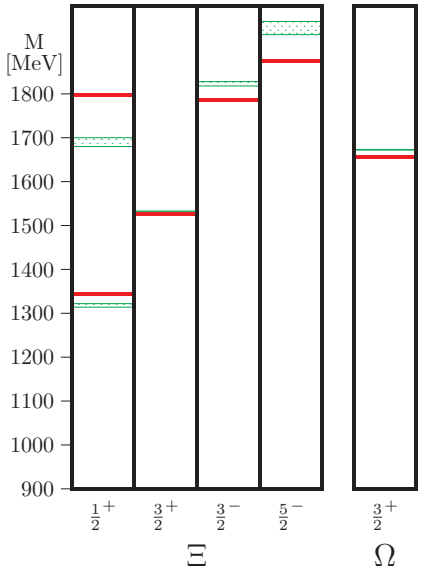

Figure 4.3: The same as in Fig. 4.1 for Ξ and Ω baryons.

Chapter 5

The Universal RCQM

The CQM has a long history, and it has made important contributions to the understanding of many hadron properties, think only of the fact that the systematization of hadrons in the standard particle-data base [65] follows the valence-quark picture. Over the decades the CQM has ripened into a stage where its formulation and solution are well based on a relativistic (or more generally Poincaré-invariant) quantum theory. Relativistic constituent-quark models (RCQM) have been developed by several groups, however, with limited domains of validity. Of course, it is desirable to have a framework as universal as possible for the description of all kinds of hadron processes in the low- and intermediate-energy regions. This is especially true in view of the advent of ever more data on heavy-baryon spectroscopy from present and future experimental facilities.

Here, we present a universal RCQM (URCQM) that comprises all known baryons with flavors u, d, s, c, and b within a single framework. There have been only a few efforts so far to extend a CQM from light- to heavy-flavor baryons. We may mention, for example, the approach by the Bonn group who have developed a RCQM, based on the 't Hooft instanton interaction, along a microscopic theory solving the Salpeter equation [66] and extended their model to charmed baryons [88], still not yet covering bottom baryons. A further quark-model attempt has been undertaken by the Mons-Liège group relying on the large-N_c expansion [68,69], partially extended to heavy-flavor baryons [70]. Similarly, efforts are invested to expand other approaches to heavy baryons, such as the employment of Dyson-Schwinger equations together with either quark-diquark or three-quark calculations [15, 93]. Also an increased amount of more refined lattice-QCD results has by now

become available on heavy-baryon spectra (see, e.g., the recent work by Liu et al. [87] and references cited therein).

Similar to the earlier RCQM our URCQM is based on the invariant mass operator

$$\hat{M} = \hat{M}_{\text{free}} + \hat{M}_{\text{int}} \,, \tag{5.0.1}$$

where the free part corresponds to the total kinetic energy of the three-quark system and the interaction part contains the dynamics of the constituent quarks Q. In the rest frame of the baryon, where its three-momentum $\vec{P} = \sum_i^3 \vec{k}_i^2 = 0$, we may express the terms as

$$\hat{M}_{\text{free}} = \sum_{i=1}^{3} \sqrt{\hat{m}_i^2 + \hat{\vec{k}}_i^2} \,, \tag{5.0.2}$$

$$\hat{M}_{\text{int}} = \sum_{i<j}^{3} \hat{V}_{ij} = \sum_{i<j}^{3} (\hat{V}_{ij}^{\text{conf}} + \hat{V}_{ij}^{\text{hf}}) \,. \tag{5.0.3}$$

Here, the $\hat{\vec{k}}_i$ correspond to the three-momentum operators of the individual quarks with rest masses m_i and the Q-Q potentials $\hat{V}_{ij}$ are composed of confinement and hyperfine interactions. By employing such a mass operator $\hat{M}^2 = \hat{P}^\mu \hat{P}_\mu$, with baryon four-momentum $\hat{P}_\mu = (\hat{H}, \hat{P}_1, \hat{P}_2, \hat{P}_3)$, the Poincaré algebra involving all ten generators $\{\hat{H}, \hat{P}_i, \hat{J}_i, \hat{K}_i\}$, $(i = 1, 2, 3)$, or equivalently $\{\hat{P}_\mu, \hat{J}_{\mu\nu}\}$, $(\mu, \nu = 0, 1, 2, 3)$, of time and space translations, spatial rotations as well as Lorentz boosts, can be guaranteed. The solution of the eigenvalue problem of the mass operator $\hat{M}$ yields the relativistically invariant mass spectra as well as the baryon eigenstates (the latter, of course, initially in the standard rest frame).

We adopt the confinement depending linearly on the Q-Q distance r_{ij}

$$V_{ij}^{\text{conf}}(\vec{r}_{ij}) = V_0 + C r_{ij} \tag{5.0.4}$$

with the strength $C = 2.33$ fm^{-2}, corresponding to the string tension of QCD. The parameter $V_0 = -402$ MeV is only necessary to set the ground state of the whole baryon spectrum, i.e., the proton mass; it is irrelevant, if one considers only level spacings.

The hyperfine interaction is most essential to describe all of the baryon excitation spectra. In a unified model the hyperfine potential must be explicitly flavor-dependent. Otherwise, e.g., the N and Λ spectra with their distinct level orderings could not be reproduced simultaneously. At least for baryons with flavors u, d, and s the type of hyperfine interaction taking into account SBχS has been most successful over the past

years. Obviously, it grabs the essential degrees of freedom governing the behavior of low-energy baryons [73–75]. The RCQM constructed along this dynamical concept, i.e., on Goldstone-boson exchange (GBE), has provided a comprehensive description of all light and strange baryons [18, 76]. This is not only true with regard to the spectroscopy but to a large extent also for other baryon properties, like electromagnetic and axial form factors [77] and a number of other reaction observables (for a concise summary see ref. [78]). It has been tempting to extend this successful concept even to the heavier flavors c and b. By such studies one should in addition learn about the proper light-heavy and heavy-heavy hyperfine Q-Q interactions. Some exploratory work in this direction had already been undertaken some time ago in ref. [79], hinting to promising results also for charm and bottom baryons.

Therefore we have advocated for the hyperfine interaction of our universal RCQM the $SU(5)_F$ GBE potential

$$V_{\rm hf}(\vec{r}_{ij}) = \left[V_{24}(\vec{r}_{ij}) \sum_{a=1}^{24} \lambda_i^a \lambda_j^a + V_0(\vec{r}_{ij}) \lambda_i^0 \lambda_j^0\right] \vec{\sigma}_i \cdot \vec{\sigma}_j \,. \tag{5.0.5}$$

Here, we take into account only its spin-spin component, which produces the most important hyperfine forces for the baryon spectra. While $\vec{\sigma}_i$ represent the Pauli spin matrices of $SU(2)_S$, the λ_i^a are the generalized Gell-Mann flavor matrices of $SU(5)_F$ for quark i. In addition to the exchange of the pseudoscalar 24-plet also the flavor-singlet is included because of the U(1) anomaly. The radial form of the GBE potential resembles the one of the pseudoscalar meson exchange

$$V_\beta(\vec{r}_{ij}) = \frac{g_\beta^2}{4\pi} \frac{1}{12 m_i m_j} \left[\mu_\beta^2 \frac{e^{-\mu_\beta r_{ij}}}{r_{ij}} - 4\pi\delta(\vec{r}_{ij})\right] \tag{5.0.6}$$

for $\beta = 24$ and $\beta = 0$. Herein the δ-function must be smeared out leading to [76, 80]

$$V_\beta(\vec{r}_{ij}) = \frac{g_\beta^2}{4\pi} \frac{1}{12 m_i m_j} \left[\mu_\beta^2 \frac{e^{-\mu_\beta r_{ij}}}{r_{ij}} - \Lambda_\beta^2 \frac{e^{-\Lambda_\beta r_{ij}}}{r_{ij}}\right]. \tag{5.0.7}$$

Contrary to the earlier GBE RCQM [18], which uses several different exchange masses μ_γ and different cut-offs Λ_γ, corresponding to $\gamma = \pi$, K, and η=η_8 mesons, we here managed to get along with a universal GBE mass μ_{24} and a single cut-off Λ_{24} for the 24-plet of $SU(5)_F$. Only the singlet exchange comes with another mass μ_0 and another cut-off Λ_0

$(g_0/g_{24})^2$	Λ_{24} [fm^{-1}]	Λ_0 [fm^{-1}]
1.5	3.55	7.52

Table 5.1: Free parameters of the present URCQM determined by a best fit to the baryon spectra.

Fixed Parameters						
Quark masses [MeV]				Exchange masses [MeV]		Coupling
$m_u = m_d$	m_s	m_c	m_b	μ_{24}	μ_0	$g_{24}^2/4\pi$
340	480	1675	5055	139	958	0.7

Table 5.2: Fixed parameters of the present URCQM predetermined from phenomenology and not varied in the fitting procedure.

with a separate coupling constant g_0. Consequently the number of open parameters in the hyperfine interaction could be kept as low as only three (see Tab. 5.1).

All other parameters entering the model have judiciously been predetermined by existing phenomenological insights. In this way the constituent quark masses have been set to the values as given in Tab. 5.2. The 24-plet Goldstone-boson (GB) mass has been assumed as the value of the π mass and similarly the singlet mass as the one of the η'. The universal coupling constant of the 24-plet has been chosen according to the value derived from the π-N coupling constant via the Goldberger-Treiman relation.

5.1 Spectra

We have calculated the baryon spectra of the relativistically invariant mass operator $\hat{M}$ to a high accuracy both by the stochastic variational method [81] as well as the modified Faddeev integral equations [82, 83]. The present universal RCQM produces the spectra in the light and strange sectors with similar or even better quality than the previous GBE RCQM [18] (see Figs. 5.2 and 5.3). Most importantly, the right level orderings specifically in the N, Δ and Λ spectra as well as all other SU(3)$_F$ ground and excited states are reproduced in accordance with phenomenology. The reasons are exactly the same as for the previous GBE RCQM, which has already been extensively discussed in the lit-

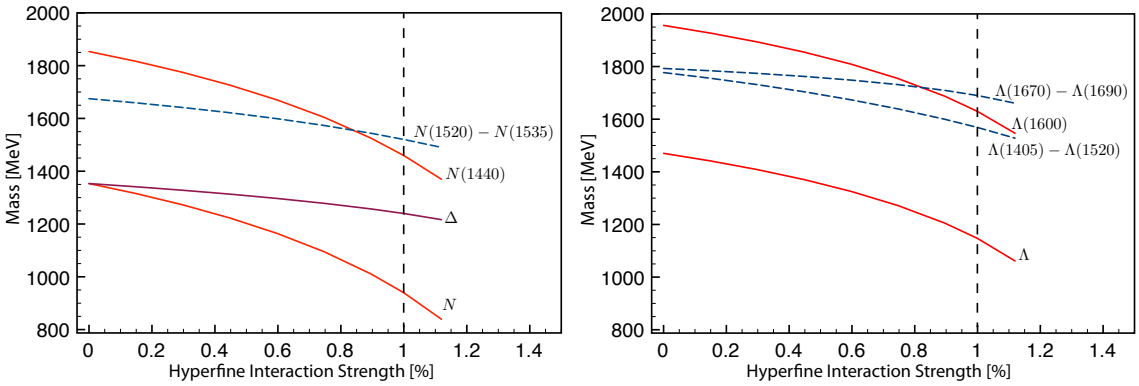

Figure 5.1: We see here the correct level ordering of the nucleon, the Roper, and $N(1520)$. This is a very important feature that was first realized in the original RCQM and has been reproduced in the new universal model.

erature [18, 74, 76]. Unfortunately, the case of the $\Lambda(1405)$ excitation could still not be resolved. It remains as an intriguing problem for all three-quark CQMs.

What is most interesting in the context of the present work are the very properties of the light-heavy and heavy-heavy Q-Q hyperfine interactions. Can the GBE dynamics reasonably account for them? In Figs. 5.4 and 5.5 we show the spectra of all charm and bottom baryons that experimental data with at least three- or four-star status by the PDG [65] are available for [‡]. As is clearly seen, our URCQM can reproduce all levels with respectable accuracy. In the Λ_c and Σ_c spectra some experimental levels are not known with regard to their spin and parity J^P. They are shown in the right-most columns of Fig. 5.4. Obviously they could easily be accommodated in accordance with the theoretical spectra, once their J^P's are determined. Furthermore the model predicts some additional excited states for charm and bottom baryons that are presently missing in the phenomenological data base.

5.2 Heavy Baryons

[‡]Only Ξ_c and Ξ_b are missing, as we are presently not in the position to calculate baryons with three different constituent-quark masses.

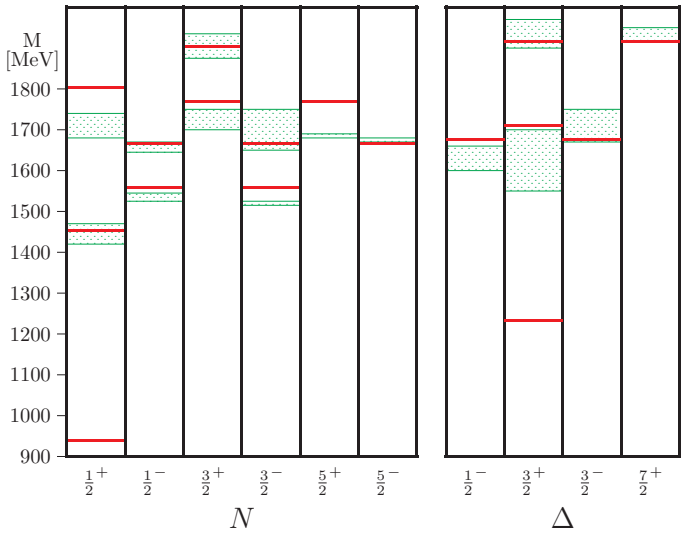

Figure 5.2: Nucleon and Δ excitation spectra (solid/red levels) as produced by the URCQM in comparison to phenomenological data [65] (the gray/blue lines and shadowed/blue boxes show the masses and their uncertainties).

5.2.1 Single Heavy

Of course, the presently available data base on charm and bottom baryon states is not yet very rich and thus not particularly selective for tests of effective Q-Q hyperfine forces. The situation will certainly improve with the advent of further data from ongoing and planned experiments. Beyond the comparison to experimental data, we note that the theoretical spectra produced by our present URCQM are also in good agreement with existing lattice-QCD results for heavy-flavor baryons. This is especially true for the charm baryons vis-à-vis the recent work by Liu et al. [87].

We emphasize that the most important ingredients into the universal RCQM are relativity, or more generally Poincaré invariance, and a hyperfine interaction that is derived from an interaction Lagrangian built from effective fermion (constituent quark) and boson (Goldstone boson) fields connected by a pseudoscalar coupling [74]. It appears that such kind of dynamics is quite appropriate for constituent quarks of any flavor. The effects of the hyperfine forces do not at all become tentatively small for baryons with charm and bottom flavors. In some cases at least the heavy-light interactions are of the same importance for the level spacings as the light-light interactions. This has already been seen

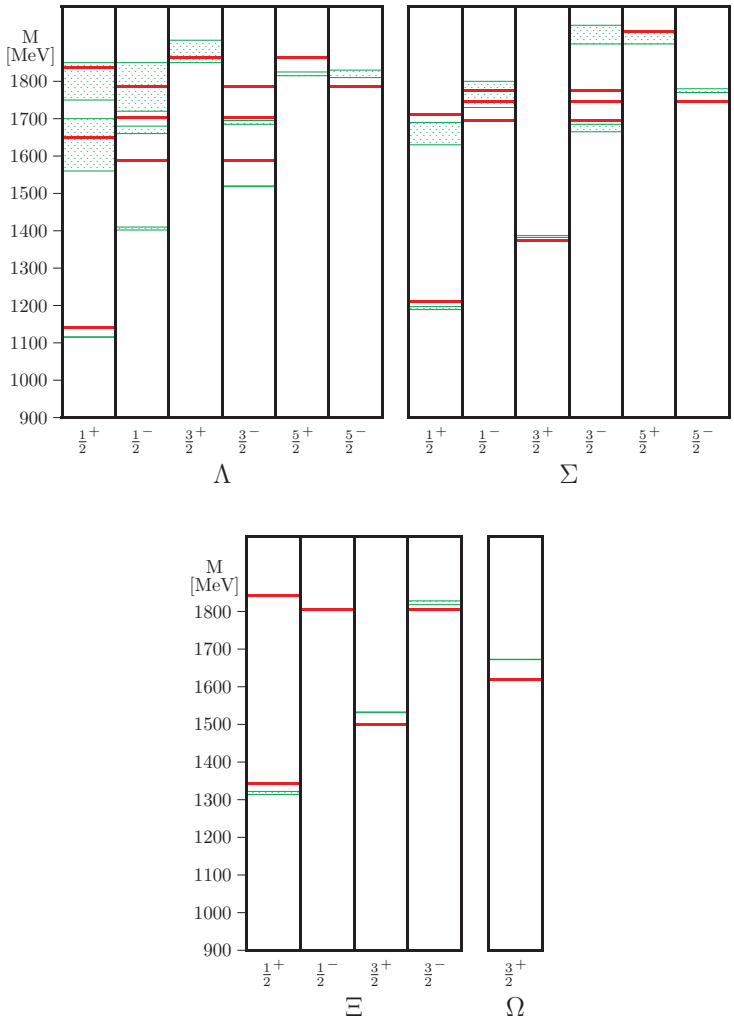

Figure 5.3: Same as Fig. 5.2 but for the strange baryons.

for charm baryons in the work by the Bonn group [88] and is also true for our URCQM (as will be detailed in ref. [84] too). It is furthermore in line with findings from earlier lattice-QCD calculations [85].

As a result we have demonstrated by the proposed URCQM that a universal description of all known baryons is possible in a single model. Here, we have considered only the baryon masses (eigenvalues of the invariant mass operator $\hat{M}$). Beyond spectroscopy the present model will be subject to further tests with regard to the baryon eigenstates, which are simultaneously obtained from the solution of the eigenvalue problem of $\hat{M}$. They must prove reasonable in order to make the model a useful tool for the treatment of all kinds of baryons reactions within a universal framework.

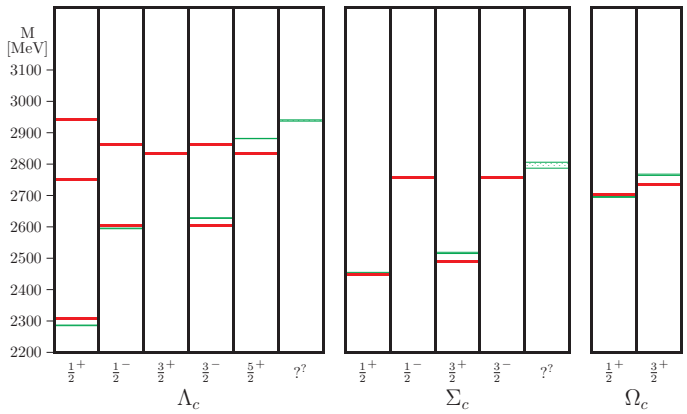

Figure 5.4: Same as Fig. 5.2 but for charm baryons.

5.2.2 Importance of Hyperfine Interaction?

It is sometimes said with regard to heavy baryon spectroscopy that the most important interaction is the confinement while the hyperfine interaction plays little to no role. We have investigated this behavior and the results for the single heavy baryons are shown in figures 5.6 5.7 and 5.8. The baryon energy levels with confinement only are shown by the light blue lines on the left-hand side of each column. The magenta lines in the middle of each column include confinement for all three quarks plus the hyperfine interaction "turned on" only between light quarks. The full calculation with confinement and hyperfine interaction for all three quarks is shown by the red lines on the right side of each column.

As we see, in fact, the hyperfine interaction plays an essential role also in heavy baryons. This is in general true for both the light-light and light-heavy parts. Of course, there are some levels, where the latter plays a minor role. One glaring example, where both types produce level shifts of similar magnitudes is the $\frac{1}{2}^+$ Λ_c state. A similar behavior is found for the Σ_c $\frac{1}{2}^+$ states. Only as soon a bottom quark is involved the light-heavy hyperfine interaction becomes small (see Fig. 5.8).

5.2.3 Double Heavy

In the case of double heavy baryons there has been the claim of the Ξ_{cc} measurement by the SELEX group at Fermilab in 2002 [86]. This baryon has never been independently

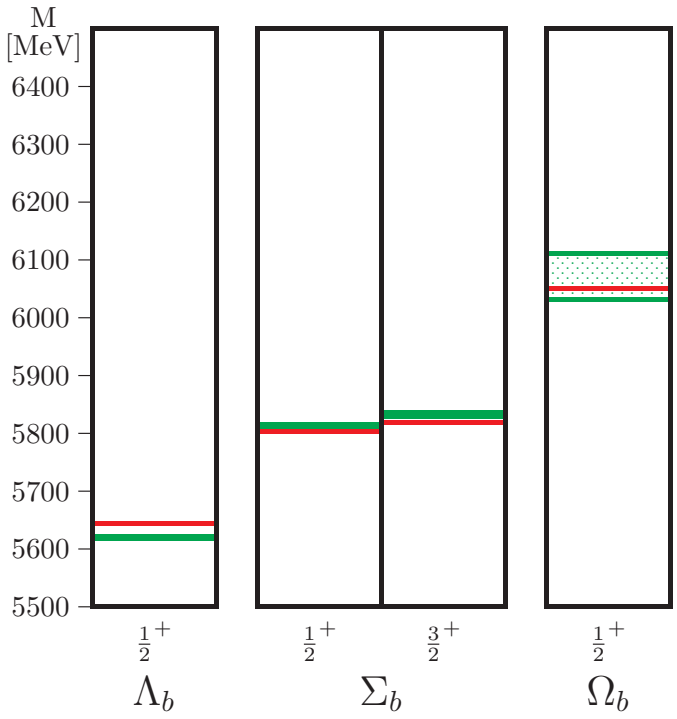

Figure 5.5: Same as Fig. 5.2 but for bottom baryons.

reproduced and is currently ranked by the particle data group with a one star rating which means ”evidence of existence of poor”. We always consider experiment the final verdict in physics, however, given the dubious nature of this measurement we employ additional comparison of our results with the lattice QCD [87] and a relativistically covariant quark model based on the Bethe-Salpeter equation in instantaneous approximation [88]. The results are shown in Fig. 5.9. We see that the experimental value [86] lies roughly 100 MeV below all theoretical predictions. We look forward to the resolution of this curious measurement, however it is a bit discouraging that more than ten years later there has not been an independent confirmation or update.

5.2.4 Triple Heavy

To date no triple heavy baryons have been observed experimentally. Here we list our predictions. Mention something about the types of comparisons as well, e.g.; Bethe-Salpeter equation in instantaneous approximation [88]; Quark Model [89]; Relativistic Quark Model [90]; Relativistic Quark Model [91]; Lattice QCD [92]; DSE [93]; potential

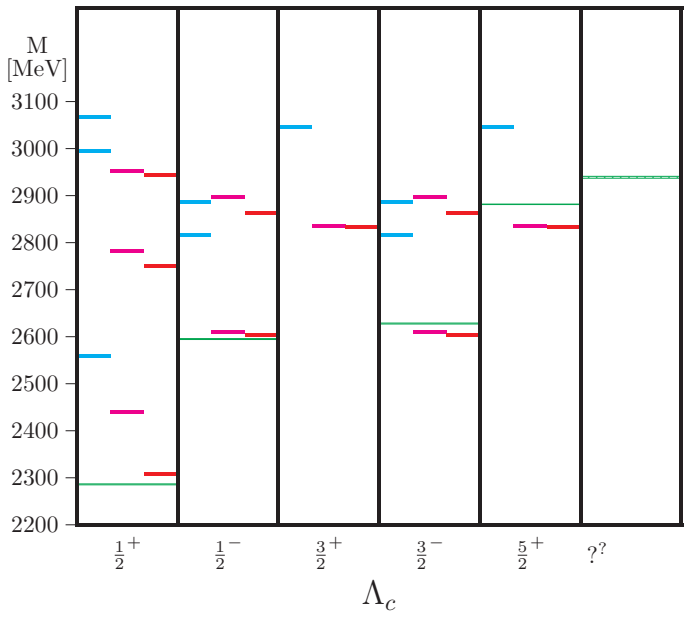

Figure 5.6: Evolution of the Λ_c baryon. The three-quark system with confinement only is shown in light blue on the left hand side of each column. The magenta line in the middle of each column includes confinement for all three quarks plus the hyperfine interaction "turned on" between only light-light quark interactions. The full calculation with confinement and hyperfine interaction for all three quarks is shown by the red line on the right side of each column.

Non-Relativistic Quantum Chromodynamics (pNRQCD) [94];

5.3 Form Factors

The physics behind the baryon form factors is the idea of probing the structure of the baryon. Of course, depending on what one uses as a probe one will gain will different insights. For example, by probing the baryon with a photon (electromagnetic interaction) one can learn something about the electromagnetic structure. In contrast, by probing with a W or Z (weak interaction) one will learn about the axial structure. Another possibility exists in probing the baryon with a spin-2 graviton (gravitational interaction). Let us first look at the general formalism in connection with form factors. The hadronic current

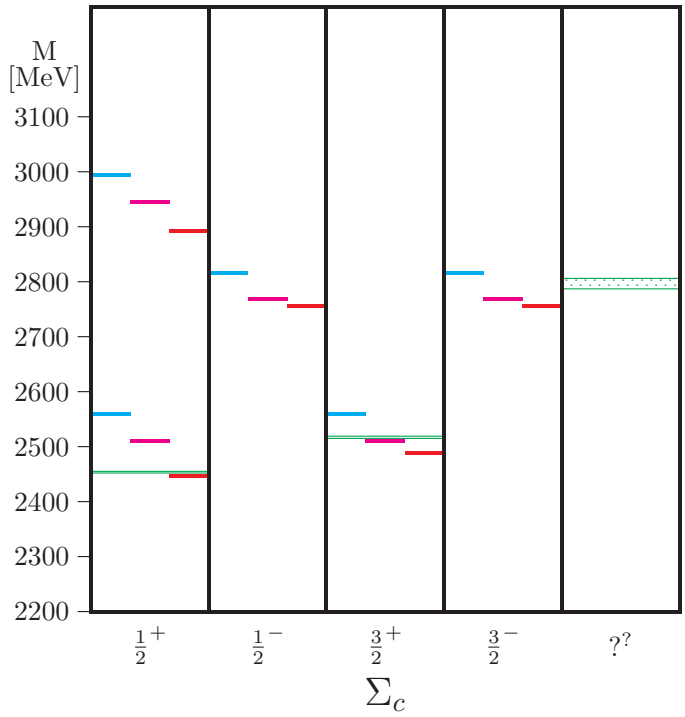

Figure 5.7: Same as Fig. 5.6 for the Σ_c baryons.

operator must satisfy the following conditions [95]:

$$\frac{\partial J^\mu(x)}{\partial x^\mu} = 0 \qquad \text{(current conservation)}, \tag{5.3.8}$$

$$U(\Lambda)J_\mu(x)U(\Lambda)^{-1} = (\Lambda^{-1})^\nu_\mu J_\nu(\Lambda x) \qquad \text{(Lorentz covariance)}, \tag{5.3.9}$$

$$[P^\nu, J^\mu(x)] = i\frac{\partial J^\mu(x)}{\partial x_\nu} \qquad \text{(space-time covariance)}. \tag{5.3.10}$$

Current conservation, $\partial_\mu J^\mu = 0$, requires

$$(P^\mu_f - P^\mu_i)\,\langle V', M', J', \Sigma'|\, J_\mu\, |V, M, J, \Sigma\rangle = 0\,, \tag{5.3.11}$$

where P^μ_i and P^μ_f are the initial and final four-momenta respectively. The Lorentz boosts

$$\Lambda_c(v_{\rm in}) = \Lambda_c^{-1}(v_{\rm f}) = \begin{pmatrix} \cosh\frac{\Delta}{2} & 0 & 0 & -\sinh\frac{\Delta}{2} \\ 0 & 1 & 0 & 0 \\ 0 & 0 & 1 & 0 \\ -\sinh\frac{\Delta}{2} & 0 & 0 & \cosh\frac{\Delta}{2} \end{pmatrix} \tag{5.3.12}$$

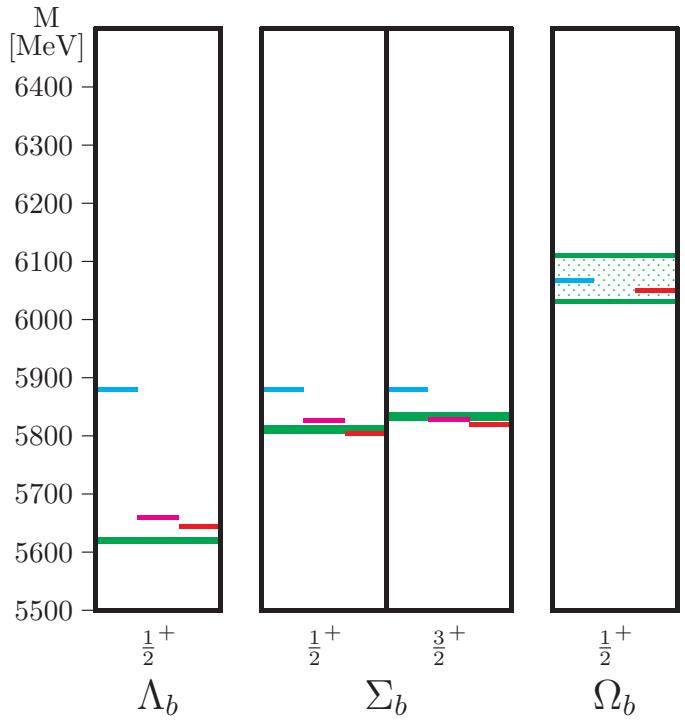

Figure 5.8: Same as Fig. 5.6 for the single bottom baryons Λ_b, Σ_b, and Ω_b.

are such that

$$\Lambda_c^{-1}(v_{\rm f})\Lambda_c(v_{\rm in}) = \begin{pmatrix} \cosh\Delta & 0 & 0 & -\sinh\Delta \\ 0 & 1 & 0 & 0 \\ 0 & 0 & 1 & 0 \\ -\sinh\Delta & 0 & 0 & \cosh\Delta \end{pmatrix}, \tag{5.3.13}$$

where Δ is defined through

$$\sinh\frac{\Delta}{2} = \frac{Q}{2M}, \tag{5.3.14}$$

with M the mass of the baryon and $Q^2 = -q_\mu q^\mu$. In the Breit frame (B) the initial and final four-momenta are given as

$$P_i^\mu(B) = MV_i^\mu = M(\cosh\frac{\Delta}{2}, 0, 0, -\sinh\frac{\Delta}{2}), \tag{5.3.15}$$

$$P_f^\mu(B) = MV_f^\mu = M(\cosh\frac{\Delta}{2}, 0, 0, \sinh\frac{\Delta}{2}). \tag{5.3.16}$$

The invariant momentum transfer along the z-axis is $q^\mu(B) = (0, 0, 0, Q)$. We can write it as

$$q^2(B) = -Q^2 = (P_f(B) - P_i(B))^2 = -4M^2(\sinh\frac{\Delta}{2})^2. \tag{5.3.17}$$

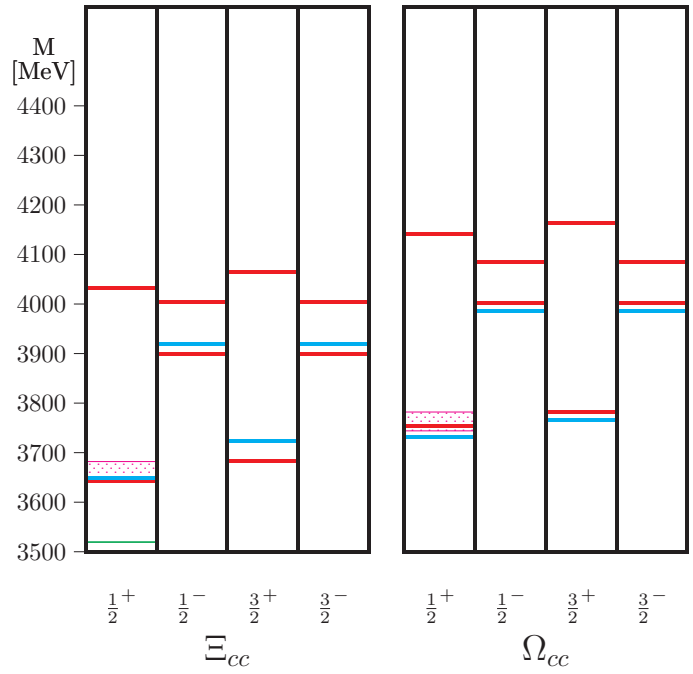

Figure 5.9: Double-charm baryons. The prediction of the URCQM is shown by the red lines. The green line shows the experimental value from the SELEX collaboration [86]. The pink box shows the results from a Lattice QCD calculation with uncertainties [87]. The light blue line is the result of the Bonn group [88].

We can define the invariant form factors in the Breit frame as

$$2MF^{\mu}_{\Sigma'\Sigma}(Q^2) = \langle V_f, M', J', \Sigma' | J^{\mu}(0) | V_i, M, J, \Sigma \rangle \tag{5.3.18}$$

In order to fulfill current conservation the ($\mu = 3$) component of the standard current matrix element must vanish in the Breit frame, because the momentum transfer $q^{\mu}(B) = P^{\mu}_f(B) - P^{\mu}_i(B)$ has a nonvanishing z-component. For spin J particles we should have $(2J + 1)$ independent form factors.

5.3.1 Elastic Electric and Magnetic Form Factors

Considering spin 1/2 particles we get two (one electric and one magnetic) elastic form factors as expected. We can write the matrix elements

$$\langle V_f, M, J = \frac{1}{2}, \Sigma' | J^{\mu}(0) | V_i, M, J = \frac{1}{2}, \Sigma \rangle = \tag{5.3.19}$$
$$\bar{u}(P_f, \Sigma') \left[F_1(Q^2)\gamma^{\mu} + \frac{i}{2M} F_2(Q^2)\sigma^{\mu\nu} q_{\nu}(B) \right] u(P_i, \Sigma)$$

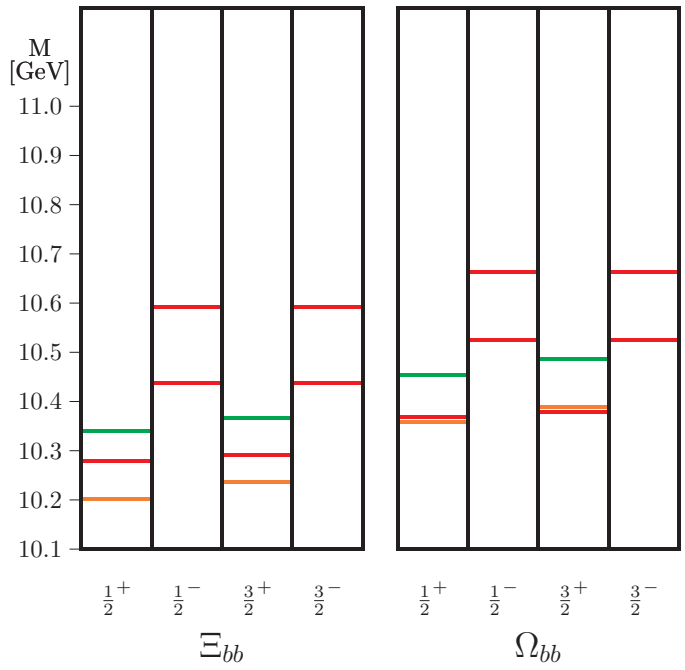

Figure 5.10: Double-bottom baryons. The prediction of the URCQM is shown by the red lines. The green line shows the theoretical value from Roberts and Pervin [89]. The orange line shows the theoretical value from Ebert *et al.* [90].

where $u(P,\Sigma)$ is the Dirac spinor with four-momentum P and spin projection Σ. F_1 is the Dirac and F_2 is the Pauli form factor. The spinor normalization is $\bar{u}(P,\Sigma')u(P,\Sigma) = 2M\delta_{\Sigma\Sigma'}$. Explicitly we write it as

$$u(P,\Sigma) = \sqrt{E+M}\begin{pmatrix} \chi_\Sigma \\ \frac{\vec{\sigma}\cdot\vec{P}}{E+M}\chi_\Sigma \end{pmatrix}, \tag{5.3.20}$$

where χ_Σ is the two-component Pauli spinor. We can relate the Dirac and Pauli form factors to the invariant form factors $F^\mu_{\Sigma'\Sigma}$ as follows:

$$F^{\mu=0}_{\Sigma'\Sigma}(Q^2) = \chi^\dagger_{\Sigma'}\left[F_1(Q^2) - \frac{Q^2}{4M^2}F_2(Q^2)\right]\chi_\Sigma \tag{5.3.21}$$

$$\vec{F}_{\Sigma'\Sigma}(Q^2) = \chi^\dagger_{\Sigma'}\frac{i|\vec{q}(B)|}{2M}[F_1(Q^2)+F_2(Q^2)](\vec{\sigma}\times\hat{z})\chi_\Sigma \tag{5.3.22}$$

In addition the invariant form factors are related to the electric and magnetic Sachs form factors

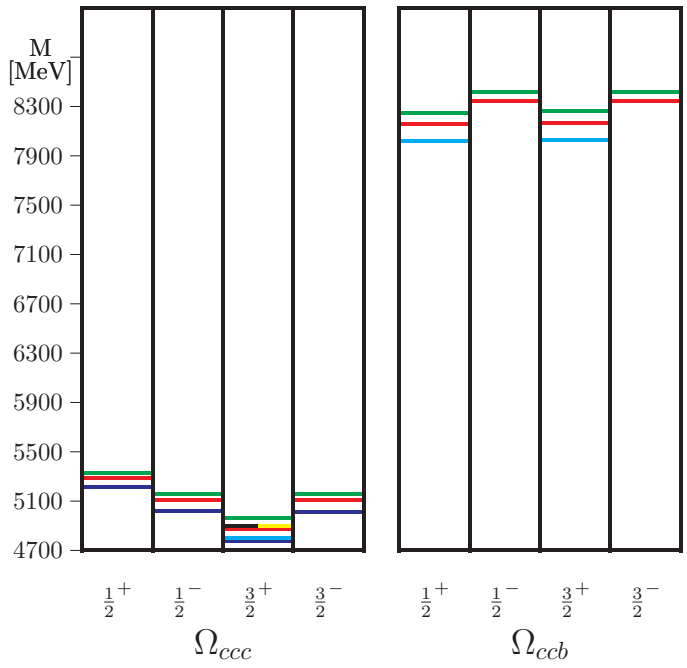

Figure 5.11: Mostly-charm baryons. The prediction of the URCQM is shown by the red lines. The green line shows the theoretical value from Roberts and Pervin [89]. The light blue line shows the theoretical value from Martynenko [91]. The dark blue line is the result of the Bonn group [88]. The yellow line is Llanes-Estrada, *et al.* [94]. The black line is Sanchis-Alepuz, *et al.* [93]

$$G_E(Q^2) = F^{\mu=0}_{\frac{1}{2}\frac{1}{2}}(Q^2) \tag{5.3.23}$$

$$G_M(Q^2) = \frac{2M}{Q} F^{\mu=1}_{\frac{1}{2}\frac{-1}{2}}(Q^2) \tag{5.3.24}$$

In the case of spin 3/2 baryons (i.e. Δ and Ω), the Sachs form factors are given by

$$G_E(Q^2) = \frac{1}{2}\left(F^{\mu=0}_{\frac{1}{2}\frac{1}{2}}(Q^2) + F^{\mu=0}_{\frac{3}{2}\frac{3}{2}}(Q^2)\right) \tag{5.3.25}$$

$$G_M(Q^2) = \frac{6M}{5Q}\left(F^{\mu=1}_{\frac{1}{2}\frac{-1}{2}}(Q^2) + \sqrt{3}F^{\mu=1}_{\frac{3}{2}\frac{1}{2}}(Q^2)\right). \tag{5.3.26}$$

5.3.2 Axial Form Factor

In the case of the axial form factor at the baryonic level we have

$$\langle V_f, M, J = \frac{1}{2}, \Sigma' | A^\mu_a(0) | V_i, M, J = \frac{1}{2}, \Sigma\rangle = \bar{u}(P_f, \Sigma')\left[g_A \gamma^\mu \gamma_5 \frac{\tau_a}{2}\right] u(P_i, \Sigma)\,. \tag{5.3.27}$$

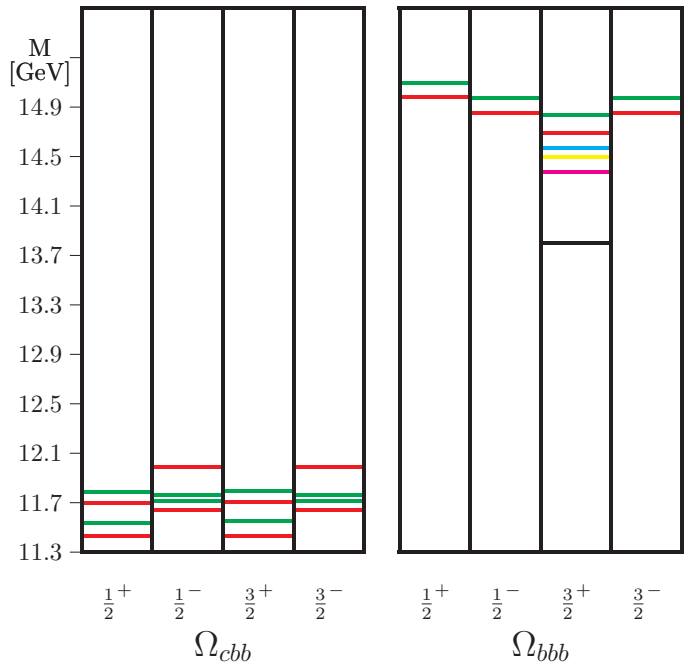

Figure 5.12: Mostly-charm baryons. The prediction of the URCQM is shown by the red lines. The green line shows the theoretical value from Roberts and Pervin [89]. The light blue line shows the theoretical value from Martynenko [91]. The magenta line is the result of the Meinel [92]. The yellow line is Llanes-Estrada, *et al.* [94]. The black line is Sanchis-Alepuz, *et al.* [93]

At the quark level in the point form spectator model we have the matrix element of the axial current operator $\hat{A}^\mu_a$ between (free) three-particle states $|k_1, k_2, k_3; \sigma_1, \sigma_2, \sigma_3\rangle$. We assume the form

$$\begin{aligned}\langle k_1, k_2, k_3; \sigma_1', \sigma_2', \sigma_3' \big| \hat{A}^\mu_a |k_1, k_2, k_3; \sigma_1, \sigma_2, \sigma_3\rangle = \\ 3 \langle k_1, \sigma_1' \big| \hat{A}^\mu_{a,\mathrm{SM}} |k_1, \sigma_1\rangle 2\omega_2 2\omega_3 \delta_{\sigma_2\sigma_2'} \delta_{\sigma_3\sigma_3'} .\end{aligned} \tag{5.3.28}$$

In the situation where quark 1 is the active point like quark, and quarks 2 and 3 are the spectators we have the form

$$\langle k_1, \sigma_1' \big| \hat{A}^\mu_{a,\mathrm{SM}} |k_1, \sigma_1\rangle = \bar{u}(k_1, \sigma_1') g_A^q \gamma^\mu \gamma_5 \frac{\tau_a}{2} u(k_1, \sigma_1) , \tag{5.3.29}$$

where $u(k_1, \sigma_1)$ is the usual quark spinor and $g_A^q = 1$ the quark axial charge. Detailed calculation can be found in the literature [23, 96, 97].

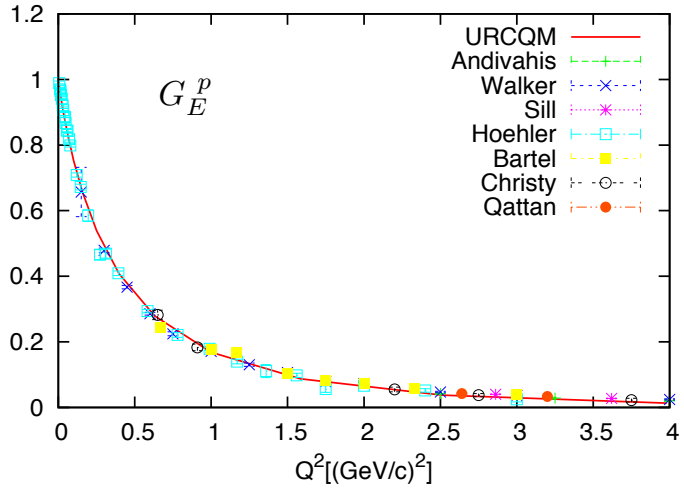

Figure 5.13: URCQM prediction for the proton electric form factor in the point-form spectator model (PFSM). Experimental data with error bars are also given for comparison.

5.3.3 Electric Radii Squared

The electric radii squared is defined as

$$r_{ch}^2 \equiv -\frac{6}{G_E(0)} \frac{dG_E(Q^2)}{d(Q^2)}\Big|_{Q^2=0} \tag{5.3.30}$$

5.3.4 Magnetic Moments

The magnetic moment is defined as

$$G_M(Q^2 = 0) \tag{5.3.31}$$

We see that the URCQM compares well with experiment and previous work in the RCQM [98].

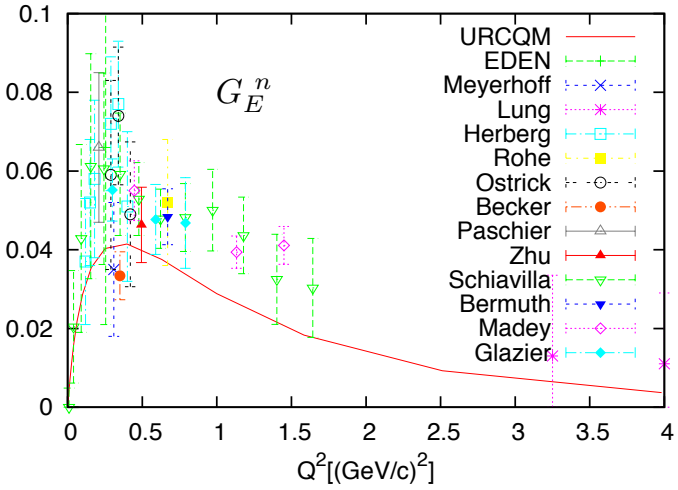

Figure 5.14: URCQM prediction for the neutron electric form factor in the PFSM. Experimental data with error bars are also given for comparison.

5.4 Gravitational Form Factor

In the same way that the well known Pauli and Dirac electric form factors tell us about the electric structure of particles, the gravitational form factor tells us about the matter distributions within hadrons. Experimentally to probe a particle in this way would require one to perform scattering experiments using a massless spin-2 particle (graviton) as a probe. Currently this lies outside the reach of experimental capabilities, however this has not been an obstacle to the theoretical community. Several different approaches have been taken toward this problem, generalized parton distributions (GPD's) [99], holographic QCD (AdS/QCD) [100–104], chiral quark models [105], light cone representations [104, 106], heavy baryon chiral perturbation theory [107], and lattice QCD [108] to name only a few. Within these approaches we see a long history of investigation of both bosonic and fermionic matter distributions. In this work we present a calculation of a gravitational form factor in a Poincaré invariant constituent quark model within the point form spectator model approximation (PFSM).

The point form is characterized by the fact that only the four-momentum operator $\hat{P}^\mu$ is affected by interactions. All other generators of the Poincaré group remain interaction-free. As a result the spatial rotations and, most importantly, the Lorentz boosts are purely

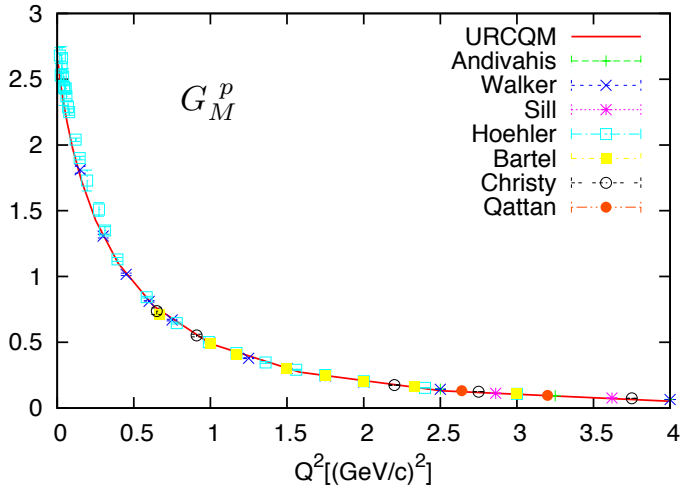

Figure 5.15: URCQM prediction for the proton magnetic form factor in the PFSM. Experimental data with error bars are also given for comparison.

kinematic. Consequently, the theory is manifestly covariant. The $\{QQQ\}$ Hilbert space $\mathcal{H}$ is spanned by the free states

$$|p_1,\sigma_1;p_2,\sigma_2;p_3,\sigma_3\rangle = |p_1,\sigma_1\rangle \otimes |p_2,\sigma_2\rangle \otimes |p_3,\sigma_3\rangle\,, \tag{5.4.32}$$

which are direct products of free single-particle states $|p_i,\sigma_i\rangle$, with p_i and σ_i denoting the individual (free) four-momenta and spin projections, respectively. In point form, instead of working with the usual three-body states in Eq. (5.4.32), one introduces so-called velocity states. They can be constructed by applying a specific Lorentz boost $B(v)$ to the free three-body states $|k_1,\mu_1;k_2,\mu_2;k_3,\mu_3\rangle$ in the centre-of-momentum frame (for which $\sum_i \vec{k}_i = 0$):

$$\begin{aligned} |v;\vec{k}_1,\mu_1;\vec{k}_2,\mu_2;\vec{k}_3,\mu_3\rangle &= U_{B(v)}|k_1,\mu_1;k_2,\mu_2;k_3,\mu_3\rangle \\ &= \prod_{i=1}^{3}\sum_{\sigma_i} D^{\frac{1}{2}}_{\sigma_i\mu_i}[R_W(k_i,B(v))]|p_1,\sigma_1;p_2,\sigma_2;p_3,\sigma_3\rangle\,. \end{aligned} \tag{5.4.33}$$

These velocity states also span the whole Hilbert space $\mathcal{H}$. They have the important advantage that under general Lorentz transformations the occurring Wigner D-functions are the same for all three particles and the individual momenta are all rotated by the same amount (what is not the case for the three-particle states of Eq. (5.4.32)). Of course, the practical calculations are facilitated a lot by expressing the baryon mass eigenstates $|\Psi_B\rangle$

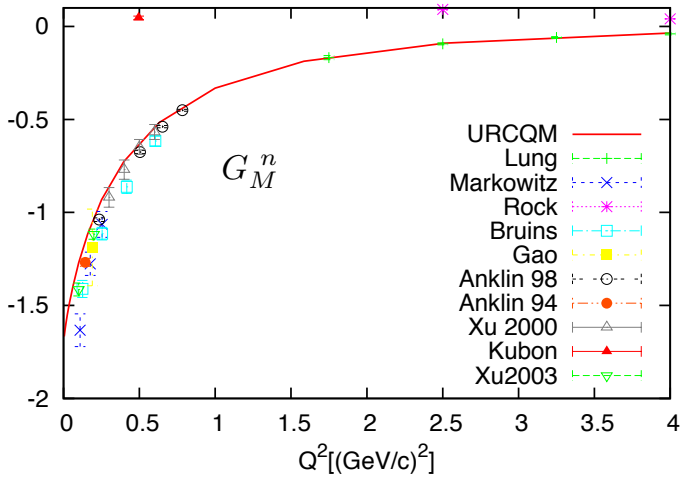

Figure 5.16: URCQM prediction for the neutron magnetic form factor in the PFSM. Experimental data with error bars are also given for comparison.

in the velocity-state representation

$$\langle v; \vec{k}_1, \mu_1; \vec{k}_2, \mu_2; \vec{k}_3, \mu_3 | v_B, M_B, J, \Sigma \rangle \sim \delta^3(\vec{v} - \vec{v}_B) \Psi_{M_B J \Sigma}(\vec{k}_1, \mu_1; \vec{k}_2, \mu_2; \vec{k}_3, \mu_3) \,, \qquad (5.4.34)$$

where $\vec{v}$ and $\vec{v}_B$ are the total three-velocities of the bra and ket states, respectively.

5.4.1 Point Form Spectator Model

Here we outline the spectator model construction. The general translational-invariant amplitude between certain incoming and outgoing baryon states, $|V, M, J, \Sigma\rangle$ and $\langle V', M', J', \Sigma'|$, is given by

$$\langle V', M', J', \Sigma' | \hat{O} | V, M, J, \Sigma \rangle = \qquad (5.4.35)$$
$$= \langle V', M', J', \Sigma' | \hat{O}_{\mathrm{rd}} | V, M, J, \Sigma \rangle \, 2MV_0 \delta^3 \left(M\vec{V} - M'\vec{V}' - \vec{Q} \right) ,$$

where $\hat{O}$ represents any electromagnetic, weak, or hadronic operator, and $\hat{O}_{\mathrm{rd}}$ is its reduced part. The baryon states are eigenstates of the four-velocity operator $\hat{V}$, the interacting mass operator $\hat{M}$, the (total) spin operator $\hat{J}$, and its z-component $\hat{\Sigma}$ (the corresponding letters without a hat denoting their eigenvalues). The factor in front of the δ-function is the invariant measure ensuring the correct normalization and transformation properties of the states. The δ-function itself expresses the overall momentum conservation of the transition amplitude under the four-momentum transfer $Q^\mu = P^\mu - P'^\mu$ (for on-shell particles).

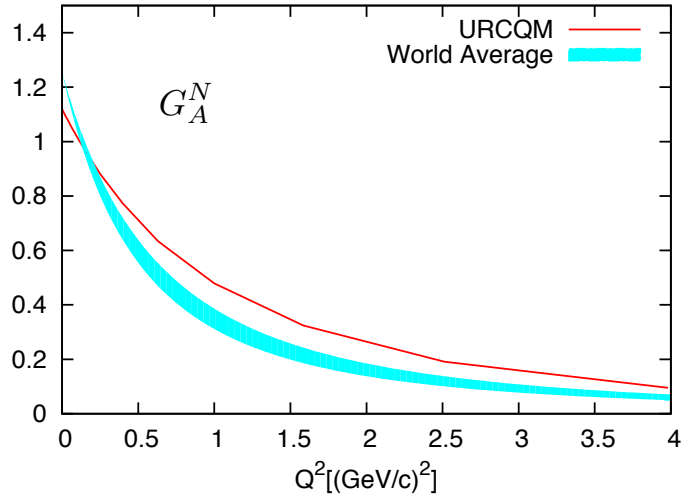

Figure 5.17: URCQM prediction for the axial form factor in PFSM. We compare with the world average using a dipole fit.

With the appropriate basis representations of the baryon eigenstates and inclusion of the necessary Lorentz transformations the expression for the transition amplitude becomes

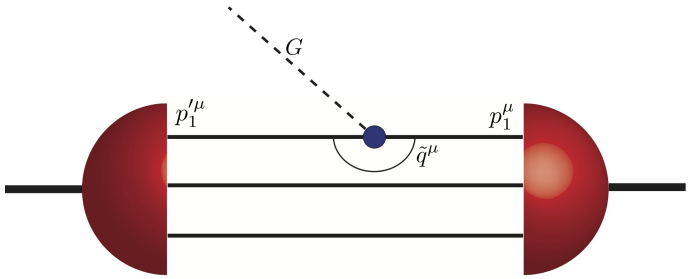

Figure 5.18: Here we see the graviton coupling with a quark inside the nucleon in the point form spectator model

$$\langle V', M', J', \Sigma' | \hat{O} | V, M, J, \Sigma \rangle = \frac{2}{MM'} \sum_{\sigma_i \sigma_i'} \sum_{\mu_i \mu_i'} \int d^3\vec{k}_2 d^3\vec{k}_3 d^3\vec{k}_2' d^3\vec{k}_3'$$
$$\sqrt{\frac{(\omega_1 + \omega_2 + \omega_3)^3}{2\omega_1 2\omega_2 2\omega_3}} \sqrt{\frac{\left(\omega_1' + \omega_2' + \omega_3'\right)^3}{2\omega_1' 2\omega_2' 2\omega_3'}} \Psi^{\star}_{M' J' \Sigma'} \left(\vec{k}_1', \vec{k}_2', \vec{k}_3'; \mu_1', \mu_2', \mu_3'\right)$$
$$\prod_{\sigma_i'} D^{\star \frac{1}{2}}_{\sigma_i' \mu_i'} \left\{R_W \left[k_i'; B\left(V'\right)\right]\right\} \left\langle p_1', p_2', p_3'; \sigma_1', \sigma_2', \sigma_3' \right| \hat{O}_{\mathrm{rd}} \left| p_1, p_2, p_3; \sigma_1, \sigma_2, \sigma_3 \right\rangle$$
$$\prod_{\sigma_i} D^{\frac{1}{2}}_{\sigma_i \mu_i} \left\{R_W \left[k_i; B\left(V\right)\right]\right\} \Psi_{MJ\Sigma} \left(\vec{k}_1, \vec{k}_2, \vec{k}_3; \mu_1, \mu_2, \mu_3\right)$$
$$2MV_0 \delta^3 \left(M\vec{V} - M'\vec{V}' - \vec{Q}\right) . \tag{5.4.36}$$

The integral measures stem from the completeness relation of the velocity states (see Eq. (5.4.34)), where the integrations over the velocities have already been performed exploiting the δ-functions in the velocity-state representations of the baryon states. In this formula the individual quark momenta $\vec{k}_i$ (and similarly $\vec{k}_i'$) are restricted by the rest-frame condition $\sum_i \vec{k}_i = \vec{0}$. The Wigner rotations stem from the Lorentz transformations to the boosted incoming and outgoing states, which have nonzero total momenta $\vec{P} = M\vec{V}$ and $\vec{P}' = M'\vec{V}'$, respectively. The wave functions $\Psi^{\star}_{M' J' \Sigma'}$ and $\Psi_{MJ\Sigma}$ denote the (rest-frame) velocity-state representations of the baryon states. The reduced operator $\hat{O}_{\mathrm{rd}}$ remains sandwiched between the free three-quark states. The spectator-model approximation of the current operator in point form (the PFSM) is defined by the expression Here the momentum transfer to the struck quark is given by

$$p_1^{\mu} - p'^{\mu}_1 = \tilde{q}^{\mu} , \tag{5.4.37}$$

where $\tilde{q}^{\mu} \neq Q^{\mu}$ is uniquely determined by the overall momentum conservation and the two spectator conditions. The relation between p_1 and p_1' is complicated, because the transferred momentum $\tilde{q}$ to the active quark inherits nontrivial interaction-dependent contributions [114]. Writing the Belinfante energy momentum tensor matrix element in its most general form for a spin 1/2 particle [115] we have

$$\langle N(p') | \Theta^{\mu\nu}(0) | N(p) \rangle =$$
$$= \bar{u}(p') \left[\gamma^{(\mu} \bar{P}^{\nu)} A(Q^2) + \tfrac{i}{2M} \bar{P}^{(\mu} \sigma^{\nu)} B(Q^2) + \tfrac{q^{\mu} q^{\nu} - q^2 g^{\mu\nu}}{M} C(Q^2) \right] u(p) . \tag{5.4.38}$$

where $q^\mu = (P' - P)^\mu$, $\bar{P}^\mu = \frac{1}{2}(P' + P)^\mu$, $a^{(\mu}b^{\nu)} = \frac{1}{2}(a^\mu b^\nu + a^\nu b^\mu)$, and $u(p)$ is the spinor of the nucleon system. For the nucleon gravitational form factor we insert

$$\langle p'_1, \sigma'_1; p'_2, \sigma'_2; p'_3, \sigma'_3 | \Theta^{\mu\nu}(0) | p_1, \sigma_1; p_2, \sigma_2; p_3, \sigma_3 \rangle = \tag{5.4.39}$$
$$= 3\mathcal{N} \langle p'_1, \sigma'_1 | \Theta^{\mu\nu}_{\text{spec}}(0) | p_1, \sigma_1 \rangle 2E_2 \delta^3(\vec{p}_2 - \vec{p}'_2) 2E_3 \delta^3(\vec{p}_3 - \vec{p}'_3) \delta_{\sigma_2\sigma'_2} \delta_{\sigma_3\sigma'_3}$$

into Eq. (5.4.36). It has been shown previously that $B(Q^2)$ can be interpreted as the anomalous gravitomagnetic moment [118] and must vanish due to the Einstein equivalence principle. The $C(Q^2)$ term also drops out [117]. We are left with the task of calculating $A(Q^2)$. The energy momentum tensor matrix elements in the point form spectator model reduce to

$$A(q^2) = \langle p'_1, \sigma'_1 | \Theta^{00}_{\text{spec}}(0) | p_1, \sigma_1 \rangle \tag{5.4.40}$$

To get this element we start with

$$\left\langle p'_1, p'_2, p'_3; \sigma'_1, \sigma'_2, \sigma'_3 \right| \hat{\Theta}^{\mu\nu}_{\text{rd,PFSM}} \left| p_1, p_2, p_3; \sigma_1, \sigma_2, \sigma_3 \right\rangle = \tag{5.4.41}$$
$$= 3\mathcal{N} \bar{u}\left(p'_1, \sigma'_1\right) \gamma^{(\mu} \bar{P}^{\nu)} u\left(p_1, \sigma_1\right) 2p_{20} \delta^3\left(\vec{p}_2 - \vec{p}'_2\right) 2p_{30} \delta^3\left(\vec{p}_3 - \vec{p}'_3\right) \delta_{\sigma_2\sigma'_2} \delta_{\sigma_3\sigma'_3} .$$

Looking explicitly at the Θ^{00} element at the quark level we have:

$$\langle p'_1, \sigma'_1 | \Theta^{00}_{\text{spec}}(0) | p_1, \sigma_1 \rangle = \tag{5.4.42}$$
$$= \bar{u}(p'_1, \sigma'_1) \left(\frac{\gamma^0 P'^0 + \gamma^0 P^0}{2} \right) u(p_1, \sigma_1) = \left(\frac{E'_1 + E_1}{2} \right) \bar{u}(p'_1, \sigma'_1) \gamma^0 u(p_1, \sigma_1)$$

We insert this relation into Eq. 5.4.36 to get our $A(Q^2)$ on the nucleon level.

5.5 Results

Our result for $A(Q^2)$ is plotted in Fig. 5.19. In physics comparison with experiment is always the preeminent goal however, as stated in the introduction at the present moment there is no experimental data to compare with for this quantity. Instead we compare with other theoretical groups. We compare with a holographic soft wall model [100]. In addition we compare with a gravitationally coupled Pomeron model [103] parameterized from cross section data of pp and $p\bar{p}$ scattering from the CDF $\sqrt{s} = 1800$ GeV data set.

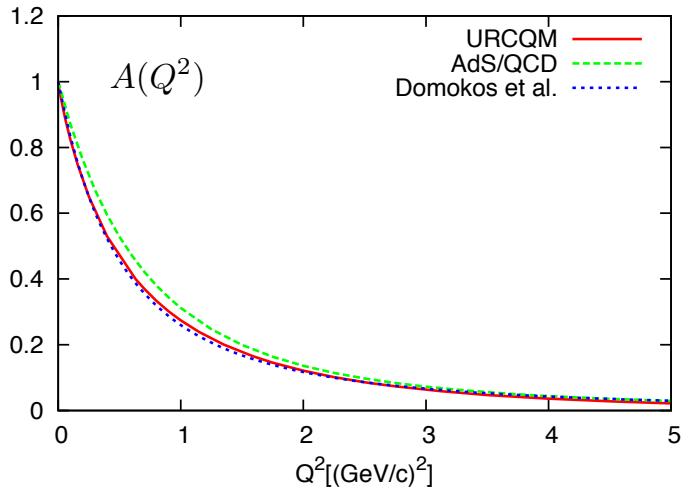

Figure 5.19: PFSM model result (URCQM) for the nucleon gravitational form factor $A(Q^2)$ compared to a holographic (AdS/QCD) model [100] and a parameterization of a gravitationally coupled Pomeron model (Domokos *et al.*) [103].

Baryon	J^P	URCQM	GBE	Experiment
N(939)	$\frac{1}{2}^+$	939	939	938-940
N(1440)	$\frac{1}{2}^+$	1454	1459	1420-1470
N(1520)	$\frac{3}{2}^-$	1558	1519	1515-1525
N(1535)	$\frac{1}{2}^-$	1558	1519	1525-1545
N(1650)	$\frac{1}{2}^-$	1666	1647	1645-1670
N(1675)	$\frac{5}{2}^-$	1666	1647	1670-1680
N(1700)	$\frac{3}{2}^-$	1666	1647	1650-1750
N(1710)	$\frac{1}{2}^+$	1804	1776	1680-1740
Δ(1232)	$\frac{3}{2}^+$	1234	1240	1231-1233
Δ(1600)	$\frac{3}{2}^+$	1710	1718	1550-1700
Δ(1620)	$\frac{1}{2}^-$	1675	1642	1600-1660
Δ(1700)	$\frac{3}{2}^-$	1675	1642	1670-1750
Λ(1116)	$\frac{1}{2}^+$	1141	1136	1116
Λ(1405)	$\frac{1}{2}^-$	1589	1556	1401-1410
Λ(1520)	$\frac{3}{2}^-$	1589	1556	1519-1521
Λ(1600)	$\frac{1}{2}^+$	1650	1625	1560-1700
Λ(1670)	$\frac{1}{2}^-$	1702	1682	1660-1680
Λ(1690)	$\frac{3}{2}^-$	1702	1682	1685-1695
Λ(1800)	$\frac{1}{2}^-$	1787	1778	1720-1850
Λ(1810)	$\frac{1}{2}^+$	1837	1799	1750-1850
Λ(1830)	$\frac{5}{2}^-$	1787	1778	1810-1830
Σ(1193)	$\frac{1}{2}^+$	1210	1180	1189-1197
Σ(1385)	$\frac{3}{2}^+$	1374	1389	1383-1387
Σ[1560]	$\frac{1}{2}^-$	1695	1677	1546-1576
Σ[1620]	$\frac{1}{2}^-$	1745	1736	1594-1643
Σ(1660)	$\frac{1}{2}^+$	1711	1616	1630-1690
Σ(1670)	$\frac{3}{2}^-$	1695	1677	1665-1685
Σ[1690]	$\frac{3}{2}^+$	1892	1865	1670-1727
Σ(1750)	$\frac{1}{2}^-$	1776	1759	1730-1800
Σ(1775)	$\frac{5}{2}^-$	1745	1736	1770-1780
Σ(1880)	$\frac{1}{2}^+$	1950	1911	1806-2025
Σ[1940]	$\frac{3}{2}^-$	1745	1736	1900-1950
Σ	$\frac{3}{2}^-$	1776	1759	-
Ξ(1318)	$\frac{1}{2}^+$	1342	1348	1315-1321
Ξ(1530)	$\frac{3}{2}^+$	1501	1528	1532-1535
Ξ[1690]	$\frac{1}{2}^+$	1842	1805	1680-1700
Ξ(1820)	$\frac{3}{2}^-$	1805	1792	1818-1828
Ξ[1950]	$\frac{5}{2}^-$	1865	1881	1935-1965
Ω	$\frac{3}{2}^+$	1620	1656	1673.45±0.29

Table 5.3: Light and strange spectra for URCQM and GBE hyperfine interactions calculated via SVM. All values are given in MeV.

Baryon	J^P	URCQM	Experiment
Λ_c	$\frac{1}{2}^+$	2308	2286.46±0.14
$\Lambda_c(2595)$	$\frac{1}{2}^-$	2604	2592.25±0.28
$\Lambda_c(2625)$	$\frac{3}{2}^-$	2604	2628.11±0.19
Λ_c	$\frac{1}{2}^+$	2750	-
Λ_c	$\frac{3}{2}^+$	2834	-
$\Lambda_c(2880)$	$\frac{5}{2}^+$	2834	2881.53±0.35
$\Lambda_c(2940)$	$\frac{1}{2}^+$	2943	2938-2941♥
$\Sigma_c(2455)$	$\frac{1}{2}^+$	2447	2452-2455
$\Sigma_c(2520)$	$\frac{3}{2}^+$	2489	2517-2519
$\Sigma_c(2800)$	$\frac{1}{2}^-$	2756	2787-2811♥
$\Sigma_c(2800)$	$\frac{3}{2}^-$	2756	2787-2811♥
Ω_c	$\frac{1}{2}^+$	2703	2694-2697
$\Omega_c(2770)$	$\frac{3}{2}^+$	2732	2764-2768
Ξ_{cc}	$\frac{1}{2}^+$	3673	3519-3520

Table 5.4: Single charm spectra for URCQM. All values are given in MeV. ♥This state is noted in the PDG [65] with J^P assignment $?^?$.

Baryon	J^P	URCQM	Experiment
Λ_b	$\frac{1}{2}^+$	5644	5619.4±0.7
Σ_b	$\frac{1}{2}^+$	5804	5809-5817
Σ_b^*	$\frac{3}{2}^+$	5819	5831-5837
Ω_b	$\frac{1}{2}^+$	6050	6031-6111

Table 5.5: Single bottom spectra for URCQM. All values are given in MeV.

Baryon	J^P	URCQM
Ξ_{cc}	$\frac{1}{2}^+$	3642
Ξ_{cc}	$\frac{3}{2}^+$	3683
Ξ_{cc}	$\frac{1}{2}^-$	3899
Ξ_{cc}	$\frac{3}{2}^-$	3899
Ξ_{cc}	$\frac{1}{2}^-$	4004
Ξ_{cc}	$\frac{3}{2}^-$	4004
Ξ_{cc}	$\frac{1}{2}^+$	4032
Ξ_{cc}	$\frac{3}{2}^+$	4064
Ω_{cc}	$\frac{1}{2}^+$	3753
Ω_{cc}	$\frac{3}{2}^+$	3783
Ω_{cc}	$\frac{1}{2}^-$	4002
Ω_{cc}	$\frac{3}{2}^-$	4002
Ω_{cc}	$\frac{1}{2}^-$	4084
Ω_{cc}	$\frac{3}{2}^-$	4084
Ω_{cc}	$\frac{1}{2}^+$	4141
Ω_{cc}	$\frac{3}{2}^+$	4084
Ξ_{bb}	$\frac{1}{2}^+$	10279
Ξ_{bb}	$\frac{3}{2}^+$	10292
Ξ_{bb}	$\frac{1}{2}^-$	10437
Ξ_{bb}	$\frac{3}{2}^-$	10437
Ξ_{bb}	$\frac{3}{2}^+$	10553
Ξ_{bb}	$\frac{1}{2}^+$	10573
Ξ_{bb}	$\frac{1}{2}^-$	10593
Ξ_{bb}	$\frac{3}{2}^-$	10593
Ω_{bb}	$\frac{1}{2}^+$	10369
Ω_{bb}	$\frac{3}{2}^+$	10378
Ω_{bb}	$\frac{1}{2}^-$	10525
Ω_{bb}	$\frac{3}{2}^-$	10525
Ω_{bb}	$\frac{3}{2}^+$	10641
Ω_{bb}	$\frac{1}{2}^+$	10635
Ω_{bb}	$\frac{1}{2}^-$	10664
Ω_{bb}	$\frac{3}{2}^-$	10664

Table 5.6: Double heavy baryon spectra. Predictions from the URCQM. All values are given in MeV.

Baryon	J^P	URCQM
Ω_{ccc}	$\frac{3}{2}^+$	4876
Ω_{ccc}	$\frac{1}{2}^-$	5106
Ω_{ccc}	$\frac{3}{2}^-$	5106
Ω_{ccc}	$\frac{3}{2}^+$	5248
Ω_{ccc}	$\frac{1}{2}^+$	5291
Ω_{ccc}	$\frac{1}{2}^+$	5293
Ω_{ccc}	$\frac{1}{2}^-$	5440
Ω_{ccc}	$\frac{3}{2}^-$	5440
Ω_{ccb}	$\frac{1}{2}^+$	8160
Ω_{ccb}	$\frac{3}{2}^+$	8163
Ω_{ccb}	$\frac{1}{2}^-$	8344
Ω_{ccb}	$\frac{3}{2}^-$	8344
Ω_{ccb}	$\frac{1}{2}^-$	8393
Ω_{ccb}	$\frac{3}{2}^-$	8393
Ω_{ccb}	$\frac{1}{2}^+$	8478
Ω_{ccb}	$\frac{3}{2}^+$	8480
Ω_{cbb}	$\frac{1}{2}^+$	11429
Ω_{cbb}	$\frac{3}{2}^+$	11432
Ω_{cbb}	$\frac{1}{2}^-$	11644
Ω_{cbb}	$\frac{3}{2}^-$	11644
Ω_{cbb}	$\frac{1}{2}^+$	11700
Ω_{cbb}	$\frac{3}{2}^+$	11702
Ω_{cbb}	$\frac{1}{2}^-$	11985
Ω_{cbb}	$\frac{3}{2}^-$	11985
Ω_{bbb}	$\frac{3}{2}^+$	14692
Ω_{bbb}	$\frac{1}{2}^-$	14851
Ω_{bbb}	$\frac{3}{2}^-$	14851
Ω_{bbb}	$\frac{3}{2}^+$	14961
Ω_{bbb}	$\frac{1}{2}^+$	14984
Ω_{bbb}	$\frac{1}{2}^+$	14987
Ω_{bbb}	$\frac{1}{2}^-$	15095
Ω_{bbb}	$\frac{3}{2}^-$	15095

Table 5.7: Triple heavy baryon spectra. Predictions from the URCQM. All values are given in MeV.

Property	Theory [fm^2]	Experiment [fm^2]
Proton	0.851	0.769(28)
Neutron	-0.127	-0.1161(22)
Σ^-	0.463	0.6084±0.156

Table 5.8: Electric radii squared.

Particle	Theory	Experiment
P	2.694	2.792847356(23)
N	-1.697	-1.9130427(5)
Λ	-0.706	-0.613(4)
Σ^+	2.151	2.458(10)
Σ^-	-0.805	-1.160(25)
Ξ^0	-1.219	-1.250(14)
Ξ^-	-0.629	-0.6507(25)
Δ^+	2.10	$2.7^{+1.0}_{-1.3} \pm 1.5 \pm 3$
Δ^{++}	4.197	3.7-7.5
Ω^-	-1.583	-2.02(5)

Table 5.9: Magnetic moments calculated from the universal model.

Chapter 6

The AdS/QCD Correspondence

6.1 The AdS/CFT Correspondence

There has been a deep historical connection between the pursuit of understanding the physics of strongly coupled systems and string theory. String theory was proposed as an explanation for the Regge trajectory pattern on bound states. This is the noted pattern that when the angular momentum of hadronic excitations J are plotted versus the mass or energy squared they form a pattern of lines. This pattern could be easily explained by representing the mesons for example as two quarks bound together by a string. With the emergence of QCD in the early 70's this stringy explanation was abandoned however the ideas of string theory persisted into a theory of quantum gravity. In 1997 it seems these ideas finally came full circle. When Maldacena first conjectured the correspondence between a geometrical (gravitational) theory in anti-de Sitter space (AdS) and a conformal field theory (CFT) [119] he generated a sensation in the theoretical physics community. The reason for the interest was that the correspondence allowed one to relate a geometrical theory on the boundary of some higher n-dimensional space to a (n-1)-dimensional conformal field theory via the holographic principle [120]. Geometrically anti-de Sitter space corresponds to a maximally symmetric spacetime with a negative cosmological constant. The AdS/CFT duality has the interesting feature that when one side of the correspondence is strongly coupled the other side is weakly coupled and vice versa. A current goal amongst physicists is to extend our understanding of AdS/CFT to a possible dS/CFT. This could be fruitful in several ways. The first is that de Sitter space-time has a

positive cosmological curvature therefore relates with current observations of the observable universe. The second is the double edged sword that a de Sitter spacetime cannot be supersymmetric. This poses the positive possibility that we can do away with supersymmetric theories that so far have not shown their signature in the experimental data. The downside is that without the added symmetry the dS/CFT correspondence is much less well understood. I will briefly review the essentials points of the correspondence here, however, readers interested in a deeper discussion should refer to [121] and references therein.

6.1.1 Dp-Branes

The correspondence is best motivated by studying Dp-brane dynamics [122]. A Dp-brane is a volume of spacetime that exists in p spatial dimensions. For example our usual Minkowski space can be thought of as a D3-brane, (3+1) dimensions living a higher ten-dimensional spacetime. In string theory D-brane's are objects in ten-dimensional spacetime where strings can end. The low energy excitations of a D-Brane can be described by a $\mathcal{N} = 4$ supersymmetric $U(1)$ gauge theory. Extending this one can "stack" up N D-branes to make a supersymmetric $U(N)$ gauge theory. This theory can be decoupled into $U(N) = SU(N) \times U(1)$, where the $U(1)$ part corresponds to the center of mass motion of the stack of branes. Given what we know about the standard model one can already see the significance of this type of non-abelian group structure.[‡] We can write down the action for a D3-brane

$$S = \int d^{10}x \tag{6.1.1}$$

we can vary the action to get the metric

$$ds^2_{10} = H^{-1/2}\eta^{\mu\nu}dx_\mu dx_\nu + H^{1/2}(dr^2 + r^2 d\Omega^2_5) \tag{6.1.2}$$

where

$$H = 1 + \frac{R^4}{r^4}\,. \tag{6.1.3}$$

R is the radius of the throat and r is the radius of the circle surrounding the throat as shown in Fig. 6.1. Here $d\Omega_5$ is the five-sphere metric. We see that when $r >> R$ then $H \simeq 1$

[‡]Although it must be stressed that to our current knowledge the standard model is *not* supersymmetric!

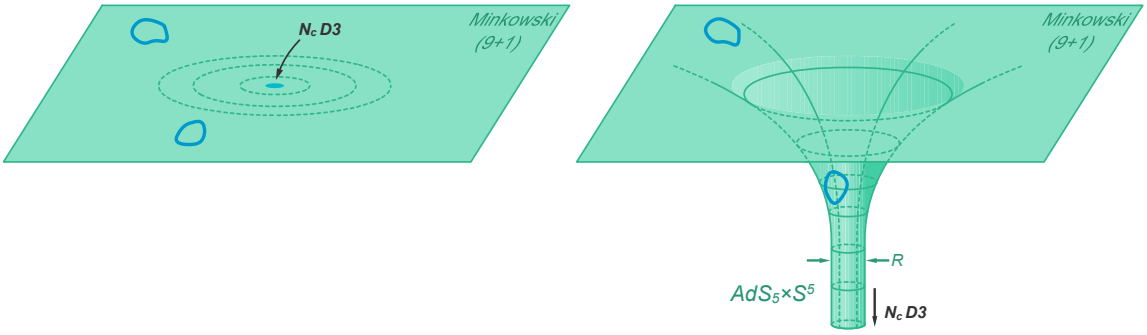

Figure 6.1: Flat spacetime on the left. On the right spacetime is deformed by a stack of D3-branes. Figure taken from [123]

the spacetime is basically flat. In the near horizon limit when $R^4/r^4 >> 1$ gravitational effects become strong and our metric is

$$ds^2 = \frac{r^4}{R^4}\eta^{\mu\nu}dx_\mu dx_\nu + \frac{R^4}{r^4}(dr^2 + r^2 d\Omega_5^2) \tag{6.1.4}$$

we can make a change of variable, $z = R^2/r$ so our metric becomes

$$ds^2 = \frac{R^2}{z^2}(\eta^{\mu\nu}dx_\mu dx_\nu + dz^2) + R^2 d\Omega_5^2 \tag{6.1.5}$$

We can now see transparently that the metric is $AdS_5 \times S^5$.

$$\underbrace{\frac{R^2}{z^2}(\eta^{\mu\nu}dx_\mu dx_\nu + dz^2)}_{AdS_5} + \underbrace{R^2 d\Omega_5^2}_{S^5} \tag{6.1.6}$$

6.1.2 Holography

The holographic principle has origins in Bekenstein and Hawkings' analysis of black hole thermodynamics [120]. This first work showed that one can encode the degrees of freedom within the volume of a black hole simply by understanding its area.

The holographic principle in the context of the AdS/CFT correspondence allows us to encode the physics from the $(d+1)$-dimensional bulk theory into a d-dimensional gauge theory. It seems clear that the d-dimensional x^μ coordinates for a point within the bulk correspond to the x^μ position within the gauge theory. However, it is less clear how the radial r or z component is encoded into the field theory.

One approach is to define your gauge theory as is done in most "real" quantum field theories, as a function of an energy scale. In a conformal field theory the resulting effective field theory will be independent of E but in a non-conformal theory such as QCD

this result is a useful tool. If we consider a scale transformation $x^\mu \to \lambda x^\mu$, where λ is a generic scale factor, we can also rescale the energy via $E \to E/\lambda$. In addition this scale transformation can be performed in the AdS metric (6.1.5), telling us that when $x^\mu \to \lambda x^\mu$ we also must have $z \to z/\lambda$ as a symmetry of the metric. Thus we can now relate both z and r from the bulk theory to an energy scale in the gauge theory

$$E \sim \frac{1}{z} \sim r \,. \tag{6.1.7}$$

One now gets a better understanding as to how the holographic coordinates z and r in the bulk are related to degrees of freedom in the dual gauge theory. For example if one wishes to propose a theory without any degrees of freedom integrated out then this corresponds to the limit where $E \to \infty$. We see from the relation in Eq. (6.1.7) that this implies as $z \to 0$ then $r \to \infty$. As you integrate out higher-momentum degrees of freedom the dual gauge theory gets projected inwards towards the horizon.

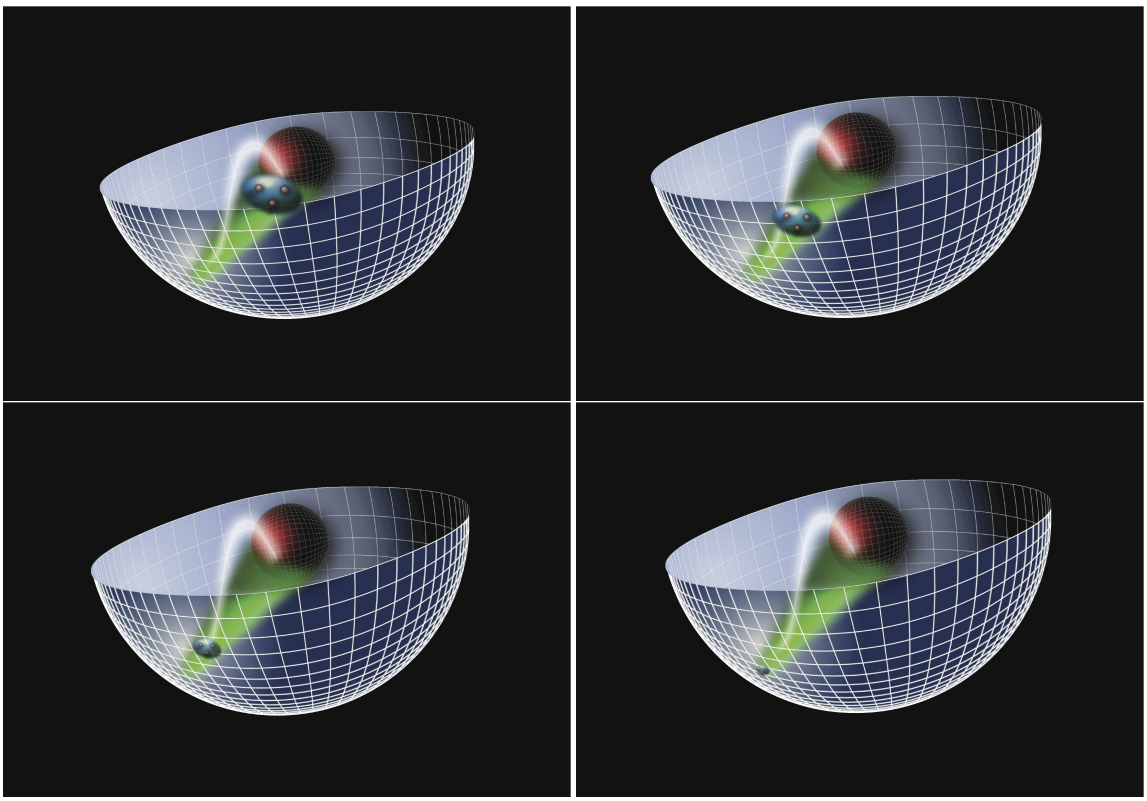

Figure 6.2: Holographic projection of the gauge theory via the holographic coordinate z.

Why does holography give us (3+1) not (9+1)?

One important point is that naively one may ask why, when speaking of the ten-dimesional spacetime $AdS_5 \times S^5$, does one get a (3+1)-dimensional theory on the boundary instead of a (9+1)-dimensional one as one would expect from a 10-dimensional bulk? Here it is important to note that one can Weyl rescale the metric in Eq. (6.1.6) as so

$$\underbrace{R^2(\eta^{\mu\nu}dx_\mu dx_\nu + dz^2)}_{AdS_5} + \underbrace{z^2R^2d\Omega_5^2}_{S^5} \ . \tag{6.1.8}$$

This makes clear that at the boundary when $z = 0$, that the five-sphere disappears leaving only AdS_5 to contribute to when the holographic principle is applied, allowing us to go from a 5-dimensional theory in the bulk, to a 4-dimensional theory on the boundary.

6.2 AdS/QCD

We know that QCD in the usual sense is not a conformal field theory. The next section explains the attempt to go from AdS/CFT to AdS/QCD. It should be stated up front that although it is often argued in the literature that holographic QCD is dual to ”real” QCD, we will take a more conservative approach; in the sense that what is presented in the following sections, is what should be understood as a model that captures many of the features that we know exist in real QCD, for example confinement and chiral symmetry.

The two most obvious differences between ”real” QCD and the $\mathcal{N} = 4$ super Yang-Mills theory that is the result of the usual type IIB $AdS_5 \times S^5$ correspondence, is that at our present level of understanding, QCD is neither conformal nor supersymmetric. The problem of breaking the supersymmetry was resolved first by Witten [124], in which he was able to show a description of large N_c gauge theories in four dimensions without supersymmetry. The next task is to break the conformal symmetry. This is done in a number of ways.

First one should note there are essentially two different approaches to AdS/QCD. The first is what is commonly called the ”top-down” approach. This approach uses string theory as the general motivation and starting point. From the string side one tries to build a theory that resembles some holographic dual to QCD. An example of one of the most

popular top-down models is the Sakai-Sugimoto model [125, 126]. This model relies on the embedding of D8 and anti-D8-branes into a D4 background. By playing around with different geometries one can break not only the conformal symmetry but also create behavior that mimics chiral symmetry breaking. Due to these features Sakai and Sugimoto were able to produce spectra and form factors for both baryons and mesons [127, 128].

The other type of approach, and the one that we are most interested in in this thesis, is what is known as the "bottom-up" approach. This approach is motivated by QCD and simply uses the gauge/gravity correspondence as a way to gain insight into the strong coupling regime. We look specifically at the bottom-up model known as light-front holography.

6.2.1 QCD on the Light Cone

Let's begin by looking at the $SU(3)_C$ Lagrangian of QCD[‡]

$$\mathcal{L}_{\text{QCD}} = \sum_n \bar{\psi}_n \left(i\gamma^\mu D_\mu - m_n \right) \psi_n - \tfrac{1}{4} G^a_{\mu\nu} G^{a\,\mu\nu}. \tag{6.2.9}$$

summed over n flavors, the covariant derivative is defined as $D_\mu = \partial_\mu - ig_s A^a_\mu T^a$ and $G^a_{\mu\nu} = \partial_\mu A^a_\nu - \partial_\nu A^a_\mu + g_s c^{abc} A^b_\mu A^c_\nu$ is the gluon field strength tensor. $\left[T^a, T^b\right] = ic^{abc}T^c$ where a, b, c are $SU(3)_C$ color indices.

A review of light-cone notation can be found in Appendix D.2. We can express the hadron four-momentum generator $P = (P^+, P^-, P_\perp)$, $P^\pm = P^0 \pm P^3$, in terms of the dynamical fields, the Dirac field ψ_+ (where $\psi_\pm = \Lambda_\pm \psi$, $\Lambda_\pm = \gamma^0\gamma^\pm$), and the transverse field $A_\perp$. Specifically we will work in light-cone gauge where $A^+ = 0$, quantized on the light front at fixed light-cone time, x^+.

$$P^- = \int dx^- d^2x_\perp \bar{\psi}_+ \gamma^+ \frac{(i\nabla_\perp)^2 + m^2}{i\partial^+} \psi_+ + (\text{interactions}), \tag{6.2.10}$$

$$P^+ = \int dx^- d^2x_\perp \bar{\psi}_+ \gamma^+ i\partial^+ \psi_+, \tag{6.2.11}$$

$$P_\perp = \int dx^- d^2x_\perp \bar{\psi}_+ \gamma^+ i\nabla_\perp \psi_+, \tag{6.2.12}$$

A physical hadron in 3+1 dimensional Minkowski space with four-momentum P_μ

[‡]This is Eq. (1.1.1) reproduced here for convenience.

and invariant hadronic mass states $P_\mu P^\mu = \mathcal{M}^2$ is determined by the Lorentz-invariant Hamiltonian equation for the relativistic bound-state system

$$H_{LF}|\psi(P)\rangle = \mathcal{M}^2|\psi(P)\rangle, \tag{6.2.13}$$

where $H_{LF} \equiv P_\mu P^\mu = P^- P^+ - P_\perp^2$. The hadronic state $|\psi\rangle$ is an expansion in multiparticle Fock eigenstates $|n\rangle$ of the free light-front Hamiltonian, $|\psi\rangle = \sum_n \psi_n|\psi\rangle$. The Fock components $\psi_n(x_i, \mathbf{k}_{\perp i}, \lambda_i)$ are independent of P^+ and $P_\perp$ and depend only on the momentum fraction $x_i = k_i^+/P^+$, the transverse momentum $\mathbf{k}_{\perp i}$ and spin component λ_i^z. To ensure conservation of momentum we require that, $\sum_{i=1}^n x_i = 1$ and $\sum_{i=1}^n \mathbf{k}_{\perp i} = 0$.

As first shown by Brodsky and de Teramond [17], it is possible to derive so-called light-front holography, using a first semiclassical approximation to transform the fixed light-front time bound-state Hamiltonian equation of motion in QCD (6.2.13), to a corresponding wave equation in AdS space. We expand the initial and final hadronic states in terms of its Fock components. We may simplify the calculation by choosing the frame $P = (P^+, \mathcal{M}^2/P^+, \vec{0}_\perp)$ where $P^2 = P^+P^-$. This results in

$$\mathcal{M}^2 = \sum_n \int [dx_i]\left[d^2k_{\perp i}\right] \sum_q \left(\frac{k_{\perp q}^2 + m_q^2}{x_q}\right) |\psi_n(x_i, k_{\perp i})|^2 + (\text{interactions}), \tag{6.2.14}$$

plus similar terms for antiquarks and gluons ($m_g = 0$). The integrals in (6.2.14) are over the internal coordinates of the n constituents for each Fock state

$$\int [dx_i] \equiv \prod_{i=1}^n \int dx_i\, \delta\Big(1 - \sum_{j=1}^n x_j\Big), \quad \int \left[d^2k_{\perp i}\right] \equiv \prod_{i=1}^n \int \frac{d^2k_{\perp i}}{2(2\pi)^3}\, 16\pi^3\, \delta^{(2)}\Big(\sum_{j=1}^n k_{\perp j}\Big), \tag{6.2.15}$$

with phase space normalization

$$\sum_n \int [dx_i] \left[d^2k_{\perp i}\right] |\psi_n(x_i, k_{\perp i})|^2 = 1. \tag{6.2.16}$$

Each constituent of the light-front wavefunction (LFWF) $\psi_n(x_i, k_{\perp i}, \lambda_i)$ of a hadron is on its respective mass shell $k_i^2 = k_i^+ k_i^- - k_{\perp i}^2 = m_i^2$, $i = 1, 2 \cdots n$. Therefore,

$$k_i^- = \left(k_{\perp i}^2 + m_i^2\right)/x_i P^+ \,. \tag{6.2.17}$$

However, it is important to note that the LFWF represents a state which is off the light-front energy shell

$$P^- - \sum_i^n k_i^- < 0\,, \tag{6.2.18}$$

for a stable hadron. The invariant mass of the constituents $\mathcal{M}_n$ is

$$\mathcal{M}_n^2 = \Big(\sum_{i=1}^n k_i^\mu\Big)^2 = \sum_i \frac{k_{\perp i}^2 + m_i^2}{x_i}. \tag{6.2.19}$$

The LFWF, $\psi_n(x_i, \mathbf{k}_{\perp i}, \lambda_i)$ can be expanded in terms of $n-1$ independent position coordinates $\mathbf{b}_{\perp j}$, $j = 1, 2, \ldots, n-1$, conjugate to the relative coordinates $k_{\perp i}$, where the sum over position coordinates, $\sum_{i=1}^n b_{\perp i} = 0$. Alternatively we may express Eq. (6.2.14) in terms of the internal impact coordinates $b_{\perp j}$;

$$\mathcal{M}^2 = \sum_n \prod_{j=1}^{n-1} \int dx_j\, d^2b_{\perp j}\, \psi_n^*(x_j, b_{\perp j}) \sum_q \left(\frac{-\nabla^2_{b_{\perp q}} + m_q^2}{x_q}\right) \psi_n(x_j, b_{\perp j}) + (\text{interactions}). \tag{6.2.20}$$

The normalization is defined by

$$\sum_n \prod_{j=1}^{n-1} \int dx_j d^2\mathbf{b}_{\perp j} \left|\psi_n(x_j, \mathbf{b}_{\perp j})\right|^2 = 1. \tag{6.2.21}$$

To ensure conformal invariance the underlying classical QCD Lagrangian must be expressed in terms of massless quarks [129]. Due to this requirement, in this thesis with regards to AdS/QCD, we will work only in the chiral limit, therefore confining our studies to the light hadron sector. With this restriction it is clear how one proceeds to map the equations of motion and transition matrix elements to their corresponding conformal AdS expressions.

As a simple example let us consider a two-parton hadronic bound state. In the limit of zero quark mass, $m_q \to 0$

$$\mathcal{M}^2 = \int_0^1 \frac{dx}{x(1-x)} \int d^2b_\perp\, \psi^*(x, b_\perp) \left(-\nabla^2_{b_\perp}\right) \psi(x, b_\perp) + (\text{interactions}). \tag{6.2.22}$$

We can factor the light front wavefunction in terms of angular dependence ϕ, longitudinal depenence, $X(x)$ and the transverse mode $\varphi(\zeta)$ by introducing the impact-space variable ζ. Specifically for a two parton state as $\zeta = x(1-x)\mathbf{b}_\perp^2$

$$\psi(x, \zeta, \varphi) = e^{iL\varphi} X(x) \frac{\phi(\zeta)}{\sqrt{2\pi\zeta}}, \tag{6.2.23}$$

To simplify we write the Laplacian in circular cylindrical coordinates

$$\nabla_\zeta^2 = \frac{1}{\zeta}\frac{d}{d\zeta}\left(\zeta\frac{d}{d\zeta}\right) + \frac{1}{\zeta^2}\frac{\partial^2}{\partial\varphi^2}\,. \tag{6.2.24}$$

Next we factor out the angular dependence of the modes in terms of the SO(2) Casimir representation L^2 orbital angular momentum in the transverse plane. Using the factored form of the wave function we write

$$\mathcal{M}^2 = \int d\zeta\,\phi^*(\zeta)\,\sqrt{\zeta}\left(-\frac{d^2}{d\zeta^2} - \frac{1}{\zeta}\frac{d}{d\zeta} + \frac{L^2}{\zeta^2}\right)\frac{\phi(\zeta)}{\sqrt{\zeta}} + \int d\zeta\,\phi^*(\zeta)U(\zeta)\phi(\zeta), \tag{6.2.25}$$

where $L = |L^z|$. Since we work in the chiral limit ($m_q \to 0$) the longitudinal mode decouples. We can now see that the eigenvalue equation $P_\mu P^\mu\,|\phi\rangle = M^2\,|\phi\rangle$ can be written in a general form as a light-front wave equation for ϕ

$$\left(-\frac{d^2}{d\zeta^2} - \frac{1-4L^2}{4\zeta^2} + U(\zeta)\right)\phi(\zeta) = \mathcal{M}^2\phi(\zeta)\,. \tag{6.2.26}$$

This is a relativistic light-front Schrödinger equation. The confinement properties of QCD can be introduced via the effective interaction $U(\zeta)$ as will be shown in section 6.3. Extension to n-parton systems can be done by introducing an x-weighted impact parameter where $x = x_n$ is the longitudinal momentum fraction of the active quark and the impact parameter for a $n-1$ spectator system is

$$\zeta = \sqrt{\frac{x}{1-x}}\Big|\sum_{j=1}^{n-1} x_j b_{\perp j}\Big|\,. \tag{6.2.27}$$

6.2.2 Hadrons in AdS Space

The action for a spin J field in AdS_{d+1} space-time is given by

$$S = \int d^d x\,dz\,\sqrt{g}\,e^{\varphi(z)}\Big(g^{NN'}g^{M_1M_1'}\cdots g^{M_JM_J'}D_N\Phi_{M_1\cdots M_J}D_{N'}\Phi_{M_1'\cdots M_J'} - \mu^2 g^{M_1M_1'}\cdots g^{M_JM_J'}\Phi_{M_1\cdots M_J}\Phi_{M_1'\cdots M_J'} + \cdots\Big), \tag{6.2.28}$$

where the $\varphi(z)$ is the dilation background field, $\sqrt{g} = (R/z)^{d+1}$, and D_M is the covariant derivative. M, N run over $1, \cdots, d+1$. AdS coordinates, $x^M = (x^\mu, z)$, are written in terms

of the usual Minkowski coordinates x^μ and the holographic variable z. The dilaton background breaks the conformal symmetry by introducing an energy scale. It is a function of the holographic coordinate z. It vanishes hence restores conformality in the ultraviolet limit as $z \to 0$. We can express the effective action in terms of AdS fields $\Phi_J \equiv \Phi_{\mu_1 \cdots \mu_J}$

$$S = \int d^d x\, dz\, \sqrt{g_J}\, e^{\varphi(z)} \Big(g^{NN'} \partial_N \Phi_J \partial_{N'} \Phi_J - \mu^2 \Phi_J^2 \Big), \tag{6.2.29}$$

where the metric determinant is defined as $\sqrt{g_J} = (R/z)^{d+1-2J}$. If we vary the action in Eq. (6.2.29) we get the AdS wave equation for the spin-J mode Φ_J

$$\left[-\frac{z^{d-1-2J}}{e^{\varphi(z)}} \partial_z \left(\frac{e^{\varphi(z)}}{z^{d-1-2J}} \partial_z \right) + \left(\frac{\mu R}{z} \right)^2 \right] \Phi(z)_J = \mathcal{M}^2 \Phi(z)_J, \tag{6.2.30}$$

Here the eigenmode Φ_J is normalized following

$$R^{d-1-2J} \int_0^\infty \frac{dz}{z^{d-1-2J}}\, e^{\varphi(z)} \Phi_J^2(z) = 1. \tag{6.2.31}$$

Furthermore, we see that according to the scaling behavior of the AdS field near $z \to 0$, $\Phi_J = z^\tau$. It follows that the AdS mass μ obeys the relation

$$(\mu R)^2 = (\tau - J)(\tau - d + J). \tag{6.2.32}$$

6.2.3 Light-Front Holographic Mapping

Now that we have an eigenvalue equation for hadrons in QCD on the light cone (6.2.26) and also an eigenvalue equation for hadron within AdS space (6.2.30) we can make a profound connection by mapping one equation to another. The first identification we must make is realizing the connection between the z direction in AdS space and the impact parameter in a QCD bound state ζ. Following this logic in Eq. (6.2.29) we make the substitution $z \to \zeta$ and

$$\phi_J(\zeta) = (\zeta/R)^{-3/2+J} e^{\varphi(\zeta)/2} \Phi_J(\zeta)\,. \tag{6.2.33}$$

For $d = 4$ we can identify the form of the effective potential $U(\zeta)$ by comparing the form of the the QCD light-front wave equation (6.2.26) to Eq. (6.2.29)

$$U(\zeta) = \frac{1}{2}\varphi''(\zeta) + \frac{1}{4}\varphi'(\zeta)^2 \frac{2J-3}{2z} \varphi'(\zeta)\,. \tag{6.2.34}$$

This light-front holographic mapping also tells us how the fifth dimensional AdS mass μ is related to the kinematical generators in front form, specifically the angular momentum projections in the light-front $\hat{z}$ direction L^z, S^z, and J^z.

$$(\mu R)^2 = -(2-J)^2 + L^2 \tag{6.2.35}$$

As stated before the angular momentum projections are kinematical generators in the front-form so they are natural quantum numbers to label the eigenstates.

Some important points to note. The result of this mapping gives us a heuristic guide for a model of QCD via the mapping from AdS space to a light-front holographic wave function. It should not be mistaken for a solution of QCD. Eq. (6.2.26) is a linear-quantum mechanical equation of states in Hilbert space while on the other hand Eq. (6.2.30) is a classical equation of gravity. Now that we have made this connection we need a way to implement confinement. The need for confinement also requires us to break the conformality of the theory. I will mention two possibilites for doing this, namely the so called hard-wall and soft-wall models.

6.3 Conformal Symmetry Breaking

6.3.1 The Hard-Wall Model for Mesons

The hard-wall model within AdS/QCD was first introduced by Polchinski and Strassler [130,138]. This model is the analog of the well known MIT bag model [132]. This type of model allows the quarks and anti-quarks to propagate freely within a certain radius, however, there is sharp wall disallowing propagation outside of this boundary. Confinement is implemented in this manner as a sharp cut-off in the potential

$$U(\zeta) = \begin{cases} 0 & \text{if} \quad \zeta \leq \frac{1}{\Lambda_{\rm QCD}}, \\ \infty & \text{if} \quad \zeta > \frac{1}{\Lambda_{\rm QCD}}. \end{cases} \tag{6.3.36}$$

The eigenvalues for the light-front wave equation (6.2.26) for this potential are determined by the boundary conditions

$$\phi(z = 1/\Lambda_{QCD}) = 0\,. \tag{6.3.37}$$

The result can be given in terms of the roots of Bessel functions

$$\mathcal{M}_{L,k} = \beta_{L,k}\Lambda_{QCD}\,. \tag{6.3.38}$$

The eigenmodes are nomalized as

$$\int_0^{\Lambda_{\rm QCD}^{-1}} d\zeta\, \phi^2(\zeta) = 1\,. \tag{6.3.39}$$

Explicitly this gives

$$\phi_{L,k}(\zeta) = \frac{\sqrt{2}\Lambda_{QCD}}{J_{1+L}(\beta_{L,k})}\sqrt{\zeta}J_L(\zeta\beta_{L,k}\Lambda_{QCD})\,. \tag{6.3.40}$$

Results for mesons in the hard wall model are plotted below as originally shown in [133]. Although the results are reasonable the hard wall model has some shortcomings that we

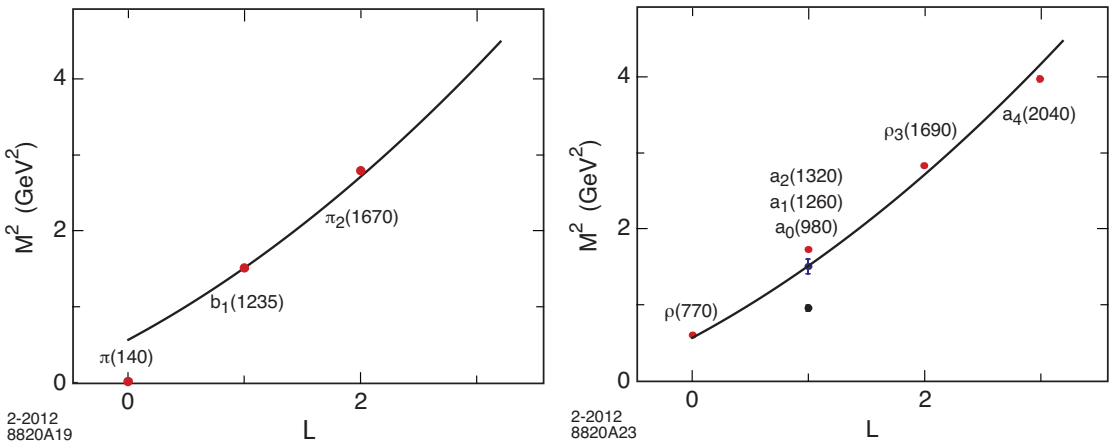

Figure 6.3: $I = 1$ light-meson orbital states in the hard wall model for $\Lambda_{\rm QCD} = 0.32$ GeV: pseudoscalar mesons (left) and vector mesons (right). Figure taken from Ref. [134] however the behavior was first shown in Ref. [133].

would like to improve on. One problem is the degeneracy of the meson model with respect to the orbital quantum number L. This results in the failure to describe the important $L = |L^z| = 1$ triplet splitting. Another shortcoming is the failure to reproduce the well known Regge trajectory dependence. Namely, that when we take the asymptotic expansion of the Bessel function for large arguments, we see that in fact the mass scales as $\mathcal{M} \sim 2n + L$, which disagrees with the usual Regge dependence $\mathcal{M}^2 \sim n + L$, found in nature.

6.3.2 The Soft-Wall Model for Mesons

As opposed to the hard and physically undesirable cut-off in Eq. (6.3.36) it was proposed to introduce a smooth dilaton profile $\varphi(z)$ to simulate confinement [135]. The dilaton background breaks the conformal invariance of the theory but as we will see also leads to

the correct Regge trajectory behavior.

$$V(z) = mc^2\sqrt{g_{00}} = mc^2 R\frac{e^{\pm 3\kappa^2 z^2/4}}{z}. \tag{6.3.41}$$

Mathematically both the positive and negative solution of the dilaton profile are valid however we must take the positive solution based on physical arguments. In the case of the negative solution the potential decreases monotonically so an object at the boundary of the AdS space is unbounded from below and hence can fall to an infinitely large value of z [136]. Taking the positive value for the dilaton profile

$$\varphi(z) = e^{+\kappa^2 z^2} \tag{6.3.42}$$

we get the result for the effective potential in the mesonic soft wall model

$$U(\zeta) = \kappa^4\zeta^2 + 2\kappa^2(J-1)\,. \tag{6.3.43}$$

With this effective potential we can solve for the eigenfunctions $\phi_{n,L}(\zeta)$

$$\phi_{n,L}(\zeta) = \kappa^{1+L}\sqrt{\frac{2n!}{(n+L)!}}\,\zeta^{1/2+L}e^{-\kappa^2\zeta^2/2}L_n^L(\kappa^2\zeta^2)\,. \tag{6.3.44}$$

This leaves us simply to solve for the eigenvalues which give us the masses of the mesonic bound state

$$\mathcal{M}^2_{n,J,L} = 4\kappa^2\left(n + \frac{J+L}{2}\right). \tag{6.3.45}$$

We can see this gives the correct Regge trajectories that we know from experiment as well as resolves the important $L = |L^z| = 1$ triplet splitting that was absent in the hard wall model.

6.4 Baryons

Similar to the case of mesons one can have either a hard or soft wall model for baryons. In this thesis we will look only at the soft wall model. Interested readers may find extensive coverage of the hard wall model in [134].

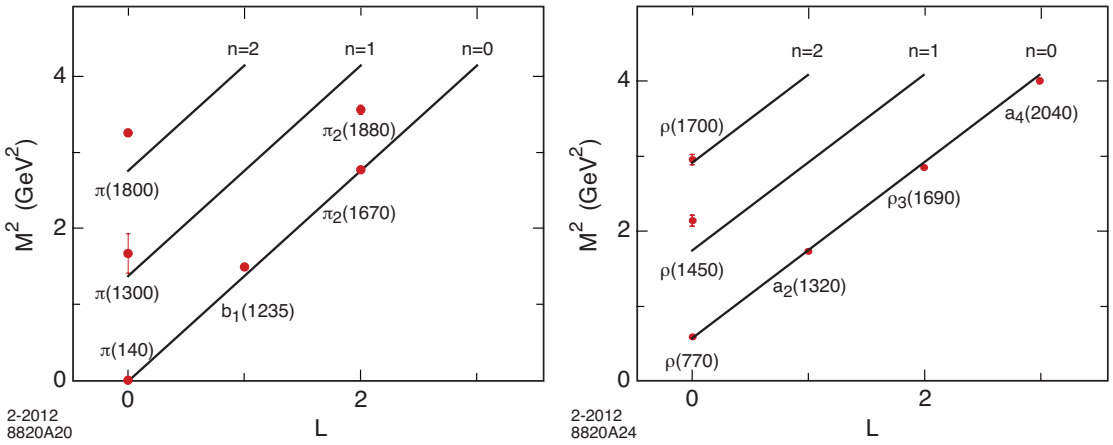

Figure 6.4: $I = 1$ parent and daughter Regge trajectories for the π-meson family (left) with $\kappa = 0.59$ GeV; and the ρ-meson family (right) with $\kappa = 0.54$ GeV. Figure taken from Ref. [134]

6.4.1 Soft-Wall Model for Baryons

What makes baryons much different from mesons in terms of the soft-wall is that they are fermions. It has been shown that in AdS space fermion fields cannot break conformality by introducing a dilaton profile in the soft-wall. It was shown in Ref. [137] that the dilaton profile can be rotated away leaving the action still conformally invariant.

Beginning with the fermionic AdS action, we introduce a potential $V(z)$ to explicitly break the conformal symmetry.

$$S_F = \int d^d x\, dz\, \sqrt{g} \left(\frac{i}{2} \bar{\Psi} e_A^M \Gamma^A D_M \Psi - \frac{i}{2} (D_M \bar{\Psi}) e_A^M \Gamma^A \Psi - \mu \bar{\Psi} \Psi - V(z) \bar{\Psi} \Psi \right). \tag{6.4.46}$$

The variation of the action (6.4.46) leads to the Dirac equation in AdS space

$$\left[i \left(z \eta^{MN} \Gamma_M \partial_N + \frac{d}{2} \Gamma_z \right) - \mu R - R V(z) \right] \Psi = 0. \tag{6.4.47}$$

By making the correspondence between the holographic variable z and the transverse light front coordinate ζ we can identify the corresponding light front wave equation in physical space time. We write the 2×2 spinor component representation for $d = 4$ as

$$\begin{aligned} \frac{d}{d\zeta} \psi_+ + \frac{\nu+}{\zeta} \psi_+ + U(\zeta) \psi_+ &= \mathcal{M} \psi_-, \\ -\frac{d}{d\zeta} \psi_- + \frac{\nu+}{\zeta} \psi_- + U(\zeta) \psi_- &= \mathcal{M} \psi_+, \end{aligned} \tag{6.4.48}$$

where $U(\zeta)$ is some as yet unknown effective confining potential which can be related to the potential $V(z)$ that we introduced in the action via the light-front Dirac equation

as $U(\zeta) = \frac{R}{\zeta}V(\zeta)$. For the ansatz $U(\zeta) = \kappa^2\zeta$, where κ is the parameter that previously appeared in the soft-wall dilaton profile, the AdS Dirac equation results in

$$\left(-\frac{d^2}{d\zeta^2} - \frac{1-4\nu^2}{4\zeta^2} + \kappa^4\zeta^2 + 2(\nu+1)\kappa^2\right)\psi_+(\zeta) = \mathcal{M}^2\psi_+(\zeta), \tag{6.4.49}$$

and

$$\left(-\frac{d^2}{d\zeta^2} - \frac{1-4(\nu+1)^2}{4\zeta^2} + \kappa^4\zeta^2 + 2\nu\kappa^2\right)\psi_-(\zeta) = \mathcal{M}^2\psi_-(\zeta). \tag{6.4.50}$$

We know the light front equation $H_{\rm LF}\psi_\pm = \mathcal{M}^2\psi_\pm$, has the two-component solution

$$\psi_+(\zeta) \sim \zeta^{\frac{1}{2}+\nu}e^{-\kappa^2\zeta^2/2}L_n^\nu(\kappa^2\zeta^2), \qquad \psi_-(\zeta) \sim \zeta^{\frac{3}{2}+\nu}e^{-\kappa^2\zeta^2/2}L_n^{\nu+1}(\kappa^2\zeta^2), \tag{6.4.51}$$

where both the plus and minus solutions have equal probability when properly normalized. This allows us to write the general solution for the eigenvalues of the mass operator as

$$\mathcal{M}^2 = 4\kappa^2(n+\nu+1), \tag{6.4.52}$$

where n is the principle quantum number and ν is a free parameter which we will use to set the overall mass scale. There are an extensive number of arguments regarding the best way to set this parameter ranging from scaling behavior, chiral symmetry, to pure physical reasons that can be found in Ref. [134]. For our purposes we simply state the result,

$$\nu_+ = L + \frac{S}{2} - \frac{1}{4} \qquad , \qquad \nu_- = L + \frac{S}{2} + \frac{1}{4} \tag{6.4.53}$$

where L is orbital quantum number and S is the internal spin i.e., $S = \frac{1}{2}$ or $\frac{3}{2}$. Therefore we have the mass operator for the positive parity baryons as

$$\mathcal{M}^{2\,(+)}_{n,L,S} = 4\kappa^2\left(n + L + \frac{S}{2} + \frac{3}{4}\right), \tag{6.4.54}$$

and the mass operator for the negative parity baryons as

$$\mathcal{M}^{2\,(-)}_{n,L,S} = 4\kappa^2\left(n + L + \frac{S}{2} + \frac{5}{4}\right). \tag{6.4.55}$$

The Regge trajectories for the positive parity baryons are shown in Fig. 6.5.

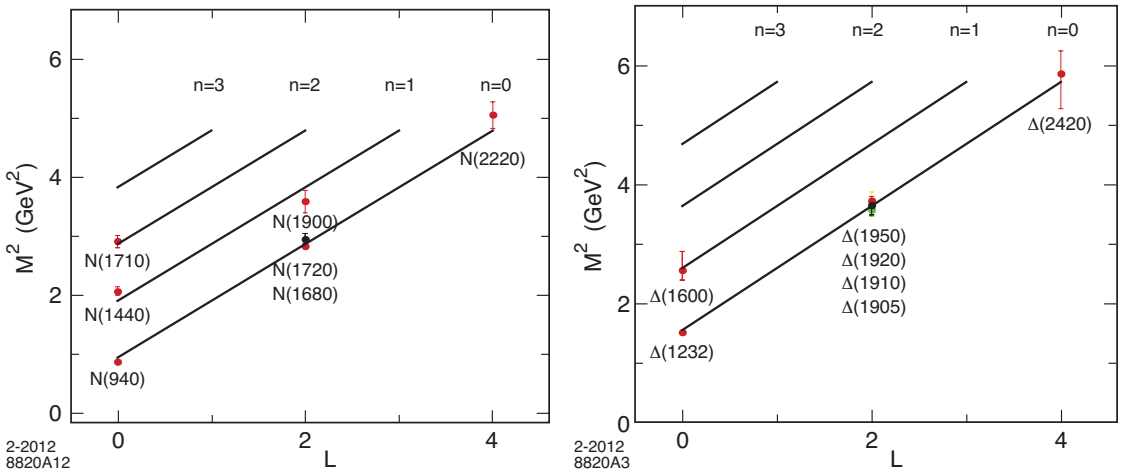

Figure 6.5: Regge trajectories for the N (left) and Δ (right) baryons in the soft wall model. Experimental values from the PDG [65] are plotted as points with corresponding error bars.

6.5 Form Factors

In AdS/CFT the hadronic matrix elements for the electromagnetic current take the form of a convolution of string modes, for the initial and final hadrons with the external electromagnetic source which propagates in the the AdS space. In the Polchinski-Strassler formalism with minimal coupling, the form factor takes the form

$$\int d^4x\, dz\, \sqrt{g}\, A^M(x,z)\Phi^*_{P'}(x,z) \overleftrightarrow{\partial}_M \Phi_P(x,z) \sim (2\pi)^4\delta^4\left(P' - P - q\right)\epsilon_\mu (P + P')^\mu F(q^2). \tag{6.5.56}$$

$\Phi_P(x,z)$ is a normalizable mode representing a hadronic state, i.e. $\Phi_P(x,z) = e^{-i\cdot Px}\Phi(z)$, with hadronic mass given as usual, namely $P_\mu P^\mu = \mathcal{M}^2$. The M superscript indicates Minkowski plus the holographic coordinate, $x^M = (x^\mu, z)$, such that M runs from 1 to 5. P and P' are the initial and final four-momentum respectively of the particle being probed. The four-momentum transferred by the photon is q, with polarization ϵ_μ. We identify the right hand side of Eq. (6.5.56) as the space-like QCD electromagnetic current in physical

space time. To see this let us consider an electromagnetic probe propagating in AdS space polarized along the Minkowski coordinates ($Q^2 = -q^2 > 0$)

$$A(x,z)_\mu = \epsilon_\mu e^{-iQ\cdot x} V(Q^2,z), \qquad A_z = 0 \tag{6.5.57}$$

where $V(Q^2,z)$ equals 1 at zero momentum transfer due to our normalization of the bulk (inside AdS) solutions to the total charge operator. This ensures the boundary limit $A_\mu(x,z\to 0) = \epsilon_\mu e^{-iQ\cdot x}$. This defines our boundary conditions as

$$V(Q^2 = 0, z) = V(Q^2, z = 0) = 1\ . \tag{6.5.58}$$

The propagation of the external current inside the AdS space can be described by the the AdS wave equation

$$[z^2\partial_z^2 - z\partial_z - z^2Q^2]V(Q^2,z) = 0 \tag{6.5.59}$$

with boundary conditions as before, explicitly

$$V(Q^2,z) = zQK_1(zQ) \tag{6.5.60}$$

where $K_n(x)$ is the modified Bessel function of the second kind. If we substitute the normalized $\Phi(x^\mu,z)_P = e^{-iP\cdot x}\Phi(z)$ into Eq. (6.5.56) we see

$$\langle P'|J^\mu(0)|P\rangle = (P+P')^\mu\, R^3 \int \frac{dz}{z^3}\Phi(z)V(Q^2,z)\Phi(z)\ . \tag{6.5.61}$$

where R is the radius of the AdS space. The form factor in AdS space is given in the holographic coordinate z, as the overlap of the normalizable modes Φ_P and $\Phi_{P'}$ dual to the incoming and outgoing hadrons with the non-normalizable mode $V(Q^2,z)$ dual to the external source [138]. Thus from

$$\langle P'|J^\mu(0)|P\rangle = (P+P')^\mu\, F(Q^2)\ . \tag{6.5.62}$$

we can identify the AdS form factor in the hard wall model explicitly as

$$F(Q^2) = R^3 \int \frac{dz}{z^3}\Phi(z)V(Q^2,z)\Phi(z) \tag{6.5.63}$$

Using the integral representation of $V(Q^2,z)$

$$V(Q^2,z) = \int_0^1 dx\, J_0\left(zQ\sqrt{\frac{1-x}{x}}\right), \tag{6.5.64}$$

we write the hard-wall AdS electromagnetic form-factor as

$$F(Q^2) = R^3 \int_0^1 dx \int \frac{dz}{z^3} J_0\left(zQ\sqrt{\frac{1-x}{x}}\right)\Phi^2(z). \tag{6.5.65}$$

We can compare this result directly for with the form factor in the front form. We compute the matrix elements in the front form for the plus component of the current J^+. This choice is wise because it allows us to avoid coupling to Fock states with different numbers of constituents. By expanding the final and initial meson states in terms of Fock components we obtain the classic Drell-Yan-West expression in the q^+ frame

$$F_M(q^2) = \sum_n \int [dx_i]\left[d^2k_{\perp i}\right] \sum_j e_j \psi^*_{n/M}(x_i, k'_{\perp i}, \lambda_i)\psi_{n/M}(x_i, k_{\perp i}, \lambda_i), \tag{6.5.66}$$

where $[dx_i]\left[d^2k_{\perp i}\right]$ is the phase space factor. The final state light cone Fock components for the struck constituent quark is $\mathbf{k}'_{\perp,i} = \mathbf{k}_{\perp,i} + (1-x_i)\mathbf{q}_\perp$ while each spectator is $\mathbf{k}'_{\perp,i} = \mathbf{k}_{\perp,i} - x_i\mathbf{q}_\perp$ As first shown by Soper [139] this expression for the form factor can also be written in impact space as a sum of overlap terms of light front wave functions for the $j = 1, 2, \cdots, n-1$ spectators.

$$F_M(q^2) = \sum_n \prod_{j=1}^{n-1} \int dx_j d^2b_{\perp j} \exp\Big(iq_\perp \cdot \sum_{j=1}^{n-1} x_j b_{\perp j}\Big) \left|\psi_{n/M}(x_j, b_{\perp j})\right|^2 . \tag{6.5.67}$$

This corresponds to a change of transverse momentum $x_j\mathbf{q}_\perp$ for each of the $n-1$ spectators with $\sum_{i=1}^n \mathbf{b}_{\perp,i} = 0$. Let us consider for example the π^+ valence Fock state $|u\bar{d}\rangle$. For $n = 2$, Eq. (6.5.67) becomes

$$F_{\pi^+}(q^2) = 2\pi \int_0^1 \frac{dx}{x(1-x)} \int \zeta d\zeta\, J_0\left(\zeta q\sqrt{\frac{1-x}{x}}\right)\left|\psi_{u\bar{d}/\pi}(x,\zeta)\right|^2, \tag{6.5.68}$$

where $\zeta^2 = x(1-x)\mathbf{b}_\perp^2$ and $F_{\pi^+}(q=0) = 1$. Now that we have the form factor in AdS space, Eq. (6.5.65) and the form factor in usual front form, Eq. (6.5.68) we can see the relationship of severable variables. Most importantly the identification of the holographic variable z with the transverse light front impact variable ζ. We can simplify the AdS form factor expression even more. Now that we have the exact expression for the form factor in AdS, Eq. (6.5.65), we explicitly write the string mode $\Phi^\tau(z)$ in the soft-wall model for twist τ in the lowest radial $n = 0$ and orbital $L = 0$ mode

$$\Phi^\tau(z) = \frac{1}{R^{3/2}}\sqrt{\frac{2P_\tau}{\Gamma(\tau-1)}}\,\kappa^{\tau-1} z^\tau e^{-\kappa^2 z^2/2}, \tag{6.5.69}$$

which is normalized accordingly

$$\langle \Phi^\tau | \Phi^\tau \rangle = \int \frac{dz}{z^3} e^{-\kappa^2 z^2} \Phi^\tau(z)^2 = P_\tau \, . \tag{6.5.70}$$

P_τ is the probability for the twist τ mode in Eq. (6.5.69). In the soft wall model the electromagnetic bulk to boundary propagator can be written as

$$V(Q^2, z) = \Gamma\left(1 + \frac{Q^2}{4\kappa^2}\right) U\left(\frac{Q^2}{4\kappa^2}, 0, \kappa^2 z^2\right), \tag{6.5.71}$$

where $\Gamma(a)$ is the gamma function and $U(a, b, c)$ is the Tricomi confluent hypergeometric function. For the general case the multiplication of these two special functions result in the exact integral equation

$$\Gamma(a) U(a, b, z) = \int_0^\infty e^{-zt} t^{a-1} (1+t)^{b-a-1} dt \, . \tag{6.5.72}$$

Writing the soft wall bulk to boundary in the integral representation we get

$$V(Q^2, z) = \kappa^2 z^2 \int_0^1 \frac{dx}{(1-x)^2} \, x^{\frac{Q^2}{4\kappa^2}} e^{-\kappa^2 z^2 x/(1-x)}. \tag{6.5.73}$$

In the limit that $Q^2 \to \infty$ this simply reduces to the solution for the AdS wave equation as given in Eq. (6.5.60). Plugging in the string mode $\Phi^\tau(z)$ and the bulk to boundary propagator $V(Q^2, z)$ for the soft wall model into the equation for the hadronic form factor

$$F(Q^2) = R^3 \int \frac{dz}{z^3} e^{-\kappa^2 z^2} \Phi(z) V(Q^2, z) \Phi(z) \tag{6.5.74}$$

and computing the integral we end up with a solution for the hadronic form factor in a beautiful multipole form

$$F_\tau(Q^2) = \frac{P_\tau}{\left(1 + \frac{Q^2}{M_\rho^2}\right)\left(1 + \frac{Q^2}{M_{\rho'}^2}\right) \cdots \left(1 + \frac{Q^2}{M_{\rho^{\tau-2}}^2}\right)}. \tag{6.5.75}$$

It is important to note that the full form factor is just the sum of all twists that contribute to the process you are looking at where the normalization is governed via Eq. (6.5.70)

$$F(0) = \sum_\tau F_\tau(0) = \sum_\tau P_\tau = 1. \tag{6.5.76}$$

Form Factor Results

Here we show the application of Eq. (6.5.75) in detail. Let us look at the case of the case of the pion form factor in detail. In principle we should take all twist contributions into our calculation.

$$F_\pi(Q^2) = \sum_\tau F_\tau(Q^2) \tag{6.5.77}$$

In AdS/QCD the twist is defined as the sum of partons plus orbital quantum number L. An important point in that for partons we only count q and $\bar{q}$ partons. The reason is the gluons are thought to be sublimated [141], meaning there are no constituent dynamical gluons. This idea is supported by the flux tube picture of QCD where the gluons are sublimated into a color confinement for quarks and antiquarks. Gluonic degrees of freedom only arise at large virtuality. Thus, the Fock expansion for the pion is

$$|\pi\rangle = \psi^{L=0}_{q\bar{q}/\pi}\,|q\bar{q}, L=0\rangle_{\tau=2} + \psi^{L=0}_{q\bar{q}q\bar{q}}\,|q\bar{q}, L=0\rangle_{\tau=4} + \psi^{L=1}_{q\bar{q}q\bar{q}}\,|q\bar{q}, L=1\rangle_{\tau=5} + \cdots\,. \tag{6.5.78}$$

In practice we can truncate at some twist depending on what accuracy we desire. In the case of the pion it is useful to take up to twist 5. This means we must sum the twist 2, 4, and 5 contributions,

$$F_\pi(Q^2) = F_{(\tau=2)}(Q^2) + F_{(\tau=4)}(Q^2) + F_{(\tau=5)}(Q^2). \tag{6.5.79}$$

For this first example it is useful and instructive to write out this equation in full detail

$$\begin{aligned} F_\pi(Q^2) = &\frac{P_2}{\left(1+\frac{Q^2}{\mathcal{M}_\rho^2}\right)} + \frac{P_4}{\left(1+\frac{Q^2}{\mathcal{M}_\rho^2}\right)\left(1+\frac{Q^2}{\mathcal{M}_{\rho'}^2}\right)\left(1+\frac{Q^2}{\mathcal{M}_{\rho''}^2}\right)} \\ &+\frac{P_5}{\left(1+\frac{Q^2}{\mathcal{M}_\rho^2}\right)\left(1+\frac{Q^2}{\mathcal{M}_{\rho'}^2}\right)\left(1+\frac{Q^2}{\mathcal{M}_{\rho''}^2}\right)\left(1+\frac{Q^2}{\mathcal{M}_{\rho'''}^2}\right)}\,. \end{aligned} \tag{6.5.80}$$

where the P_τ are fixed by Eqns. (6.5.69) and (6.5.70). In the twist-five pion case $P_2 = 0.908$, $P_4 = 0.064$, and $P_5 = 0.028$. The ground and excited ρ mass states are given as in Eq. (6.3.45), namely $\mathcal{M}^2_{n,J,L} = 4\kappa^2\left(n + \frac{J+L}{2}\right)$. One is able to make a connection between the space-like and time-like form factors by making the analytic continuation as found for example in Peskin and Schroeder [140],

$$Q^2 \to Q^2 + iQ\Gamma \tag{6.5.81}$$

where Γ is the decay width of the relevant particle. The analytic continuation allows us to calculate the space and time-like form factors using the same function. The result is shown below. Luckily for the process of $e^+e^- \to \pi^+\pi^-$ several experimental groups have

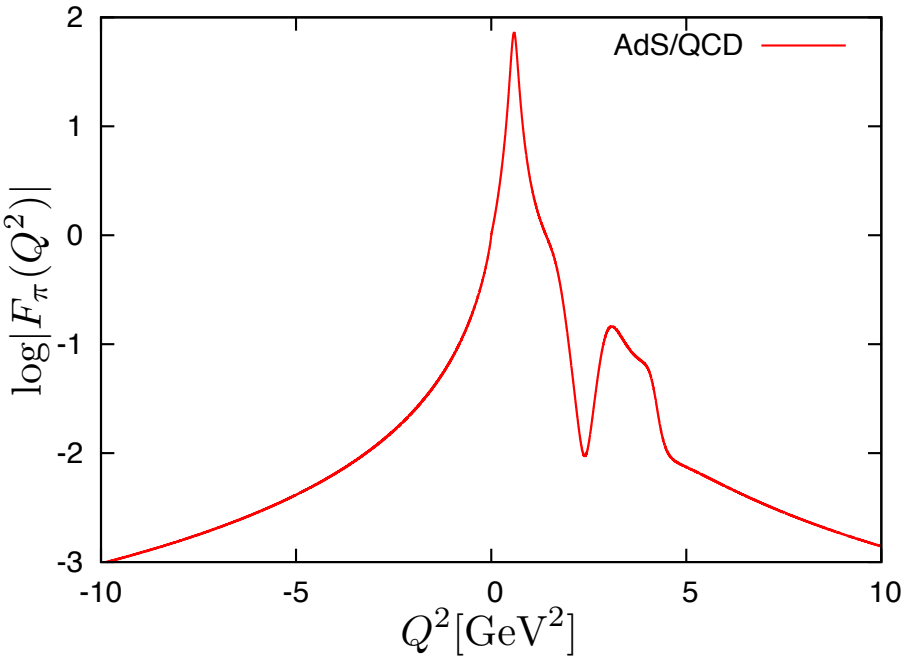

Figure 6.6: Theoretical calculation for the pion form factor in AdS/QCD taking up to twist 5 contributions into account.

measured the pion form factor. The result from Fig. 6.6 with comparison to data is shown below as it appeared in conference proceedings [142]. We see remarkable comparison with experiment especially in terms of the time like side. The next obvious step is to make this calculation for processes not yet measured in order to make pure theoretical predictions. Another process of current interest is with regard to two photon physics. Currently there are proposed experiments in Japan (KEK) and the U.S. (SLAC) that will measure some of these processes. Specifically, we calculate the process $\gamma\gamma \to \pi\omega$ where the exchange particle is the scalar 0^{++}, a-meson. The game is now played similar to the pion form factor except now we have

$$F_\tau(Q^2) = \frac{P_\tau}{\left(1+\frac{Q^2+iQ\Gamma_{a_0}}{M^2_{a_0}}\right)\left(1+\frac{Q^2+iQ\Gamma_{a_0'}}{M^2_{a_0'}}\right)\cdots\left(1+\frac{Q^2+iQ\Gamma_{a_0^{(\tau-2)}}}{M^2_{a_0^{(\tau-2)}}}\right)}. \tag{6.5.82}$$

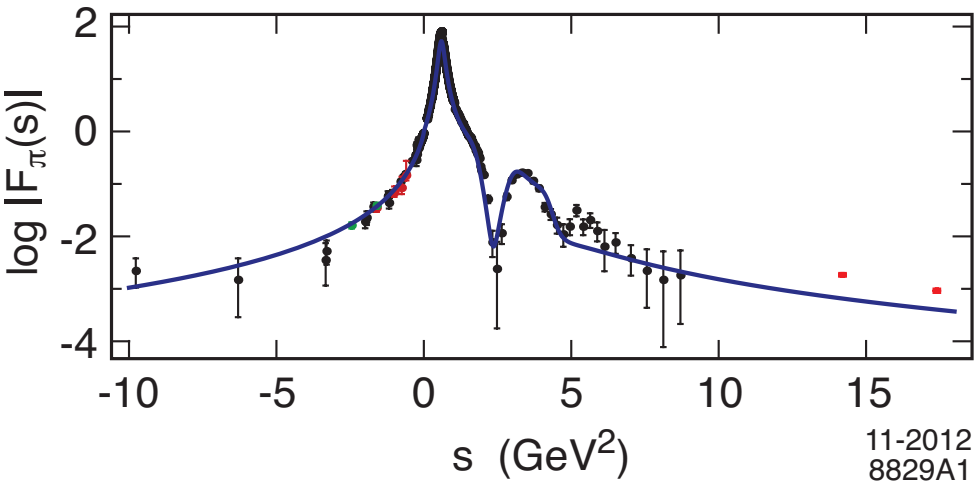

Figure 6.7: Comparison with experiment as shown in proceedings [142]. The space-like data are the compilation from Baldini *et al.* [143] (black) and JLAB data [144] (green and red). The time-like data are from the recent precise measurements from BABAR [145] (black) and CLEO [146] (red).($s = Q^2$)

again to arbitrary twist.

In Fig. 6.8 we see the full space and time-like result plotted. An important note is we don't know that the decay width is for the second excited state of the a-meson so we vary the possibilities between 25 and 275 MeV in steps of 50 MeV. It is interesting to note that the decay width Γ has no consequence on the space-like side as can be seen in Fig. 6.9. However, we see on the time-like side there are quite significant consequences. One sees that the height of the peak between 3-4 GeV^2 is governed by the decay width. A smaller decay width is related to a taller peak. Not having the experimental input can be seen as a shortcoming; however one can argue, this can be seen as an indirect way to "predict" the decay width if one has experimental form factor data similar to the pion case as in Fig. 6.7.

Nucleon Form Factors

As in the case of the universal RCQM we are interested in electromagnetic properties of the nucleon. Precisely as in Eq. (5.3.19) the general form necessary to describe the elastic

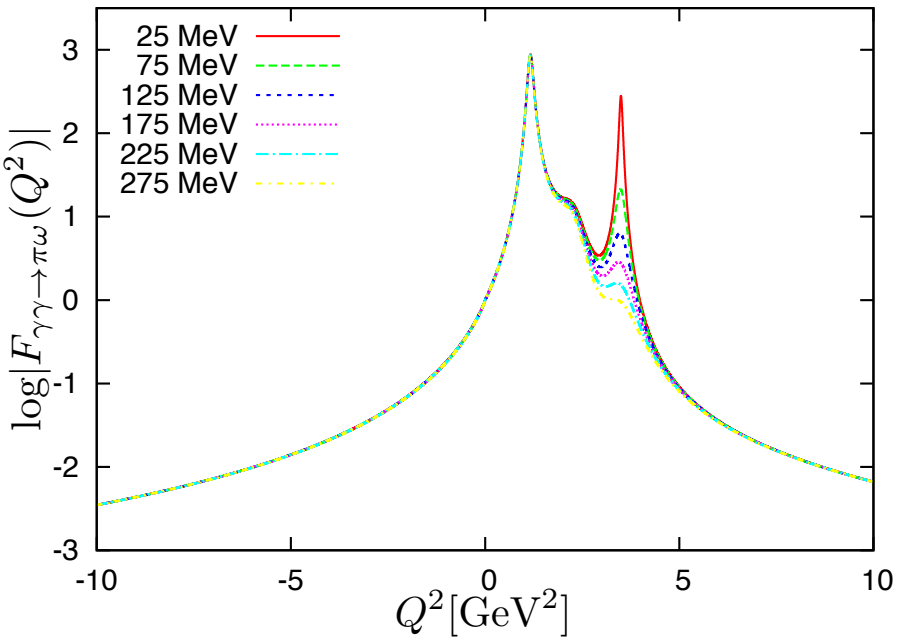

Figure 6.8: Space and time-like prediction for the $\gamma\gamma \to \pi\omega$ form factor. The third decay width of the a-meson is unknown experimentally so each colored line represents different theoretical input values.

scattering of spin $1/2$ particles is

$$\langle P'|J^\mu(0)|P\rangle = \bar{u}(P')\left[\gamma^\mu F_1(q^2) + \frac{i\sigma^{\mu\nu}q^\nu}{2\mathcal{M}}F_2(q^2)\right]u(P), \tag{6.5.83}$$

where F_1 and F_2 are the Dirac and Pauli form factors respectively and $q = P' - P$. As we did with the mesons we look at the connection between the non-local coupling of an external electromagnetic field $A^M(x,z)$ propagating in AdS space with $\Psi_P(x,z)$ being the fermionic mode.

$$\int d^4x\, dz\ \sqrt{g}\,\bar{\Psi}_{P'}(x,z)\, e^A_M\, \Gamma_A\, A^M(x,z)\Psi_P(x,z)$$
$$\sim (2\pi)^4\delta^4\left(P' - P - q\right)\epsilon_\mu u(P')\gamma^\mu F_1(q^2)u(P), \tag{6.5.84}$$

where $e^A_M = \left(\frac{R}{z}\right)\delta^A_M$ is the vielbein with curved space indices $M, N = 1, \cdots 5$ and tangent indices $A, B = 1, \cdots, 5$. The right side of Eq. (6.5.84) represents the Dirac electromagnetic form factor in physical space time. This gives the electromagnetic matrix element of the local quark current coupling to the constituents

$$J^\mu = e_q\bar{q}\gamma^\mu q\,. \tag{6.5.85}$$

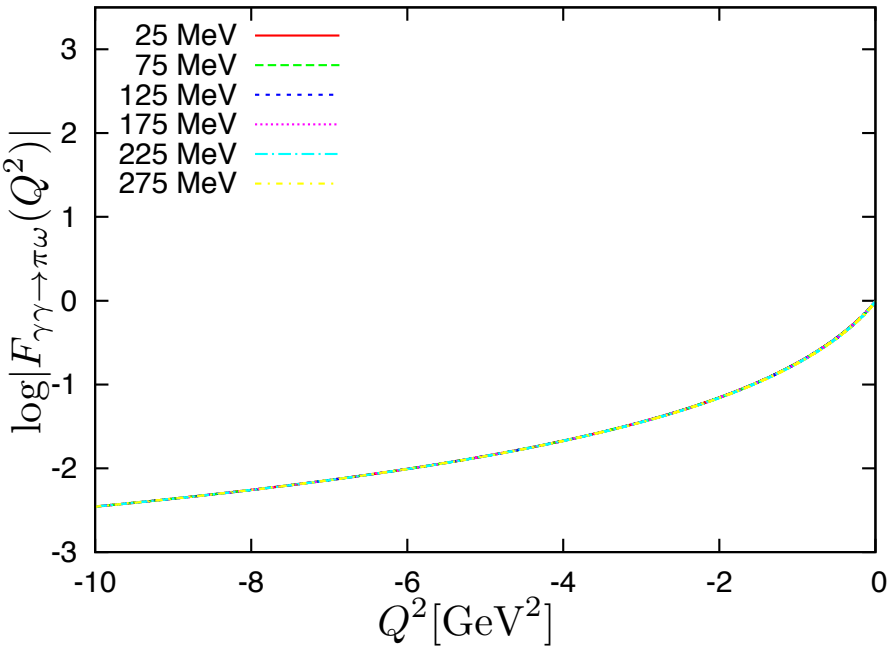

Figure 6.9: Space-like prediction for the $\gamma\gamma \to \pi\omega$ form factor. The third decay width of the a-meson is unknown experimentally so each colored line represents different theoretical input values. We see on the space-like side there is no obvious dependence on the width.

As in the case for the mesons we can identify an exact correspondence between the transverse light front impact variable ζ and the holographic variable z. This provides us with a precise mapping of the light front matrix elements J^+

$$G_\pm(Q^2) = g_\pm R^4 \int \frac{dz}{z^4} V(Q^2, z)\, \Psi_\pm^2(z)\,, \tag{6.5.86}$$

where Ψ_+ corresponds to angular momentum $L^z = 0$, and Ψ_- corresponds to angular momentum $L^z = +1$. In order to determine the value of the effective charges g_+ and g_- we must take the spin and flavor structure into account. These properties are not a priori included in AdS/QCD models so we adopt the well known SU(6) spin-flavor symmetry into our model. Explicitly we write either $N_{q\uparrow}$ or $N_{q\downarrow}$ to label the probability to find the constituent quark in either a spin up or spin down position

$$N_{u\uparrow} = \frac{5}{3}, \qquad N_{u\downarrow} = \frac{1}{3}, \qquad N_{d\uparrow} = \frac{1}{3}, \qquad N_{d\downarrow} = \frac{2}{3}, \tag{6.5.87}$$

for the proton and

$$N_{u\uparrow} = \frac{1}{3}, \qquad N_{u\downarrow} = \frac{2}{3}, \qquad N_{d\uparrow} = \frac{5}{3}, \qquad N_{d\downarrow} = \frac{1}{3}, \tag{6.5.88}$$

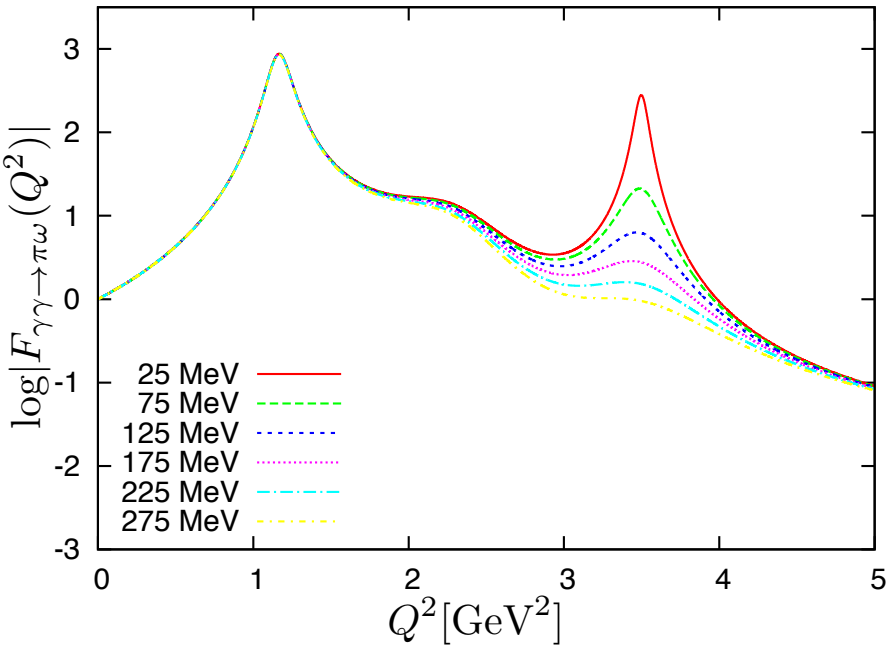

Figure 6.10: Time-like prediction for the $\gamma\gamma \to \pi\omega$ form factor. The third decay width of the a-meson is unknown experimentally so each colored line represents different theoretical input values. We see on the time-like side there is a large dependence on the width.

for the neutron. The effective charges g_+ and g_- in (6.5.86) are computed by the sum of the charges of the struck quark composed by the corresponding probability for the $L^z = 0$ and $L^z = +1$ components Ψ_+ and Ψ_-. The resulting effective charges are $g_p^+ = 1$, $g_p^- = 0$, $g_+^n = -\frac{1}{3}$ and $g_-^n = \frac{1}{3}$. Given this result we can now state in the $\mathrm{SU}(6)_{FS}$ limit the Dirac nucleon form factors are

$$F_1^p(Q^2) = R^4 \int \frac{dz}{z^4} V(Q^2, z)\, \Psi_+^2(z), \tag{6.5.89}$$

$$F_1^n(Q^2) = -\frac{1}{3} R^4 \int \frac{dz}{z^4} V(Q^2, z) \left[\Psi_+^2(z) - \Psi_-^2(z)\right], \tag{6.5.90}$$

where $F_1^p(0) = 1$ and $F_1^n(0) = 0$. As an example we write the plus and minus components of the twist-3 nucleon wave function

$$\Psi_+(z) = \frac{\sqrt{2}\kappa^2}{R^2} z^{7/2} e^{-\kappa^2 z^2/2}, \qquad \Psi_-(z) = \frac{\kappa^3}{R^2} z^{9/2} e^{-\kappa^2 z^2/2}\,. \tag{6.5.91}$$

These results are for the soft wall model with $V(Q^2, z)$ given as before in Eq. (6.5.71),

$$V(Q^2, z) = \Gamma\left(1 + \frac{Q^2}{4\kappa^2}\right) U\left(\frac{Q^2}{4\kappa^2}, 0, \kappa^2 z^2\right)\,. \tag{6.5.92}$$

The results for $F_1^{p,n}$ follow from the analytic form (6.5.75) for any twist τ. We find

$$F_1^p(Q^2) = F_+(Q^2), \tag{6.5.93}$$

and

$$F_1^n(Q^2) = -\frac{1}{3}\left(F_+(Q^2) - F_-(Q^2)\right) . \tag{6.5.94}$$

We can write the general relation between $F_+(Q^2)$ and $F_-(Q^2)$ as

$$F_+(Q^2) = F_\tau(Q^2) \qquad , \qquad F_-(Q^2) = F_{\tau+1}(Q^2) . \tag{6.5.95}$$

Here we write an explicit example for the twist-2 and twist-3 form factors

$$F_+(Q^2) = \frac{1}{\left(1+\frac{Q^2}{M_\rho^2}\right)\left(1+\frac{Q^2}{M_{\rho'}^2}\right)}, \tag{6.5.96}$$

and

$$F_-(Q^2) = \frac{1}{\left(1+\frac{Q^2}{M_\rho^2}\right)\left(1+\frac{Q^2}{M_{\rho'}^2}\right)\left(1+\frac{Q^2}{M_{\rho''}^2}\right)}. \tag{6.5.97}$$

The expression for the elastic nucleon form factor $F_2^{p,n}$ follows from (6.5.83) and has been independently derived by Abidin and Carlson [100],

$$F_2^{p,n}(Q^2) \sim \int \frac{dz}{z^3}\Psi_+(z)V(Q^2,z)\Psi_-(z). \tag{6.5.98}$$

corresponding to

$$F_2^{p,n}(Q^2) = F_-(Q^2). \tag{6.5.99}$$

Furthermore we can write the electric and magnetic nucleon Sachs form factors as

$$G_E(q^2) = F_1(q^2) - \frac{Q^2}{4M^2}F_2(Q^2) \tag{6.5.100}$$

and

$$G_M(q^2) = F_1(Q^2) + F_2(Q^2) . \tag{6.5.101}$$

The results for the proton and neutron form factors give reasonable comparison to experiment as can be seen in Figs. 6.11, 6.12, 6.13, and 6.14.

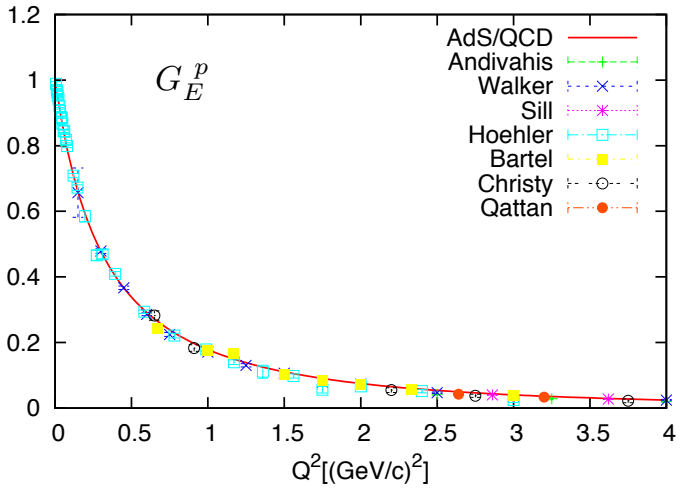

Figure 6.11: AdS/QCD prediction for the proton electric form factor. Experimental data with error bars are also given for comparison.

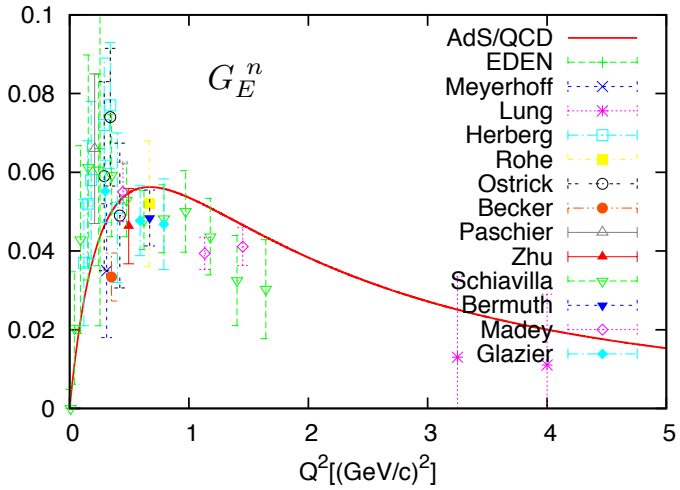

Figure 6.12: AdS/QCD prediction for the neutron electric form factor. Experimental data with error bars are also given for comparison.

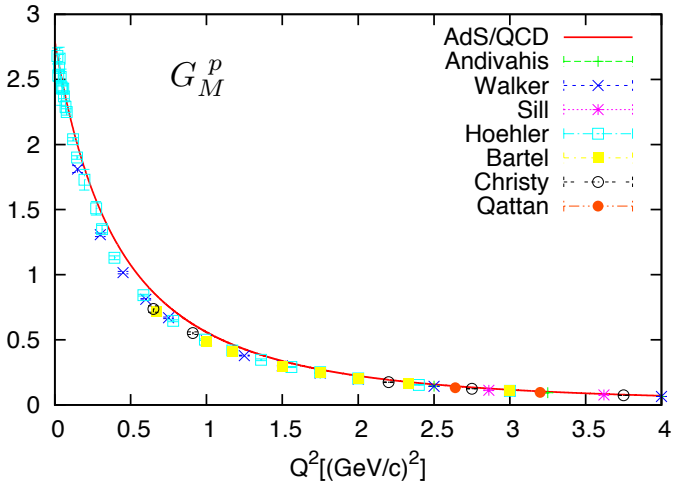

Figure 6.13: AdS/QCD prediction for the proton magnetic form factor. Experimental data with error bars are also given for comparison.

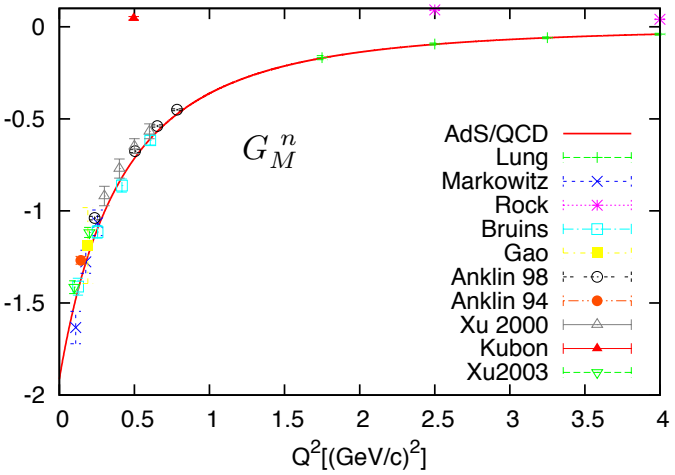

Figure 6.14: AdS/QCD prediction for the neutron magnetic form factor. Experimental data with error bars are also given for comparison.

Chapter 7

Comparison of Approaches

Thus far we have presented a universal relativistic constituent quark model as well as a model based on AdS/QCD. The starting point of each model is quite different however, with regard to observables many of the results are quite complementary to each other. In addition each model has its respective aim and strength. For example the AdS/QCD method can do well in reproducing the light meson spectra as well as space and time-like form factors in accordance with experiment. The universal RCQM has the strength of building a microscopic three-quark system for baryons, whereas the AdS/QCD model makes a quark-diquark approximation. In addition the universal RCQM gives us quite robust results with regard to heavy baryon spectroscopy. The AdS/QCD model can indeed be extended into this regime, however, current studies are still in their infancy [147]. At the moment we are limited in both models to calculate baryons with two or all three quark masses the same; for example, Ξ_c which consists of the flavors, u, s, and c, and thus has quarks of three different masses is outside our present calculational abilities. The source of this difficulty, however, lies in two different regimes for each respective model. In the case of the universal RCQM it is simply a computational issue and in fact there are some preliminary studies within a three-component Faddeev calculation that presently aim to resolve this. In the case of the AdS/QCD model the problem lies in the quark-diquark approximation. While one may consider Λ_c ([uu]c) or Λ_b ([uu]b) for example, (usc) is not possible given the current state of the theory.

In so far as we can, we now proceed with comparisons of observables we have calculated here. As may be seen in Figs. 7.1 and 7.3 in the case of the proton both models agree

can produce the electromagnetic form factors in reasonable agreement with experiments. The situation with the neutron is more interesting. As can be seen in Fig. 7.2 the neu-

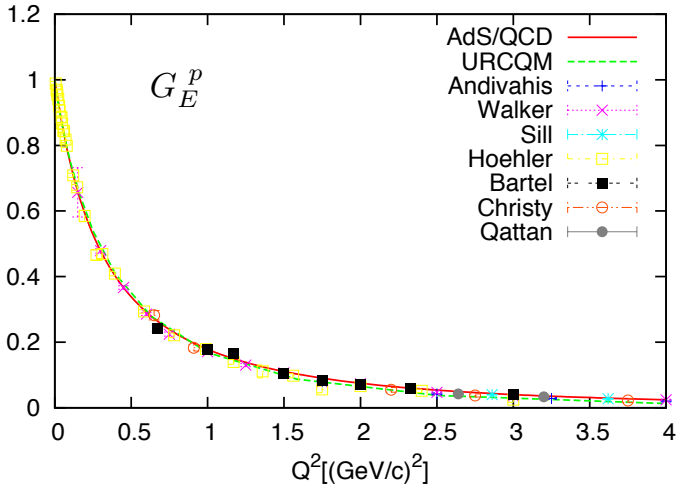

Figure 7.1: Comparison of the URCQM with AdS/QCD for the proton electric form factor. Experimental data with error bars are also given for comparison.

tron electric form factor of both models goes more or less through the experimental data points. However, the URQCM hits the error bars at the lower end while the AdS/QCD calculation hits the error bars at the upper end.

In addition below we compare the numerical spectra for three of the models we have touched on in this thesis.

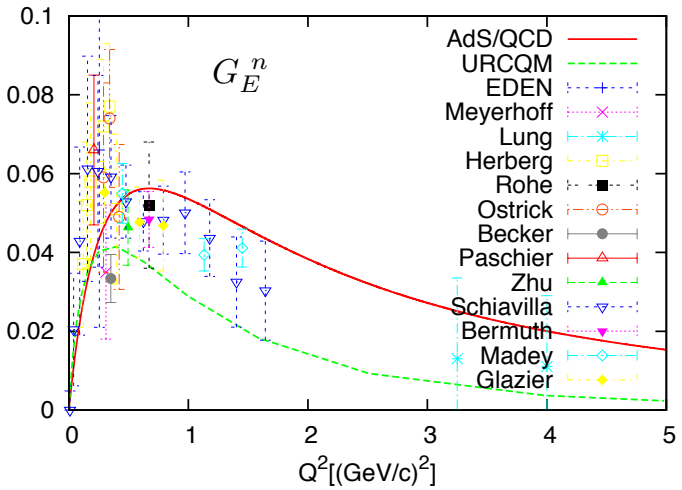

Figure 7.2: Comparison of the URCQM with AdS/QCD for the neutron electric form factor. Experimental data with error bars are also given for comparison.

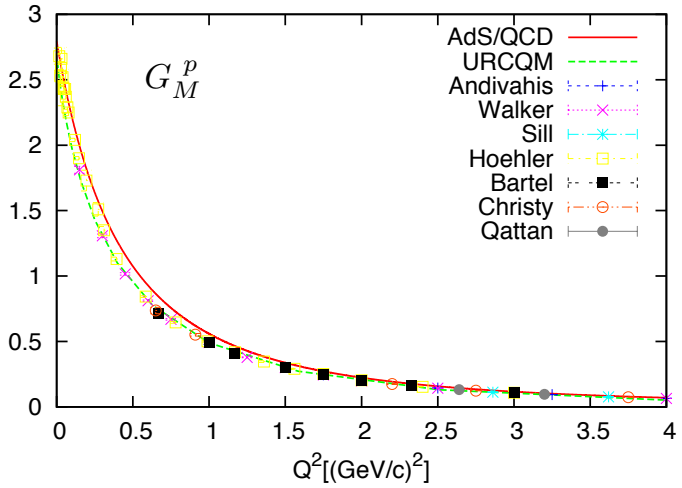

Figure 7.3: Comparison of the URCQM with AdS/QCD for the proton magnetic form factor. Experimental data with error bars are also given for comparison.

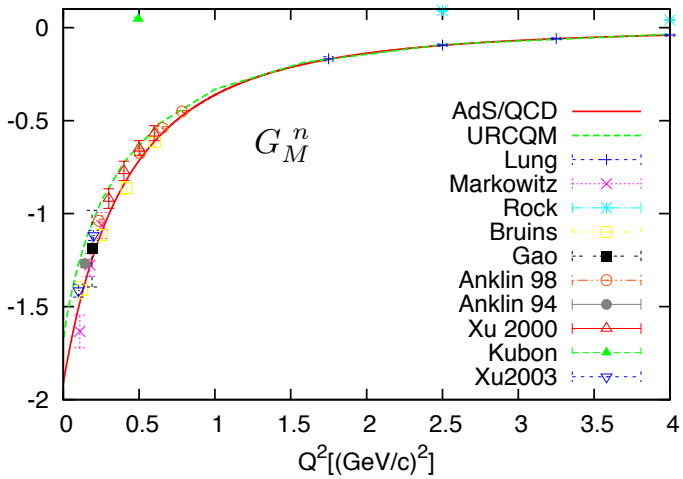

Figure 7.4: Comparison of the URCQM with AdS/QCD for the neutron magnetic form factor. Experimental data with error bars are also given for comparison.

Baryon	J^P	URCQM	OGE	AdS/QCD	Experiment
N(939)	$\frac{1}{2}^+$	939	939	1000	938-940
N(1440)	$\frac{1}{2}^+$	1454	1577	1414	1420-1470
N(1520)	$\frac{3}{2}^-$	1558	1521	1581	1515-1525
N(1535)	$\frac{1}{2}^-$	1558	1521	1581	1525-1545
N(1650)	$\frac{1}{2}^-$	1666	1690	1732	1645-1670
N(1675)	$\frac{5}{2}^-$	1666	1690	1732	1670-1680
N(1700)	$\frac{3}{2}^-$	1666	1690	1732	1650-1750
N(1710)	$\frac{1}{2}^+$	1804	1859	1732	1680-1740
Δ(1232)	$\frac{3}{2}^+$	1234	1231	1224	1231-1233
Δ(1600)	$\frac{3}{2}^+$	1710	1854	1581	1550-1700
Δ(1620)	$\frac{1}{2}^-$	1675	1621	1581	1600-1660
Δ(1700)	$\frac{3}{2}^-$	1675	1621	1581	1670-1750

Table 7.1: Comparison of the lowest-lying N and Δ levels for the URCQM, the OGE RCQM, and AdS/QCD with experiment [65].

Chapter 8

Conclusion and Outlook

In this thesis we have presented a universal RCQM and we have dealt with a model based on AdS/QCD. First for the case of the universal RCQM the quark dynamics is based on confinement and regarding the hyperfine interaction on the exchange of Goldstone bosons. The latter is motivated by the consequences of spontaneous chiral symmetry breaking of QCD in the low-energy regime. We have shown two different methods of calculating spectroscopy in RCQM's. First in Chapter 3 we showed a differential-equation approach based on the stochastic variational method (SVM). Then we have presented a modified Faddeev integral-equation method in Chapter 4.

Armed with these two powerful methods to calculate baryon masses and wave functions we extended the original RCQM based on Goldstone-boson exchange to the universal RCQM that comprises baryons of all flavor compositions, u, d, s, c, and b. The extension to heavy-flavor baryons was accomplished with surprisingly good results. Specifically we wanted to produce a framework that could accommodate all known baryons in a single model. This aim has been achieved while remarkably not expanding the number of open fit parameters that were needed for the original model in the light and strange sectors. In the case of baryons containing a single heavy (charm or bottom) quark our results agree reasonably with experiment. As we move to baryons with a larger number of heavy quarks the experimental air becomes significantly thinner. The only baryonic state measured with two heavy quarks is the Ξ_{cc}, which has been measured by only one group more than ten years ago [86]. Since this measurement there has not been any further experimental light shed on this issue. For this reason, among others, the Particle

Data Group has listed the particle with a one star rating only [65]. This is the lowest amount of confidence possible, and in their words states "*evidence of existence of poor*". This is interesting because most theoretical models, including our own, predict a ground state mass $\approx$ 100 MeV higher than the reported measurement. Due to the questionable nature of this state we have compared our results with data by lattice QCD groups [87] and from a relativistic constituent-quark model calculated with the Bethe-Salpeter equation [88]. Amongst theorists we agree well. Moving higher up the spectrum we only have our theoretical brethren to compare with. We have made comparison with a number of theoretical results ranging from lattice QCD [87, 92], quark models [89–91], and Dyson-Schwinger equations [93] to name only a few. Our universal RCQM compares well with other theoretical predictions. The results of our calculations ranging from the light sector N all the way up to Ω_{bbb} have been presented in Chapter 5. During this investigation we have found our model has many unique strengths. Namely, we have comprised all known baryons ranging from the light sector N all the way up to Ω_{bbb}. Furthermore, all positive features of the earlier GBE RCQM [18] have been kept, in particular the correct level orderings of both the N and Λ spectra. In addition we have found that our method allows the calculation of many excited states that are not currently accessible by many other theoretical methods. We hope the large number of predictions helps to illuminate the path for future studies regarding heavy-baryon spectroscopy.

In addition to spectroscopy we have applied our universal RCQM to studies of the baryon structures. Specifically, we have investigated electric, magnetic, axial, and gravitational form factors. In the cases of the electromagnetic form factors the calculations of the universal RCQM agree very will with experiment. The case of the gravitational form factor is beyond the bounds of current experimental technology. Hence our results can only be compared to other theoretical models and turn out to be quite reasonable.

Despite what has been achieved so far with the framework of the RCQM, a number of challenging problems persist. While the baryon spectroscopy now seems to be well under control, a simultaneous description of all kinds of meson spectra in a unified framework still remains open. In the baryon sector itself, the investigation of resonances, taking into account their very nature (contrary to excited bound states as in a confining quark model) still represents a demanding task. First steps in this direction are under way in our group.

Beyond the approach to low-energy QCD via RCQM's in Chapter 6 we have studied the connection between traditional light-front QCD and the corresponding equations in AdS space via the method of light-front holography. In such an approach confinement may be implemented in a number of ways. We have shown calculations in a soft-wall model that more closely mimics confinement than previously assumed dynamics. Results for meson and baryon spectroscopy reproduce the well-known Regge behavior. In addition to spectroscopy a major result has been to show a closed-form solution that comprises both space- and time-like form factors via one equation. In the case of the pion form factor we have shown good agreement with experimental results. In addition we have made predictions for other types of experiments that hopefully will be made in the near future at high-energy facilities around the globe. Additionally we have extended our mesonic form factor calculations to include baryons. We have calculated the electromagnetic form factors for both the proton and the neutron, again in good qualitative agreement with experiment.

Looking toward the future along the path of AdS/QCD we aim at applying insights from the mesonic sector to the study of baryonic processes. One particular example is, we have started preliminary studies that also concern time-like baryonic form factors. These allow us to calculate such process as the Q-dependent cross-section for $e^+e^- \rightarrow p\bar{p}$. Preliminary results are promising. In addition we hope that the small deviations at low Q^2 that arise due to the complex pole structure from the analytic continuation can give us insights into the famous experimental proton radius puzzle. Additionally another future project would be to use AdS/QCD to eliminate the factorization scale ambiguity that currently plagues high-energy experiments. The resolution of both factorization and renormalization scale ambiguities will be crucial both experimentally and theoretically as we push forward beyond the standard model. Additionally another future direction of investigation would be to make the model a full three-quark system, avoiding a quark-diquark approximation used so far. With regard to spectroscopy we would like to extend our current AdS/QCD model to heavier baryons. In this context it would certainly be quite an accomplishment to one day produce the robust spectra exhibited in the universal RCQM with similar quality.

In conclusion we see that both of these models provide complementary understanding

of the properties of QCD and represent reasonable tools to study corresponding hadron processes on the basis of existing phenomeonology. Still many open questions remain for future researchers to ponder. Even 40 years after its inception QCD remains a very interesting and elusive topic, in particular in the low-energy non-perturbative regime.

Appendix A

Generators

The GBE RCQM relies heavily on the flavor "Gell-Mann" matrices. In this Appendix we show extensive details and consequences due to considerations of the proper group constructions.

A.1 SU(3)

In SU(N) we have (N^2-1) generators, hence in SU(3) we have (3^2-1) generators. In this case we have the usual 8 "Gell-Mann" matrices. These are the 3×3 analogues of the Pauli matrices. They are Hermitian and traceless. They are normalized so that $\mathrm{Tr}(\lambda^i\lambda^j) = 2\delta_{ij}$

The following three couple the up and down quarks:

$$\lambda^1 = \begin{pmatrix} 0 & 1 & 0 \\ 1 & 0 & 0 \\ 0 & 0 & 0 \end{pmatrix} \qquad \lambda^2 = \begin{pmatrix} 0 & -i & 0 \\ i & 0 & 0 \\ 0 & 0 & 0 \end{pmatrix} \qquad \lambda^3 = \begin{pmatrix} 1 & 0 & 0 \\ 0 & -1 & 0 \\ 0 & 0 & 0 \end{pmatrix}.$$

The next ones couple the up and strange quarks:

$$\lambda^4 = \begin{pmatrix} 0 & 0 & 1 \\ 0 & 0 & 0 \\ 1 & 0 & 0 \end{pmatrix} \qquad \lambda^5 = \begin{pmatrix} 0 & 0 & -i \\ 0 & 0 & 0 \\ i & 0 & 0 \end{pmatrix}.$$

The following ones couple the down and strange quarks:

$$\lambda^6 = \begin{pmatrix} 0 & 0 & 0 \\ 0 & 0 & 1 \\ 0 & 1 & 0 \end{pmatrix} \qquad \lambda^7 = \begin{pmatrix} 0 & 0 & 0 \\ 0 & 0 & -i \\ 0 & i & 0 \end{pmatrix}.$$

Finally λ_8 mediates the coupling of all three (up, down, and strange) quarks:

$$\lambda^8 = \frac{1}{\sqrt{3}} \begin{pmatrix} 1 & 0 & 0 \\ 0 & 1 & 0 \\ 0 & 0 & -2 \end{pmatrix}.$$

A.2 SU(4)

In SU(4) we have $(4^2 - 1)$ generators, so we need 16 "Gell-Mann" matrices. The first 8 are just extensions from the SU(3) case.

Thus, these couple the up and down quarks:

$$\lambda^1 = \begin{pmatrix} 0 & 1 & 0 & 0 \\ 1 & 0 & 0 & 0 \\ 0 & 0 & 0 & 0 \\ 0 & 0 & 0 & 0 \end{pmatrix} \qquad \lambda^2 = \begin{pmatrix} 0 & -i & 0 & 0 \\ i & 0 & 0 & 0 \\ 0 & 0 & 0 & 0 \\ 0 & 0 & 0 & 0 \end{pmatrix} \qquad \lambda^3 = \begin{pmatrix} 1 & 0 & 0 & 0 \\ 0 & -1 & 0 & 0 \\ 0 & 0 & 0 & 0 \\ 0 & 0 & 0 & 0 \end{pmatrix}.$$

These couple the up and strange quarks:

$$\lambda^4 = \begin{pmatrix} 0 & 0 & 1 & 0 \\ 0 & 0 & 0 & 0 \\ 1 & 0 & 0 & 0 \\ 0 & 0 & 0 & 0 \end{pmatrix} \qquad \lambda^5 = \begin{pmatrix} 0 & 0 & -i & 0 \\ 0 & 0 & 0 & 0 \\ i & 0 & 0 & 0 \\ 0 & 0 & 0 & 0 \end{pmatrix}.$$

These couple the down and strange quarks:

$$\lambda^6 = \begin{pmatrix} 0 & 0 & 0 & 0 \\ 0 & 0 & 1 & 0 \\ 0 & 1 & 0 & 0 \\ 0 & 0 & 0 & 0 \end{pmatrix} \qquad \lambda^7 = \begin{pmatrix} 0 & 0 & 0 & 0 \\ 0 & 0 & -i & 0 \\ 0 & i & 0 & 0 \\ 0 & 0 & 0 & 0 \end{pmatrix}.$$

As before, the λ_8 mediates the exchange of up, down, and strange quarks:

$$\lambda^8 = \frac{1}{\sqrt{3}} \begin{pmatrix} 1 & 0 & 0 & 0 \\ 0 & 1 & 0 & 0 \\ 0 & 0 & -2 & 0 \\ 0 & 0 & 0 & 0 \end{pmatrix}.$$

In addition, the following ones couple the up and charm quarks:

$$\lambda^9 = \begin{pmatrix} 0 & 0 & 0 & 1 \\ 0 & 0 & 0 & 0 \\ 0 & 0 & 0 & 0 \\ 1 & 0 & 0 & 0 \end{pmatrix} \qquad \lambda^{10} = \begin{pmatrix} 0 & 0 & 0 & -i \\ 0 & 0 & 0 & 0 \\ 0 & 0 & 0 & 0 \\ i & 0 & 0 & 0 \end{pmatrix}.$$

The next ones couple the down and charm quarks:

$$\lambda^{11} = \begin{pmatrix} 0 & 0 & 0 & 0 \\ 0 & 0 & 0 & 1 \\ 0 & 0 & 0 & 0 \\ 0 & 1 & 0 & 0 \end{pmatrix} \qquad \lambda^{12} = \begin{pmatrix} 0 & 0 & 0 & 0 \\ 0 & 0 & 0 & -i \\ 0 & 0 & 0 & 0 \\ 0 & i & 0 & 0 \end{pmatrix}.$$

The following ones couple the strange and charm quarks:

$$\lambda^{13} = \begin{pmatrix} 0 & 0 & 0 & 0 \\ 0 & 0 & 0 & 0 \\ 0 & 0 & 0 & 1 \\ 0 & 0 & 1 & 0 \end{pmatrix} \qquad \lambda^{14} = \begin{pmatrix} 0 & 0 & 0 & 0 \\ 0 & 0 & 0 & 0 \\ 0 & 0 & 0 & -i \\ 0 & 0 & i & 0 \end{pmatrix}.$$

Finally analogously to λ_8, the λ_15 mediates mediates the coupling of all up, down, strange, and charm quarks:

$$\lambda^{15} = \frac{1}{\sqrt{6}} \begin{pmatrix} 1 & 0 & 0 & 0 \\ 0 & 1 & 0 & 0 \\ 0 & 0 & 1 & 0 \\ 0 & 0 & 0 & -3 \end{pmatrix}.$$

A.3 SU(5)

In SU(5) we have $(5^2 - 1)$ generators so we need 24 "Gell-Mann" matrices. Matrices $1 \rightarrow 8$ are extensions of the SU(3) case, while matrices $9 \rightarrow 15$ are extensions of the SU(4) case.

Therefore, the following couple the up and down quarks:

$$\lambda^1 = \begin{pmatrix} 0 & 1 & 0 & 0 & 0 \\ 1 & 0 & 0 & 0 & 0 \\ 0 & 0 & 0 & 0 & 0 \\ 0 & 0 & 0 & 0 & 0 \\ 0 & 0 & 0 & 0 & 0 \end{pmatrix} \quad \lambda^2 = \begin{pmatrix} 0 & -i & 0 & 0 & 0 \\ i & 0 & 0 & 0 & 0 \\ 0 & 0 & 0 & 0 & 0 \\ 0 & 0 & 0 & 0 & 0 \\ 0 & 0 & 0 & 0 & 0 \end{pmatrix} \quad \lambda^3 = \begin{pmatrix} 1 & 0 & 0 & 0 & 0 \\ 0 & -1 & 0 & 0 & 0 \\ 0 & 0 & 0 & 0 & 0 \\ 0 & 0 & 0 & 0 & 0 \\ 0 & 0 & 0 & 0 & 0 \end{pmatrix}.$$

These couple the up and strange quarks:

$$\lambda^4 = \begin{pmatrix} 0 & 0 & 1 & 0 & 0 \\ 0 & 0 & 0 & 0 & 0 \\ 1 & 0 & 0 & 0 & 0 \\ 0 & 0 & 0 & 0 & 0 \\ 0 & 0 & 0 & 0 & 0 \end{pmatrix} \quad \lambda^5 = \begin{pmatrix} 0 & 0 & -i & 0 & 0 \\ 0 & 0 & 0 & 0 & 0 \\ i & 0 & 0 & 0 & 0 \\ 0 & 0 & 0 & 0 & 0 \\ 0 & 0 & 0 & 0 & 0 \end{pmatrix}.$$

These couple the down and strange quarks:

$$\lambda^6 = \begin{pmatrix} 0 & 0 & 0 & 0 & 0 \\ 0 & 0 & 1 & 0 & 0 \\ 0 & 1 & 0 & 0 & 0 \\ 0 & 0 & 0 & 0 & 0 \\ 0 & 0 & 0 & 0 & 0 \end{pmatrix} \quad \lambda^7 = \begin{pmatrix} 0 & 0 & 0 & 0 & 0 \\ 0 & 0 & -i & 0 & 0 \\ 0 & i & 0 & 0 & 0 \\ 0 & 0 & 0 & 0 & 0 \\ 0 & 0 & 0 & 0 & 0 \end{pmatrix}.$$

As before λ_8 mediates the coupling of up, down, and strange quarks:

$$\lambda^8 = \frac{1}{\sqrt{3}} \begin{pmatrix} 1 & 0 & 0 & 0 & 0 \\ 0 & 1 & 0 & 0 & 0 \\ 0 & 0 & -2 & 0 & 0 \\ 0 & 0 & 0 & 0 & 0 \\ 0 & 0 & 0 & 0 & 0 \end{pmatrix}$$

As in SU(4), the following couple the up and charm quarks:

$$\lambda^9 = \begin{pmatrix} 0 & 0 & 0 & 1 & 0 \\ 0 & 0 & 0 & 0 & 0 \\ 0 & 0 & 0 & 0 & 0 \\ 1 & 0 & 0 & 0 & 0 \\ 0 & 0 & 0 & 0 & 0 \end{pmatrix} \quad \lambda^{10} = \begin{pmatrix} 0 & 0 & 0 & -i & 0 \\ 0 & 0 & 0 & 0 & 0 \\ 0 & 0 & 0 & 0 & 0 \\ i & 0 & 0 & 0 & 0 \\ 0 & 0 & 0 & 0 & 0 \end{pmatrix}.$$

These couple the down and charm quarks:

$$\lambda^{11} = \begin{pmatrix} 0 & 0 & 0 & 0 & 0 \\ 0 & 0 & 0 & 1 & 0 \\ 0 & 0 & 0 & 0 & 0 \\ 0 & 1 & 0 & 0 & 0 \\ 0 & 0 & 0 & 0 & 0 \end{pmatrix} \qquad \lambda^{12} = \begin{pmatrix} 0 & 0 & 0 & 0 & 0 \\ 0 & 0 & 0 & -i & 0 \\ 0 & 0 & 0 & 0 & 0 \\ 0 & i & 0 & 0 & 0 \\ 0 & 0 & 0 & 0 & 0 \end{pmatrix}.$$

These couple the strange and charm quarks:

$$\lambda^{13} = \begin{pmatrix} 0 & 0 & 0 & 0 & 0 \\ 0 & 0 & 0 & 0 & 0 \\ 0 & 0 & 0 & 1 & 0 \\ 0 & 0 & 1 & 0 & 0 \\ 0 & 0 & 0 & 0 & 0 \end{pmatrix} \qquad \lambda^{14} = \begin{pmatrix} 0 & 0 & 0 & 0 & 0 \\ 0 & 0 & 0 & 0 & 0 \\ 0 & 0 & 0 & -i & 0 \\ 0 & 0 & i & 0 & 0 \\ 0 & 0 & 0 & 0 & 0 \end{pmatrix}.$$

The λ_{15} mediates the exchange of up, down, strange, and charm quarks:

$$\lambda^{15} = \frac{1}{\sqrt{6}} \begin{pmatrix} 1 & 0 & 0 & 0 & 0 \\ 0 & 1 & 0 & 0 & 0 \\ 0 & 0 & 1 & 0 & 0 \\ 0 & 0 & 0 & -3 & 0 \\ 0 & 0 & 0 & 0 & 0 \end{pmatrix}.$$

In addition, we now have the following to couple the up and bottom quarks:

$$\lambda^{16} = \begin{pmatrix} 0 & 0 & 0 & 0 & 1 \\ 0 & 0 & 0 & 0 & 0 \\ 0 & 0 & 0 & 0 & 0 \\ 0 & 0 & 0 & 0 & 0 \\ 1 & 0 & 0 & 0 & 0 \end{pmatrix} \qquad \lambda^{17} = \begin{pmatrix} 0 & 0 & 0 & 0 & -i \\ 0 & 0 & 0 & 0 & 0 \\ 0 & 0 & 0 & 0 & 0 \\ 0 & 0 & 0 & 0 & 0 \\ i & 0 & 0 & 0 & 0 \end{pmatrix}.$$

These couple the down and bottom quarks:

$$\lambda^{18} = \begin{pmatrix} 0 & 0 & 0 & 0 & 0 \\ 0 & 0 & 0 & 0 & 1 \\ 0 & 0 & 0 & 0 & 0 \\ 0 & 0 & 0 & 0 & 0 \\ 0 & 1 & 0 & 0 & 0 \end{pmatrix} \qquad \lambda^{19} = \begin{pmatrix} 0 & 0 & 0 & 0 & 0 \\ 0 & 0 & 0 & 0 & -i \\ 0 & 0 & 0 & 0 & 0 \\ 0 & 0 & 0 & 0 & 0 \\ 0 & i & 0 & 0 & 0 \end{pmatrix}.$$

These couple the strange and bottom quarks:

$$\lambda^{20} = \begin{pmatrix} 0 & 0 & 0 & 0 & 0 \\ 0 & 0 & 0 & 0 & 0 \\ 0 & 0 & 0 & 0 & 1 \\ 0 & 0 & 0 & 0 & 0 \\ 0 & 0 & 1 & 0 & 0 \end{pmatrix} \qquad \lambda^{21} = \begin{pmatrix} 0 & 0 & 0 & 0 & 0 \\ 0 & 0 & 0 & 0 & 0 \\ 0 & 0 & 0 & 0 & -i \\ 0 & 0 & 0 & 0 & 0 \\ 0 & 0 & i & 0 & 0 \end{pmatrix}.$$

These couple the charm and bottom quarks:

$$\lambda^{22} = \begin{pmatrix} 0 & 0 & 0 & 0 & 0 \\ 0 & 0 & 0 & 0 & 0 \\ 0 & 0 & 0 & 0 & 0 \\ 0 & 0 & 0 & 0 & 1 \\ 0 & 0 & 0 & 1 & 0 \end{pmatrix} \qquad \lambda^{23} = \begin{pmatrix} 0 & 0 & 0 & 0 & 0 \\ 0 & 0 & 0 & 0 & 0 \\ 0 & 0 & 0 & 0 & 0 \\ 0 & 0 & 0 & 0 & -i \\ 0 & 0 & 0 & i & 0 \end{pmatrix}.$$

Finally, λ_{24} couples quarks of all flavors u, d, s, c, and b:

$$\lambda^{24} = \frac{1}{\sqrt{10}} \begin{pmatrix} 1 & 0 & 0 & 0 & 0 \\ 0 & 1 & 0 & 0 & 0 \\ 0 & 0 & 1 & 0 & 0 \\ 0 & 0 & 0 & 1 & 0 \\ 0 & 0 & 0 & 0 & -4 \end{pmatrix}.$$

Note on λ_0

λ_0 comes about as a generator of the U(N) group. Due to this it does not have the same constraints as the other λ matrices which are generators of the SU(N) group. Most notably, however it does not have the requirement of being traceless.

$$\det[\hat{U}] = e^{i\mathrm{Tr}[\lambda]} \tag{A.3.1}$$

In general λ_0 is given in U(N) as

$$\lambda_0 = \sqrt{\frac{2}{N}} \mathbf{1}_{N\times N} \tag{A.3.2}$$

In the case of our model this affects the coefficient of the the η' interaction. Explicitly in SU(N) we have a factor of

$$+ \frac{2}{N} V_{\eta'} \tag{A.3.3}$$

added to our potential to give the singlet representation. In group-theoretical representation it is the same 1 for all SU(N), namely, $3\otimes\bar{3} = 8\oplus 1$, $4\otimes\bar{4} = 15\oplus 1$, and $5\otimes\bar{5} = 24\oplus 1$. The larger multiplet in each one of these representations is given by the generators of the SU(N) group, while the singlet is represented by λ_0. For further discussion on this topic see Ref. [148].

Constructing Generators

Constructing the first N^2-2 generators of any SU(N) group should be evident as we must consider how to each particle can couple to each other. How to build the last matrix where all are related is not obvious though. For λ^8, λ^{15}, and λ^{24} it is clear that we must have a diagonal matrix. What is not clear is what is the coefficient of the matrix and the $N\times N$th term. We can use this simple formula to calculate this matrix

$$\lambda^{N^2-1} = \sqrt{\frac{2}{N^2-N}}\begin{pmatrix} 1 & 0 & 0 & \dots & 0 \\ 0 & 1 & 0 & \dots & 0 \\ \vdots & & & \ddots & \vdots \\ 0 & & \dots & 0 & -(N-1) \end{pmatrix} \tag{A.3.4}$$

Using this formula makes it easy to calculate the final matrix in any set of generators in SU(N). We can exemplify using the above formula for the SU(2) case, for which we have $2^2-1=3$ generators. The first two are as usual:

$$\lambda^1 = \begin{pmatrix} 0 & 1 \\ 1 & 0 \end{pmatrix} \quad , \quad \lambda^2 = \begin{pmatrix} 0 & -i \\ i & 0 \end{pmatrix}.$$

Then the third gives according to Eq. (A.3.4):

$$\lambda^3 = \sqrt{\frac{2}{2^2-2}}\begin{pmatrix} 1 & 0 \\ 0 & -1 \end{pmatrix} = \begin{pmatrix} 1 & 0 \\ 0 & -1 \end{pmatrix}$$

Thus as one would expect the formula in SU(2) gives the Pauli matrices!

Hypercharge

The hypercharge Y for baryons can be calculated using the following simple formula

$$Y = S + C + B' + T + B\,, \tag{A.3.5}$$

where S = strangeness, C = charm, B' = bottomness, T = topness, and B = baryon number. Another method is by comparing maximum and minimum charge in an isospin multiplet.

$$Y = Q_{\text{max}} + Q_{\text{min}} \, . \tag{A.3.6}$$

Take as an example is the Δ resonance multiplet. We have $\Delta^{++} \rightarrow Q_{\text{max}} = 2$ and $\Delta^{-} \rightarrow Q_{\text{min}} = -1$. So the hypercharge is simply $Y = 2 + (-1) = 1$. Every particle in an isospin multiplet has the same hypercharge.

Appendix B

Baryon Flavor Wave Functions

In all of the cases of SU(N) below all have similar symmetries [149]. Explicitly

$$N \otimes N \otimes N = \square\square\square \oplus \begin{array}{ll}\square & \square \\ \square & \end{array} \oplus \begin{array}{ll}\square & \square \\ \square & \end{array} \oplus \begin{array}{l}\square \\ \square \\ \square\end{array}. \tag{B.0.1}$$

The symmetric $\square\square\square$ and antisymmetric $\begin{array}{l}\square \\ \square \\ \square\end{array}$ states are self-evident. One always has two sets of mixed symmetry states. We distinguish them by their behavior under exchange of particles 1 and 2:

$$\psi_{\rm MS} = \begin{array}{|c|c|}\hline 1 & 2 \\ \hline 3 \\ \cline{1-1}\end{array} \quad , \quad \psi_{\rm MA} = \begin{array}{|c|c|}\hline 1 & 3 \\ \hline 2 \\ \cline{1-1}\end{array}. \tag{B.0.2}$$

Here $\psi_{\rm MS}$ is symmetric under the exchange of particles 1 and 2 and $\psi_{\rm MA}$ is antisymmetric. Hence they are called mixed-symmetric and mixed-antisymmetric states, respectively. So it is clear that now for any three-quark flavor wave function we will have sets of totally symmetric states, totally antisymmetric state, and two mixed-symmetric states.

We will quickly see how to calculate the values of Young tablaux for different configurations in SU(N). Always the calculation in terms of a ratio.

Here is how to compute the numerator: You take a diagram and put N down the diagonal. Every box to the right you add one to N. The first box to the right is $N + 1$, the second box is $N + 2$ and so on. Every box directly below contributes a factor of $N - 1$. The general scheme is shown below. Now the numerator is the the product of all terms. For example, a diagram like

$$\square\square \tag{B.0.3}$$

N	$N+1$	$N+2$
$N-1$	N	$N+1$
$N-2$	$N-1$	N
$N-3$		

yields a numerator $N(N+1)$. A diagram like

(B.0.4)

gives us a numerator $N(N+1)(N-1)$.

The next question is, how to calculate the denominator? This can be done by what is known as the method of hooks [150]. You draw a line entering the right side of a diagram and then exit out at the bottom. The number of boxes this line passes through goes in the denominator. You must consider all combinations. We will continue with our previous examples and calculate the denominator for the diagram in Eq. (B.0.3). We can enter in once and come out of the bottom giving a factor of one. Then we can go out of the second box giving us a factor of two. In total our denominator is now $2 \times 1 = 2$. Thus the total

value for this particular diagram is

$$= \frac{N(N+1)}{2 \cdot 1} \tag{B.0.5}$$

Let us also complete the other example given in Eq. (B.0.4). To calculate the denominator by the method of hooks we get $3 \times 1 \times 1 = 3$. The total value for this diagram is

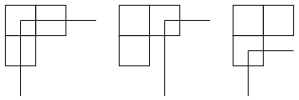

thus

$$= \frac{N(N+1)(N-1)}{3} \,. \tag{B.0.6}$$

Using the method outlined above, we can give a general formula for the representations of a baryons in SU(N):

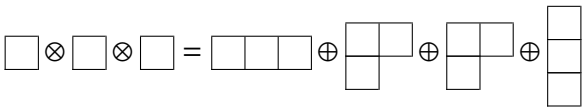

(B.0.7)

$$N \otimes N \otimes N = \frac{N(N+1)(N+2)}{6} \oplus \frac{N(N+1)(N-1)}{3} \oplus \frac{N(N+1)(N-1)}{3} \oplus \frac{N(N-1)(N-2)}{6} . \tag{B.0.8}$$

This allows us to very know easily how many representations and exactly how many of which type (i.e. symmetric, mixed-symmetric, mixed-antisymmetric, antisymmetric) to expect. There are many good references that can be found regarding Young tableaux. The preceding discussion closely followed the explanations given in Ref. [150]

Based on Eq. (B.0.8) we know what type and how many states we should have for the case of SU(3), i.e.

$$3 \otimes 3 \otimes 3 = 10_S \oplus 8_{MS} \oplus 8_{MA} \oplus 1_A \tag{B.0.9}$$

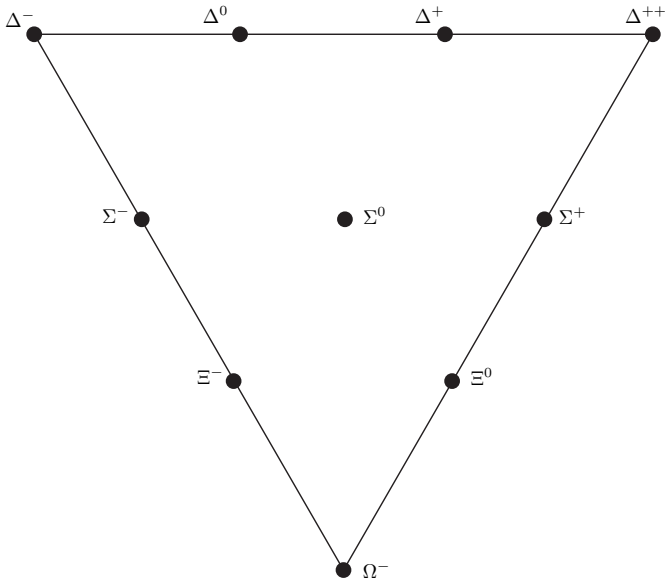

Figure B.1: Pictorial representation of the flavor-symmetric baryon decuplet with $S = \frac{3}{2}$

Baryon	Quark Content	Wave Function
Δ^{++}	uuu	uuu
Δ^{+}	uud	$\frac{1}{\sqrt{3}}(uud + udu + duu)$
Δ^{0}	udd	$\frac{1}{\sqrt{3}}(udd + dud + ddu)$
Δ^{-}	ddd	ddd
Σ^{+}	uus	$\frac{1}{\sqrt{3}}(uus + usu + suu)$
Σ^{0}	uds	$\frac{1}{\sqrt{6}}(uds + dsu + sud + dus + usd + sdu)$
Σ^{-}	dds	$\frac{1}{\sqrt{3}}(dds + dsd + sdd)$
Ξ^{0}	uss	$\frac{1}{\sqrt{3}}(uss + ssu + usu)$
Ξ^{-}	dss	$\frac{1}{\sqrt{3}}(dss + ssu + sus)$
Ω	sss	sss

Table B.1: Decuplet of totally symmetric baryon states in $SU(3)_F$

In SU(4) we get

$$4 \otimes 4 \otimes 4 = 20 \oplus 20 \oplus 20 \oplus 4$$

Therefore one has 20 symmetric states. Since $SU(3) \subset SU(4)$ we require 10 more than before. In addition one has 20 mixed-symmetric and 20 mixed-antisymmetric hence we require 12 more for each than in the previous $SU(3)_F$ case. Furthermore there are four antisymmetric states, i.e. 3 more than in $SU(3)_F$. The additional states are listed in Tabs. B.5, B.6, B.7, and B.8.

In $SU(5)_F$

$$5 \otimes 5 \otimes 5 = 35 \oplus 40 \oplus 40 \oplus 10$$

Hence one has. Since $SU(4) \subset SU(5)$ we include the previous SU(4) multiplet however we require 15 more states than before. In addition one has 40 mixed-symmetric and 40 mixed-antisymmetric hence we require 20 more for each than in the previous $SU(4)_F$ case. In addition we now have 10 totally antisymmetric states. The additional baryon states to $SU(4)_F$ are listed in Tabs. B.9, B.10, B.11, and B.12.

Baryon	Quark Content	Wave Function
P	uud	$\frac{1}{\sqrt{6}}(uud + udu - 2duu)$
N	udd	$-\frac{1}{\sqrt{6}}(dud + ddu - 2udd)$
Σ^+	uus	$\frac{1}{\sqrt{6}}(usu + suu - 2uus)$
Σ^0	sdu	$\frac{1}{\sqrt{12}}(sdu + sud + dsu + usd - 2dus - 2uds)$
Σ^-	dds	$\frac{1}{\sqrt{6}}(dsd + sdd - 2dds)$
Λ	uds	$\frac{1}{\sqrt{4}}(dsu - usd + sdu - sud)$
Ξ^-	dss	$-\frac{1}{\sqrt{6}}(dss + sds - 2ssd)$
Ξ^0	uss	$-\frac{1}{\sqrt{6}}(uss + sus - 2ssu)$

Table B.2: Octet of mixed-symmetric baryon states in $SU(3)_F$

Baryon	Quark Content	Wave Function
P	uud	$\frac{1}{\sqrt{2}}(udu - duu)$
N	udd	$\frac{1}{\sqrt{2}}(udd - dud)$
Σ^+	uus	$\frac{1}{\sqrt{2}}(usu - suu)$
Σ^0	sdu	$\frac{1}{\sqrt{4}}(dsu + usd - sud - sdu)$
Σ^-	dds	$\frac{1}{\sqrt{2}}(dsd - sdd)$
Λ	uds	$\frac{1}{\sqrt{12}}(sdu - sud + usd - dsu - 2dus + 2uds)$
Ξ^-	dss	$\frac{1}{\sqrt{2}}(dss - sds)$
Ξ^0	uss	$\frac{1}{\sqrt{2}}(uss - sus)$

Table B.3: Octet of mixed-antisymmetric baryon states in $SU(3)_F$

Baryon	Quark Content	Wave Function
Λ^0	uds	$\frac{1}{\sqrt{6}}(sdu - sud + usd - dsu + dus - uds)$

Table B.4: Singlet of fully antisymmetric baryon state in $SU(3)_F$

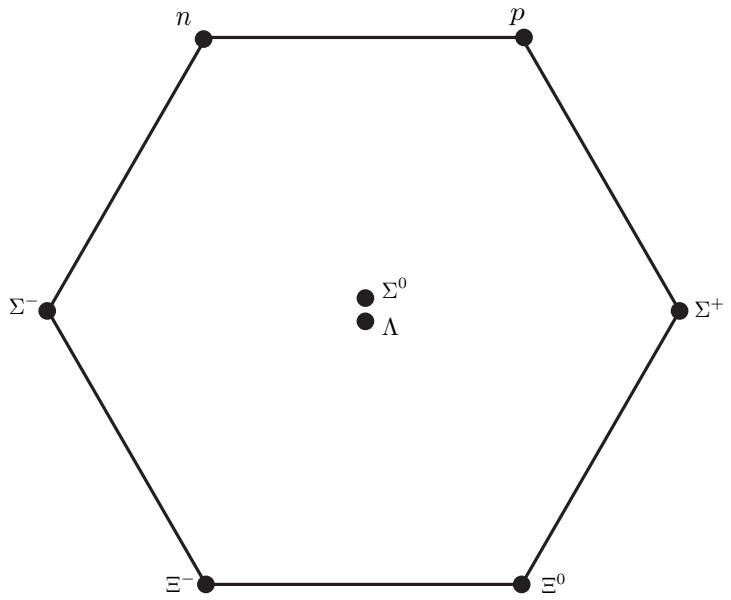

Figure B.2: Pictorial representation of the mixed-symmetric baryon octet with $S = \frac{1}{2}$

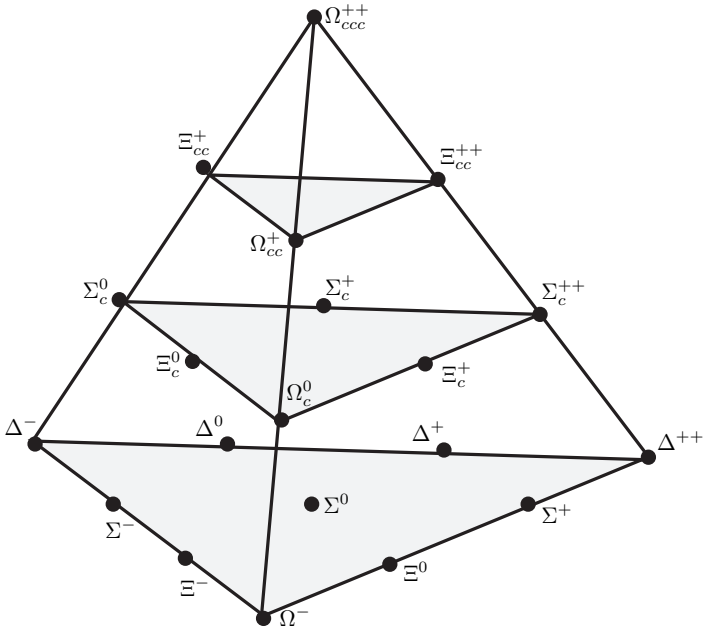

Figure B.3: Pictorial representation of the completely symmetric baryon flavor states in $\mathrm{SU}(4)_F$

Baryon	Quark Content	Wave Function
Σ_c^{++}	uuc	$\frac{1}{\sqrt{3}}(uuc + ucu + cuu)$
Σ_c^{+}	udc	$\frac{1}{\sqrt{6}}(udc + dcu + cud + duc + ucd + cdu)$
Σ_c^{0}	ddc	$\frac{1}{\sqrt{3}}(ddc + dcd + cdd)$
Ξ_c^{+}	usc	$\frac{1}{\sqrt{6}}(usc + scu + cus + suc + ucs + csu)$
Ξ_c^{0}	dsc	$\frac{1}{\sqrt{6}}(dsc + scd + cds + sdc + dcs + csd)$
Ω_c^{0}	ssc	$\frac{1}{\sqrt{3}}(ssc + scs + css)$
Ξ_{cc}^{++}	ccu	$\frac{1}{\sqrt{3}}(ccu + cuc + ucc)$
Ξ_{cc}^{+}	ccd	$\frac{1}{\sqrt{3}}(ccd + cdc + dcc)$
Ω_{cc}^{+}	ccs	$\frac{1}{\sqrt{3}}(ccs + csc + scc)$
Ω_{ccc}^{++}	ccc	ccc

Table B.5: The additional totally symmetric baryon states in SU(4)$_F$

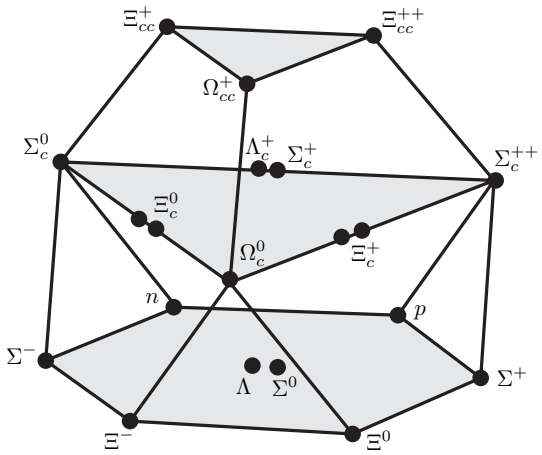

Figure B.4: Pictorial representation of the mixed-symmetric baryon flavor states in SU(4)$_F$

Baryon	Quark Content	Wave Function
Σ_c^{++}	uuc	$\frac{1}{\sqrt{6}}(uuc + ucu - 2cuu)$
Ξ_{cc}^{++}	ucc	$-\frac{1}{\sqrt{6}}(cuc + ccu - 2ucc)$
Ω_{cc}^{+}	scc	$-\frac{1}{\sqrt{6}}(csc + ccs - 2scc)$
Σ_c^{0}	ddc	$\frac{1}{\sqrt{6}}(dcd + cdd - 2ddc)$
Λ_c^{+}	cdu	$\frac{1}{\sqrt{12}}(cdu+cud+dcu+ucd-$ $2duc - 2udc)$
Ξ_{cc}^{+}	dcc	$-\frac{1}{\sqrt{6}}(dcc - cdc - 2ccd)$
Σ_c^{+}	udc	$\frac{1}{2}(dcu - ucd + cdu - cud)$
Ω_c^{0}	ssc	$\frac{1}{\sqrt{6}}(scs + css - 2ssc)$
Ξ_c^{+}	csu	$\frac{1}{\sqrt{12}}(scu + suc + csu + usc -$ $2cus - 2ucs)$
Ξ_c^{+}	usc	$\frac{1}{2}(scu - ucs + scu - cus)$
Ξ_c^{0}	dsc	$\frac{1}{2}(scd - dcs + scd - cds)$
Ξ_c^{0}	csd	$\frac{1}{\sqrt{12}}(scd + sdc + csd + dsc -$ $2cds - 2dcs)$

Table B.6: The 12 additional mixed-symmetric baryon states in $SU(4)_F$

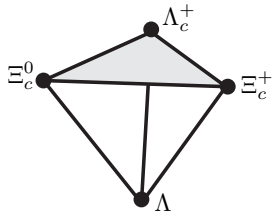

Figure B.5: Pictorial representation of the totally antisymmetric baryon states in $SU(4)_F$

Baryon	Quark Content	Wave Function
Σ_c^{++}	uuc	$\frac{1}{\sqrt{2}}(ucu - cuu)$
Σ_c^{0}	ddc	$\frac{1}{\sqrt{2}}(dcd - cdd)$
Ω_c^{0}	ssc	$\frac{1}{\sqrt{2}}(scs - css)$
Ξ_{cc}^{++}	ucc	$\frac{1}{\sqrt{2}}(ucc - cuc)$
Ξ_{cc}^{+}	dcc	$\frac{1}{\sqrt{2}}(dcc - cdc)$
Ω_{cc}^{+}	scc	$\frac{1}{\sqrt{2}}(scc - csc)$
Σ_c^{+}	udc	$\frac{1}{\sqrt{12}}(cdu - cud + ucd - dcu - 2duc + 2udc)$
Λ_c^{+}	cdu	$\frac{1}{2}(dcu - ucd + cdu - cud)$
Ξ_c^{+}	usc	$\frac{1}{\sqrt{12}}(csu - cus + ucs - scu - 2suc + 2usc)$
Ξ_c^{+}	csu	$\frac{1}{2}(scu - ucs + csu - cus)$
Ξ_c^{0}	dsc	$\frac{1}{\sqrt{12}}(csd - cds + dcs - scd - 2sdc + 2dsc)$
Ξ_c^{0}	csd	$\frac{1}{2}(scd - dcs + csd - cds)$

Table B.7: The 12 additional mixed-antisymmetric baryon states in $SU(4)_F$

Baryon	Quark Content	Wave Function
Λ_c^{+}	udc	$\frac{1}{\sqrt{6}}(sdu - sud + usd - dsu + dus - uds)$
Ξ_c^{+}	usc	$\frac{1}{\sqrt{6}}(sdu - sud + usd - dsu + dus - uds)$
Ξ_c^{0}	dsc	$\frac{1}{\sqrt{6}}(sdu - sud + usd - dsu + dus - uds)$

Table B.8: The three additional antisymmetric baryon states in $SU(4)_F$

Baryon	Quark Content	Wave Function
Σ_b^+	uub	$\frac{1}{\sqrt{3}}(uub + ubu + buu)$
Σ_b^0	udb	$\frac{1}{\sqrt{6}}(udb + dbu + bud + dub + ubd + bdu)$
Σ_b^-	ddb	$\frac{1}{\sqrt{3}}(ddb + dbd + bdd)$
Ξ_b^0	usb	$\frac{1}{\sqrt{6}}(usb + sbu + bus + sub + ubs + bsu)$
Ξ_b^-	dsb	$\frac{1}{\sqrt{6}}(dsb + sbd + bds + sdb + dbs + bsd)$
Ξ_{cb}^0	ucb	$\frac{1}{\sqrt{6}}(ucb + cbu + buc + cub + ubc + bcu)$
Ξ_{cb}^-	dcb	$\frac{1}{\sqrt{6}}(dcb + cbd + bdc + cdb + dbc + bcd)$
Ω_b^-	ssb	$\frac{1}{\sqrt{3}}(ssb + sbs + bss)$
Ω_{cb}^0	scb	$\frac{1}{\sqrt{6}}(scb + cbs + bsc + csb + sbc + bcs)$
Ω_{ccb}^+	ccb	$\frac{1}{\sqrt{3}}(ccb + cbc + bcc)$
Ξ_{bb}^0	ubb	$\frac{1}{\sqrt{3}}(ubb + bub + bbu)$
Ξ_{bb}^-	dbb	$\frac{1}{\sqrt{3}}(dbb + dbd + bbd)$
Ω_{bb}^-	sbb	$\frac{1}{\sqrt{3}}(sbb + bsb + bbs)$
Ω_{cbb}^0	cbb	$\frac{1}{\sqrt{3}}(cbb + bcb + bbc)$
Ω_{bbb}^-	bbb	bbb

Table B.9: The 15 additional totally symmetric baryon states in $SU(5)_F$

Baryon	Quark Content	Wave Function
Σ_b^+	uub	$\frac{1}{\sqrt{6}}(uub + ubu - 2buu)$
Σ_b^-	ddb	$\frac{1}{\sqrt{6}}(ddb + dbd - 2bdd)$
Ω_b^-	ssb	$\frac{1}{\sqrt{6}}(ssb + sbs - 2bss)$
Ω_{ccb}^+	ccb	$\frac{1}{\sqrt{6}}(ccb + cbc - 2bcc)$
Ξ_{bb}^0	ubb	$-\frac{1}{\sqrt{6}}(bub + bbu - 2ubb)$
Ξ_{bb}^-	dbb	$-\frac{1}{\sqrt{6}}(bdb + bbd - 2dbb)$
Ω_{bb}^-	sbb	$-\frac{1}{\sqrt{6}}(bsb + bbs - 2sbb)$
Ω_{cbb}^0	cbb	$-\frac{1}{\sqrt{6}}(bcb + bbc - 2cbb)$
Σ_b^0	udb	$\frac{1}{2}(dbu - ubd + bdu - bud)$
Ξ_b^+	usb	$\frac{1}{2}(sbu - ubs + sdu - bus)$
Ξ_{cb}^+	ucb	$\frac{1}{2}(cbu - ubc + bcu - buc)$
Ξ_b^-	dsb	$\frac{1}{2}(dbu - ubd + bdu - bud)$
Ξ_{cb}^-	dcb	$\frac{1}{2}(cbd - dbc + bcd - bdc)$
Ω_{cb}^0	scb	$\frac{1}{2}(cbs - sbc + bcs - bsc)$
Σ_b^0	bdu	$\frac{1}{\sqrt{12}}(bdu - bud + dbu + ubd - 2dub - 2udb)$
Ξ_b^+	bsu	$\frac{1}{\sqrt{12}}(bsu - bus + sbu + ubs - 2sub - 2usb)$
Ξ_{cb}^+	bcu	$\frac{1}{\sqrt{12}}(bcu - buc + cbu + ubc - 2cub - 2ucb)$
Ξ_b^-	bsd	$\frac{1}{\sqrt{12}}(bsd - bds + sbd + dbs - 2sdb - 2dsb)$
Ξ_{cb}^-	bcd	$\frac{1}{\sqrt{12}}(bcd - bdc + cbd + dbc - 2cdb - 2dcb)$
Ω_{cb}^0	bcs	$\frac{1}{\sqrt{12}}(bcs - bsc + cbs + sbc - 2csb - 2scb)$

Table B.10: The 20 additional mixed-symmetric baryon states in $SU(5)_F$

Baryon	Quark Content	Wave Function
Σ_b^+	uub	$\frac{1}{\sqrt{2}}(ubu - buu)$
Σ_b^-	ddb	$\frac{1}{\sqrt{2}}(dbd - bdd)$
Ω_b^-	ssb	$\frac{1}{\sqrt{2}}(sbs - bss)$
Ω_{ccb}^+	ccb	$\frac{1}{\sqrt{2}}(cbc - bcc)$
Ξ_{bb}^0	ubb	$\frac{1}{\sqrt{2}}(ubb - bub)$
Ξ_{bb}^-	dbb	$\frac{1}{\sqrt{2}}(dbb - bdb)$
Ω_{bb}^-	sbb	$\frac{1}{\sqrt{2}}(sbb - bsb)$
Ω_{cbb}^0	cbb	$\frac{1}{\sqrt{2}}(cbb - bcb)$
Σ_b^0	udb	$\frac{1}{\sqrt{12}}(bdu - bud + ubd - dbu - 2dub + 2udb)$
Ξ_b^+	usb	$\frac{1}{\sqrt{12}}(bsu - bus + ubs - sbu - 2sub + 2usb)$
Ξ_{cb}^+	ucb	$\frac{1}{\sqrt{12}}(bcu - buc + ubc - cbu - 2cub + 2ucb)$
Ξ_b^-	dsb	$\frac{1}{\sqrt{12}}(bsd - bds + dbs - sbd - 2sdb + 2dsb)$
Ξ_{cb}^-	dcb	$\frac{1}{\sqrt{12}}(bcd - bdc + dbc - cbd - 2cdb + 2dcb)$
Ω_{cb}^0	scb	$\frac{1}{\sqrt{12}}(bcs - bsc + sbc - cbs - 2csb + 2scb)$
Σ_b^0	bdu	$\frac{1}{2}(dbu - ubd + bdu - bud)$
Ξ_b^+	bsu	$\frac{1}{2}(sbu - ubs + bsu - bus)$
Ξ_{cb}^+	bcu	$\frac{1}{2}(dcu - ubc + bcu - buc)$
Ξ_b^-	bsd	$\frac{1}{2}(sbd - dbs + bsd - bds)$
Ξ_{cb}^-	bcd	$\frac{1}{2}(cbd - dbc + bcd - bdc)$
Ω_{cb}^0	bcs	$\frac{1}{2}(cbs - sbc + bcs - bsc)$

Table B.11: The 20 additional mixed-antisymmetric baryon states in $SU(5)_F$

Baryon	Quark Content	Wave Function
Ξ_b^0	usb	$\frac{1}{\sqrt{6}}(sdu - sud + usd - dsu + dus - uds)$
$\Xi_{cb}^{\prime +}$	ucb	$\frac{1}{\sqrt{6}}(sdu - sud + usd - dsu + dus - uds)$
$\Xi_b^{\prime -}$	dsc	$\frac{1}{\sqrt{6}}(sdu - sud + usd - dsu + dus - uds)$
Ξ_b^-	dsb	$\frac{1}{\sqrt{6}}(sdu - sud + usd - dsu + dus - uds)$
$\Xi_{cb}^{\prime 0}$	dcb	$\frac{1}{\sqrt{6}}(sdu - sud + usd - dsu + dus - uds)$
Ω_{cb}^0	scb	$\frac{1}{\sqrt{6}}(sdu - sud + usd - dsu + dus - uds)$

Table B.12: The six additional mixed-antisymmetric baryon states in SU(5)$_F$

Appendix C

Jacobi Coordinates

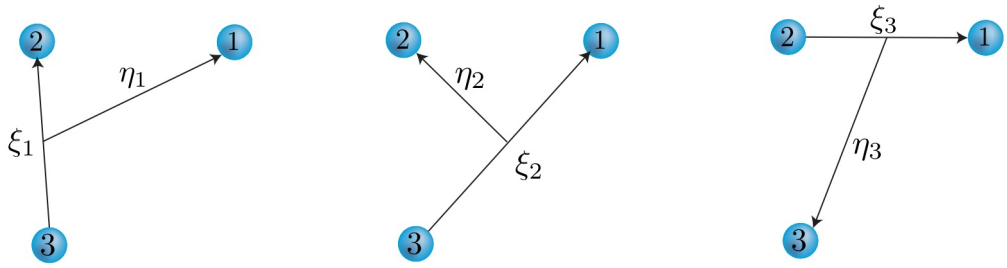

Figure C.1: Jacobi coordinates of three particles for different partitions.

A useful coordinate basis for a three-body system known as the Jacobi coordinates is shown in Fig. C.1. Each particle is respectively labeled by 1, 2, and 3. We give them each mass m_1, m_2, and m_3. Naturally we label their position vectors $\vec{r}_1$, $\vec{r}_2$, and $\vec{r}_3$. Now that we have defined these quantities we can introduce the Jacobi coordinates in configuration space,

$$\vec{\xi}_i = \vec{r}_j - \vec{r}_k \,, \tag{C.0.1}$$

$$\vec{\eta}_i = \vec{r}_i - \frac{m_j \vec{r}_j + m_k \vec{r}_k}{m_j + m_k} \,. \tag{C.0.2}$$

We have i, j, and k being elements of the set (1,2,3). We also have a restrictive condition placed on $\vec{\xi}_i$ that being (i, j, k) must form a cyclic permutation of the triplet (1,2,3). Using the center-of-mass coordinate system and separating the center-of-mass motion we have taken our three-body system down to only two Jacobi coordinates, namely $(\vec{\xi}_i, \vec{\eta}_i)$.

One can transform the set of Jacobi coordinates $(\vec{\xi}_i, \vec{\eta}_i)$ of one partition to another partition $(\vec{\xi}_j, \vec{\eta}_j)$, namely by

$$\vec{\xi}_j = -\frac{m_j}{m_j + m_k}\vec{\xi}_i - (-1)^{\epsilon}\vec{\eta}_i \,, \tag{C.0.3}$$

$$\vec{\eta}_j = (-1)^{\epsilon}\frac{Mm_k}{(m_i + m_k)(m_j + m_k)}\vec{\xi}_i - \frac{m_i}{m_i + m_k}\vec{\eta}_i \,. \tag{C.0.4}$$

We denote the sum of the masses as M. ϵ is even if (i, j, k) is an even permutation of $(1, 2, 3)$; likewise if (i, j, k) is an odd permutation of $(1, 2, 3)$ ϵ will also be odd.

Appendix D

Notation

D.1 Relativistic Quantum Mechanics

Lorentz vectors

Contravariant four-vectors of position x^μ are written as

$$x^\mu = (x^0, x^1, x^2, x^3) = (t, x, y, z) = (x^0, \vec{x}) \, . \tag{D.1.1}$$

In Minkowski space we adpot the metric tensor

$$g_{\mu\nu} = \begin{pmatrix} +1 & 0 & 0 & 0 \\ 0 & -1 & 0 & 0 \\ 0 & 0 & -1 & 0 \\ 0 & 0 & 0 & -1 \end{pmatrix} . \tag{D.1.2}$$

It follows that the covariant four-vector x_μ is given by

$$x_\mu = g_{\mu\nu} x^\nu = (x_0, x_1, x_2, x_3) = (t, -x, -y, -z) \, . \, , \tag{D.1.3}$$

The scalar product is written as

$$x \cdot p = x^\mu p_\mu = x^0 p_0 + x^1 p_1 + x^2 p_2 + x^3 p_3 = tE - \vec{x} \cdot \vec{p} \, , \tag{D.1.4}$$

with four-momentum $p^\mu = (p^0, p^1, p^2, p^3) = (E, \vec{p})$.

Dirac matrices

Up to unitary transformations, the 4×4 Dirac matrices γ^μ are defined by the Clifford algebra

$$\{\gamma^\mu, \gamma^\nu\} = \gamma^\mu\gamma^\nu + \gamma^\nu\gamma^\mu = 2g^{\mu\nu} \; . \tag{D.1.5}$$

Here, γ^0 is Hermitean and γ^k anti-Hermitean. Useful combinations are $\beta = \gamma^0$ and $\alpha^k = \gamma^0\gamma^k$, as well as

$$\sigma^{\mu\nu} = \frac{i}{2}\left(\gamma^\mu\gamma^\nu - \gamma^\nu\gamma^\mu\right) \; , \quad \gamma_5 = \gamma^5 = i\gamma^0\gamma^1\gamma^2\gamma^3 \; . \tag{D.1.6}$$

They can be expressed in terms of the 2×2 Pauli matrices

$$I = \begin{pmatrix} 1 & 0 \\ 0 & 1 \end{pmatrix}, \quad \sigma^1 = \begin{pmatrix} 0 & 1 \\ 1 & 0 \end{pmatrix}, \quad \sigma^2 = \begin{pmatrix} 0 & -i \\ i & 0 \end{pmatrix}, \quad \sigma^3 = \begin{pmatrix} 1 & 0 \\ 0 & -1 \end{pmatrix}. \tag{D.1.7}$$

The two most common representations are the Dirac and chiral representation. In the Dirac representation the γ matrices take the form

$$\gamma^0 = \begin{pmatrix} I & 0 \\ 0 & -I \end{pmatrix}, \quad \gamma^k = \begin{pmatrix} 0 & \sigma^k \\ -\sigma^k & 0 \end{pmatrix}, \tag{D.1.8}$$

$$\gamma_5 = \begin{pmatrix} 0 & +I \\ I & 0 \end{pmatrix}, \quad \alpha^k = \begin{pmatrix} 0 & \sigma^k \\ +\sigma^k & 0 \end{pmatrix}, \quad \sigma^{ij} = \begin{pmatrix} \sigma^k & 0 \\ 0 & \sigma^k \end{pmatrix}. \tag{D.1.9}$$

In the chiral representation γ_0 and γ_5 are interchanged:

$$\gamma^0 = \begin{pmatrix} 0 & +I \\ I & 0 \end{pmatrix}, \quad \gamma^k = \begin{pmatrix} 0 & \sigma^k \\ -\sigma^k & 0 \end{pmatrix}, \tag{D.1.10}$$

$$\gamma_5 = \begin{pmatrix} I & 0 \\ 0 & -I \end{pmatrix}, \quad \alpha^k = \begin{pmatrix} \sigma^k & 0 \\ 0 & -\sigma^k \end{pmatrix}, \quad \sigma^{ij} = \begin{pmatrix} \sigma^k & 0 \\ 0 & \sigma^k \end{pmatrix}. \tag{D.1.11}$$

$(i, j, k) = 1, 2, 3$ are used cyclically.

Projection operators

Combinations of Dirac matrices like the Hermitean matrices

$$\Lambda_+ = \frac{1}{2}(1 + \alpha^3) = \frac{\gamma^0}{2}(\gamma^0 + \gamma^3) \quad \text{and} \quad \Lambda_- = \frac{1}{2}(1 - \alpha^3) = \frac{\gamma^0}{2}(\gamma^0 - \gamma^3) \tag{D.1.12}$$

have projector properties, particularly

$$\Lambda_+ + \Lambda_- = \mathbf{1}\,, \quad \Lambda_+\Lambda_- = 0\,, \quad \Lambda_+^2 = \Lambda_+\,, \quad \Lambda_-^2 = \Lambda_-\,. \tag{D.1.13}$$

They are diagonal in the chiral and maximally off-diagonal in the Dirac representation:

$$(\Lambda_+)_{\text{chiral}} = \begin{pmatrix} 1 & 0 & 0 & 0 \\ 0 & 0 & 0 & 0 \\ 0 & 0 & 0 & 0 \\ 0 & 0 & 0 & 1 \end{pmatrix}, \quad (\Lambda_+)_{\text{Dirac}} = \frac{1}{2}\begin{pmatrix} 1 & 0 & 1 & 0 \\ 0 & 1 & 0 & -1 \\ 1 & 0 & 1 & 0 \\ 0 & -1 & 0 & 1 \end{pmatrix}. \tag{D.1.14}$$

Dirac spinors

The spinors $u_\alpha(p,\lambda)$ and $v_\alpha(p,\lambda)$ are solutions of the Dirac equation,[‡]

$$(\not{p} - m)\, u(p,\lambda) = 0\,, \ (\not{p} + m)\, v(p,\lambda) = 0\,. \tag{D.1.15}$$

They are orthonormal and complete:

$$\bar{u}(p,\lambda)u(p,\lambda') = -\bar{v}(p,\lambda')v(p,\lambda) = 2m\,\delta_{\lambda\lambda'}\,, \tag{D.1.16}$$

$$\sum_\lambda u(p,\lambda)\bar{u}(p,\lambda) = \not{p} + m\,, \ \sum_\lambda v(p,\lambda)\bar{v}(p,\lambda) = \not{p} - m\,. \tag{D.1.17}$$

The Gordon decomposition of the currents is useful:

$$\bar{u}(p,\lambda)\gamma^\mu u(q,\lambda') = \bar{v}(q,\lambda')\gamma^\mu v(p,\lambda) = \frac{1}{2m}\bar{u}(p,\lambda)\Big((p+q)^\mu + i\sigma^{\mu\nu}(p-q)_\nu\Big)u(q,\lambda')\,. \tag{D.1.18}$$

With $\lambda = \pm 1$, the spin projection is $s = \lambda/2$. We have the relations

$$\gamma^\mu \not{a}\gamma_\mu = -2a\,, \tag{D.1.19}$$

$$\gamma^\mu \not{a}\not{b}\gamma_\mu = 4ab\,, \tag{D.1.20}$$

$$\gamma^\mu \not{a}\not{b}\not{c}\gamma_\mu = \not{c}\not{b}\not{a}\,. \tag{D.1.21}$$

Polarization vectors

The two polarization four-vectors $\epsilon_\mu(p,\lambda)$ are labeled by the spin projections $\lambda = \pm 1$. As solutions of the free Maxwell equations they are orthonormal and complete:

$$\epsilon^\mu(p,\lambda)\,\epsilon^\star_\mu(p,\lambda') = -\delta_{\lambda\lambda'}\,, \qquad p^\mu\,\epsilon_\mu(p,\lambda) = 0\,. \tag{D.1.22}$$

[‡] we use the Feynman slash notation, $\not{p} = p_\mu\gamma^\mu$.

The star (*) refers to complex conjugation. The polarization sum is

$$d_{\mu\nu}(p) = \sum_\lambda \epsilon_\mu(p,\lambda)\epsilon_\nu^\star(p,\lambda) = -g_{\mu\nu} + \frac{\eta_\mu p_\nu + \eta_\nu p_\mu}{p^\kappa \eta_\kappa} , \tag{D.1.23}$$

with the null vector $\eta^\mu \eta_\mu = 0$.

D.2 Light-Cone Coordinates and Notation

In this thesis, when working on the light cone, we use the Brodsky-Lepage convention [151–154]. In light-cone notation general contravariant four-vectors are written as

$$x^\mu = (x^+, x^-, x^1, x^2) = (x^+, x^-, \vec{x}_\perp) . \tag{D.2.24}$$

The time-like and space-like components are defined by

$$x^+ = x^0 + x^3 , \tag{D.2.25}$$

$$x^- = x^0 - x^3 . \tag{D.2.26}$$

Here, x^+ is referred to as the light-cone time and x^- is the light-cone position. The metric tensor is

$$g_{\mu\nu} = \begin{pmatrix} 0 & \frac{1}{2} & 0 & 0 \\ \frac{1}{2} & 0 & 0 & 0 \\ 0 & 0 & -1 & 0 \\ 0 & 0 & 0 & -1 \end{pmatrix} \quad \text{and} \quad g^{\mu\nu} = \begin{pmatrix} 0 & 2 & 0 & 0 \\ 2 & 0 & 0 & 0 \\ 0 & 0 & -1 & 0 \\ 0 & 0 & 0 & -1 \end{pmatrix} \tag{D.2.27}$$

leading to

$$x^2 = x^+ x^- - \vec{x}_\perp^2 . \tag{D.2.28}$$

We define the transverse vector components $\vec{x}_\perp = (x^1, x^2)$. We can also write the product of two four-vectors as

$$u \cdot v = \frac{1}{2} u^+ v^- + \frac{1}{2} u^- v^+ - \vec{u}_\perp \cdot \vec{v}_\perp \tag{D.2.29}$$

Via the metric we see the effect of raising and lowering the indices:

$$x_- = \frac{x^0 + x^3}{2} = \frac{x^+}{2} , \tag{D.2.30}$$

$$x_+ = \frac{x^0 - x^3}{2} = \frac{x^-}{2} . \tag{D.2.31}$$

In addition we note that

$$\partial_+ = \frac{1}{2}\partial^- \qquad , \qquad \partial_- = \frac{1}{2}\partial^+ \tag{D.2.32}$$

Dirac Matrices

The light-cone Dirac matrices are related to the usual ones via

$$\gamma^{\pm} = \gamma^0 \pm \gamma^3 \,, \tag{D.2.33}$$

$$\gamma^+\gamma^+ = \gamma^-\gamma^- = 0 \,. \tag{D.2.34}$$

Alternating products are

$$\gamma^+\gamma^-\gamma^+ = 4\gamma^+ \,, \tag{D.2.35}$$

$$\gamma^-\gamma^+\gamma^- = 4\gamma^- \,. \tag{D.2.36}$$

Projection operators are written as

$$\Lambda_+ = \frac{1}{2}\gamma^0\gamma^+ = \frac{1}{4}\gamma^-\gamma^+ \qquad , \qquad \Lambda_- = \frac{1}{2}\gamma^0\gamma^- = \frac{1}{4}\gamma^+\gamma^- \,. \tag{D.2.37}$$

Dirac Spinors

$$u(p,\lambda=+1) = \frac{1}{\sqrt{p^+}}(p^+ + \beta m + \vec{\alpha}_\perp\vec{p}_\perp)\chi(\uparrow) \tag{D.2.38}$$

$$u(p,\lambda=-1) = \frac{1}{\sqrt{p^+}}(p^+ + \beta m + \vec{\alpha}_\perp\vec{p}_\perp)\chi(\downarrow) \tag{D.2.39}$$

$$v(p,\lambda=+1) = \frac{1}{\sqrt{p^+}}(p^+ - \beta m + \vec{\alpha}_\perp\vec{p}_\perp)\chi(\downarrow) \tag{D.2.40}$$

$$v(p,\lambda=-1) = \frac{1}{\sqrt{p^+}}(p^+ - \beta m + \vec{\alpha}_\perp\vec{p}_\perp)\chi(\uparrow) \tag{D.2.41}$$

where

$$\chi(\uparrow) = \frac{1}{\sqrt{2}}\begin{pmatrix}1\\0\\1\\0\end{pmatrix} \qquad , \qquad \chi(\downarrow) = \frac{1}{\sqrt{2}}\begin{pmatrix}0\\1\\0\\-1\end{pmatrix} \tag{D.2.42}$$

Polarization Vectors

The null vector is

$$\eta^\mu = (0, 2, \vec{0}) \,, \tag{D.2.43}$$

The polarization vector takes the from

$$\vec{\epsilon}_\perp(\lambda) = \frac{-1}{\sqrt{2}}(\lambda\vec{e}_x + i\vec{e}_y)\,, \tag{D.2.44}$$

where $\vec{e}_x$ and $\vec{e}_x$ are unit vectors in the p_{x^-} and p_{x^-} direction, respectively. When working in the light-cone gauge $\epsilon^+(p,\lambda) = 0$, therefore the polarization vector is

$$\epsilon^\mu(p,\lambda) = \left(0, \frac{2\vec{\epsilon}_\perp\vec{p}_\perp}{p^+}, \vec{\epsilon}_\perp\right), \tag{D.2.45}$$

which satisfies $p_\mu\epsilon^\mu(p,\lambda) = 0$.

Acknowledgements

First I must thank my academic advisors Stan Brodsky, Zoltán Papp, and Willibald Plessas. All of you have been very patient and kind in advising me throughout the period of my PhD studies. Furthermore, I appreciate the meals we ate, and the beers and wine that we drank together. I consider all of you not only advisors but friends.

Next I must thank Claudia, whom without I would be completely lost in Graz. Also the professors in the theory group that have taken the time to discuss many topics with me; Wolfgang Schweiger, Reinhard Alkofer, Christoff Gattringer, Christian Lang, and Leonid Glozman, your conversations have been truly appreciated.

I have been lucky, in the sense that during my time in Austria, I have had the opportunity to meet and enjoy many of my colleagues. Elmar, Justine, Hélios, Helena, Valentina, Mario, Ki-Seok, Valentin, and all other Mozartgasse people too numerous to mention. My time spent with you has made Graz a truly special place, both academically and socially.

I would like to thank Jogesh Pati who was so gracious to share his office with me during my time at SLAC, our conversations about life and physics were one of many highlights of my time there. Furthermore, I have been lucky to work with Matin Mojaza who has been a good friend and collaborator; additionally BJ Bjorken for inspiration, as well as many entertaining times.

Outside of the scientific environment I would like to thank my family who have always supported me. Mom, Thurston, George, Sarah, and Lola. In addition I would like to thank many of my close friends who have shaped who I have become in life; Texas Joe, Raulie, Richie, Jeff, Matt, HG, John, James, Josiah, and the rest of the Borracho/V-Room crew.

Finally, I would like to thank Ana who chose to embark on this adventure with me. It has been a great joy to travel the world with you.

Nel mezzo del cammin di nostra vita
mi ritrovai per una selva oscura,
ché la diritta via era smarrita.

List of Figures

List of Tables

Bibliography

[1] J. P. Day, K. -S. Choi and W. Plessas, Few Body Syst. **54**, 329 (2013).

[2] J. P. Day, W. Plessas and K. -S. Choi, (Bled Workshops in Physics. Vol. 13 No. 1)

[3] J. P. Day, K. -S. Choi and W. Plessas, PoS(QNP **2012**), 078.

[4] J. P. Day, W. Plessas and K. -S. Choi, arXiv:1205.6918 [hep-ph].

[5] J. P. Day and Z. Papp, Phys. Rev. D **85**, 114042 (2012) [arXiv:1202.4488 [hep-ph]].

[6] J. P. Day, K. -S. Choi and W. Plessas, (Bled Workshops in Physics. Vol. 12 No. 1)

[7] J. P. Day, K. -S. Choi and W. Plessas, arXiv:1108.3450 [hep-ph].

[8] H. Fritzsch and M. Gell-Mann, eConf C **720906V2**, 135 (1972) [hep-ph/0208010].

[9] H. Fritzsch, M. Gell-Mann and H. Leutwyler, Phys. Lett. B **47**, 365 (1973).

[10] D. J. Gross and F. Wilczek, Phys. Rev. Lett. **30**, 1343 (1973).

[11] H. D. Politzer, Phys. Rev. Lett. **30**, 1346 (1973).

[12] J. Beringer *et al.* [Particle Data Group Collaboration], Phys. Rev. D **86**, 010001 (2012).

[13] H. Leutwyler, Annals Phys. **235**, 165 (1994) [hep-ph/9311274].

[14] G. Eichmann, PhD Thesis, University of Graz (2009) arXiv:0909.0703 [hep-ph].

[15] H. Sanchis-Alepuz, PhD Thesis, University of Graz (2012) arXiv:1206.5190 [hep-ph].

[16] M. A. Shifman, Prog. Theor. Phys. Suppl. **131**, 1 (1998) [hep-ph/9802214].

[17] G. F. de Teramond and S. J. Brodsky, Phys. Rev. Lett. **102**, 081601 (2009) [arXiv:0809.4899 [hep-ph]].

[18] L. Y. Glozman, W. Plessas, K. Varga and R. F. Wagenbrunn, Phys. Rev. D **58**, 094030 (1998) [hep-ph/9706507].

[19] P. A. M. Dirac, '*The Principles of Quantum Mechanics*, 4th edn, Oxford University Press, Oxford, (1958).

[20] S. Weinberg, '*The Quantum theory of fields. Vol. 1: Foundations*, Cambridge, UK: Univ. Pr. (1995)

[21] B. Bakamjian and L. H. Thomas, Phys. Rev. **92**, 1300 (1953).

[22] P. A. M. Dirac, Rev. Mod. Phys. **21**, 392 (1949).

[23] K. S. Choi, PhD Thesis, University of Graz (2011)

[24] E. P. Biernat, PhD Thesis, University of Graz (2011) arXiv:1110.3180 [nucl-th].

[25] B. D. Keister and W. N. Polyzou, Adv. Nucl. Phys. **20**, 225 (1991).

[26] V. E. Barnes, P. L. Connolly, D. J. Crennell, B. B. Culwick, W. C. Delaney, W. B. Fowler, P. E. Hagerty and E. L. Hart *et al.*, Phys. Rev. Lett. **12**, 204 (1964).

[27] M. Gell-Mann, Phys. Lett. **8**, 214 (1964).

[28] G. Zweig, In *Lichtenberg, D. B. (Ed.), Rosen, S. P. (Ed.): Developments In The Quark Theory Of Hadrons, Vol. 1*, 22-101 and CERN Geneva - TH. 401 (REC.JAN. 64) 24p

[29] G. Zweig, PRINT-64-170.

[30] R. P. Feynman, Phys. Rev. Lett. **23**, 1415 (1969).

[31] R. P. Feynman, Conf. Proc. C **690905**, 237 (1969).

[32] J. D. Bjorken, Phys. Rev. **179**, 1547 (1969).

[33] J. D. Bjorken and E. A. Paschos, Phys. Rev. **185**, 1975 (1969).

[34] E. D. Bloom, D. H. Coward, H. C. DeStaebler, J. Drees, G. Miller, L. W. Mo, R. E. Taylor and M. Breidenbach *et al.*, Phys. Rev. Lett. **23**, 930 (1969).

[35] M. Breidenbach, J. I. Friedman, H. W. Kendall, E. D. Bloom, D. H. Coward, H. C. DeStaebler, J. Drees and L. W. Mo *et al.*, Phys. Rev. Lett. **23**, 935 (1969).

[36] J. J. Aubert *et al.* [E598 Collaboration], Phys. Rev. Lett. **33**, 1404 (1974).

[37] J. E. Augustin *et al.* [SLAC-SP-017 Collaboration], Phys. Rev. Lett. **33**, 1406 (1974).

[38] S. W. Herb, D. C. Hom, L. M. Lederman, J. C. Sens, H. D. Snyder, J. K. Yoh, J. A. Appel and B. C. Brown *et al.*, Phys. Rev. Lett. **39**, 252 (1977).

[39] S. Abachi *et al.* [D0 Collaboration], Phys. Rev. Lett. **74**, 2632 (1995) [hep-ex/9503003].

[40] F. Gursey and L. A. Radicati, Phys. Rev. Lett. **13**, 173 (1964).

[41] T. H. R. Skyrme, Nucl. Phys. **31**, 556 (1962).

[42] E. Witten, Nucl. Phys. B **223**, 422 (1983).

[43] G. S. Adkins, C. R. Nappi and E. Witten, Nucl. Phys. B **228**, 552 (1983).

[44] T. A. DeGrand, R. L. Jaffe, K. Johnson and J. E. Kiskis, Phys. Rev. D **12** (1975) 2060.

[45] R. K. Bhaduri, *Models Of The Nucleon: From Quarks To Soliton*, Addison-Wesley, Redwood City, USA, (1998)

[46] R. K. Bhaduri, L. E. Cohler and Y. Nogami, Nuovo Cim. A **65**, 376 (1981).

[47] L. Theussl, R. F. Wagenbrunn, B. Desplanques and W. Plessas, Eur. Phys. J. A **12**, 91 (2001) [nucl-th/0010099].

[48] K. Glantschnig, R. Kainhofer, W. Plessas, B. Sengl and R. F. Wagenbrunn, Eur. Phys. J. A **23**, 507 (2005) [nucl-th/0408068].

[49] R. F. Wagenbrunn, PhD Thesis, University of Graz (1998)

[50] K. Berger, PhD Thesis, University of Graz (2005)

[51] B. Sengl, PhD Thesis, University of Graz (2006)

[52] V. I. Kukulin and V. M. Krasnopolsky, J. Phys. G **3**, 795 (1977).

[53] Y. Suzuki and K. Varga, Lect. Notes Phys. M **54**, 1 (1998).

[54] L. D. Faddeev, Sov. Phys. Dokl. **6**, 384 (1961) [Dokl. Akad. Nauk Ser. Fiz. **138**, 565 (1961)].

[55] L. Y. Glozman and D. O. Riska, Phys. Rept. **268**, 263 (1996) [hep-ph/9505422].

[56] L. Y. Glozman, Z. Papp and W. Plessas, Phys. Lett. B **381**, 311 (1996) [hep-ph/9601353].

[57] L. Y. Glozman, Z. Papp, W. Plessas, K. Varga and R. F. Wagenbrunn, Phys. Rev. C **57**, 3406 (1998) [nucl-th/9705011].

[58] T. Melde, W. Plessas and B. Sengl, Phys. Rev. D **77**, 114002 (2008) [arXiv:0806.1454 [hep-ph]].

[59] Z. Papp, Few Body Syst. **26**, 99 (1999) [hep-ph/9808420].

[60] Z. Papp, A. Krassnigg and W. Plessas, Phys. Rev. C **62**, 044004 (2000) [nucl-th/0002006].

[61] J. McEwen, J. Day, A. Gonzalez, Z. Papp and W. Plessas, Few Body Syst. **47**, 225 (2010) [arXiv:1001.4062 [nucl-th]].

[62] N. W. Schellingerhout, PhD Thesis, University of Groningen (1995)

[63] E. Schmid and H. Ziegelmann; *The quantum mechanical three-body problem*, Pergamon Press, 1974.

[64] W. Glöckle; *The Quantum Mechanical Few-Body Problem*, Springer-Verlag, 1983.

[65] K. Nakamura *et al.* [Particle Data Group Collaboration], J. Phys. G **37**, 075021 (2010)

[66] U. Löring, B.C. Metsch, and H.-R. Petry, Eur. Phys. J. A **10**, 395 (2001); ibid. 447 (2001)

[67] S. Migura, D. Merten, B. Metsch, and H.-R. Petry, Eur. Phys. J. A **28**, 41 (2006)

[68] C. Semay, F. Buisseret, N. Matagne, and F. Stancu, Phys. Rev. D **75**, 096001 (2007)

[69] C. Semay, F. Buisseret, and F. Stancu, Phys. Rev. D **76**, 116005 (2007)

[70] C. Semay, F. Buisseret, and F. Stancu, Phys. Rev. D **78**, 076003 (2008)

[71] H. Sanchis-Alepuz, R. Alkofer, G. Eichmann, and R. Williams, PoS QCD-TNT-II, 041 (2011) [arXiv:1112.3214]

[72] L. Liu, H.-W. Lin, K. Orginos, and A. Walker-Loud, Phys. Rev. D **81**, 094505 (2010)

[73] A. Manohar and H. Georgi, Nucl. Phys. B **234**, 189 (1984)

[74] L.Ya. Glozman and D.O. Riska, Phys. Rept. **268**, 263 (1996)

[75] S. Weinberg, Phys. Rev. Lett. **105**, 261601 (2010)

[76] L.Ya. Glozman, Z. Papp, W. Plessas, K. Varga, and R.F. Wagenbrunn, Phys. Rev. C **57**, 3406 (1998)

[77] S. Boffi, L.Ya. Glozman, W. Klink, W. Plessas, M. Radici, and R.F. Wagenbrunn, Eur. Phys. J. A **14**, 17 (2002)

[78] W. Plessas, PoS LC 2010, 017 (2010) [arXiv:1011.0156]

[79] L.Ya. Glozman and D. O. Riska, Nucl. Phys. A **603**, 326 (1996) [Erratum ibid. A **620**, 510 (1997)]

[80] L.Ya. Glozman, Z. Papp, W. Plessas, K. Varga, and R. F. Wagenbrunn, Phys. Rev. C **61**, 019804 (2000)

[81] Y. Suzuki and K. Varga, *Stochastic Variational Approach to Quantum-Mechanical Few-Body Problems*, Lect. Notes Phys. **54**, 1 (1998)

[82] Z. Papp, A. Krassnigg, and W. Plessas, Phys. Rev. C **62**, 044004 (2000)

[83] J. McEwen, J. Day, A. Gonzalez, Z. Papp, and W. Plessas, Few-Body Syst. **47**, 225 (2010)

[84] Joseph P. Day, Ki-Seok Choi, and Willibald Plessas, to be published

[85] R. M. Woloshyn, Phys. Lett. B **476**, 309 (2000)

[86] M. Mattson *et al.* [SELEX Collaboration], Phys. Rev. Lett. **89**, 112001 (2002) [hep-ex/0208014].

[87] L. Liu, H. -W. Lin, K. Orginos and A. Walker-Loud, Phys. Rev. D **81**, 094505 (2010) [arXiv:0909.3294 [hep-lat]].

[88] S. Migura, D. Merten, B. Metsch and H. -R. Petry, Eur. Phys. J. A **28**, 41 (2006) [hep-ph/0602153].

[89] W. Roberts and M. Pervin, Int. J. Mod. Phys. A **23**, 2817 (2008) [arXiv:0711.2492 [nucl-th]].

[90] D. Ebert, R. N. Faustov, V. O. Galkin and A. P. Martynenko, Phys. Rev. D **66**, 014008 (2002) [hep-ph/0201217].

[91] A. P. Martynenko, Phys. Lett. B **663**, 317 (2008) [arXiv:0708.2033 [hep-ph]].

[92] S. Meinel, Phys. Rev. D **82**, 114514 (2010) [arXiv:1008.3154 [hep-lat]].

[93] H. Sanchis-Alepuz, R. Alkofer, G. Eichmann and R. Williams, PoS QCD **-TNT-II**, 041 (2011) [arXiv:1112.3214 [hep-ph]].

[94] F. J. Llanes-Estrada, O. I. Pavlova and R. Williams, Eur. Phys. J. C **72**, 2019 (2012) [arXiv:1111.7087 [hep-ph]].

[95] W. H. Klink, Phys. Rev. C **58**, 3587 (1998).

[96] K. -S. Choi, W. Plessas and R. F. Wagenbrunn, Phys. Rev. C **81**, 028201 (2010) [arXiv:0908.3959 [hep-ph]].

[97] K. -S. Choi, W. Plessas and R. F. Wagenbrunn, Phys. Rev. D **82**, 014007 (2010) [arXiv:1005.0337 [hep-ph]].

[98] K. Berger, R. F. Wagenbrunn and W. Plessas, Phys. Rev. D **70**, 094027 (2004) [nucl-th/0407009].

[99] M. Guidal, M. V. Polyakov, A. V. Radyushkin and M. Vanderhaeghen, Phys. Rev. D **72**, 054013 (2005) [hep-ph/0410251].

[100] Z. Abidin and C. E. Carlson, Phys. Rev. D **79**, 115003 (2009) [arXiv:0903.4818 [hep-ph]].

[101] Z. Abidin and C. E. Carlson, Phys. Rev. D **77**, 095007 (2008) [arXiv:0801.3839 [hep-ph]].

[102] Z. Abidin and C. E. Carlson, Phys. Rev. D **77**, 115021 (2008) [arXiv:0804.0214 [hep-ph]].

[103] S. K. Domokos, J. A. Harvey and N. Mann, Phys. Rev. D **80**, 126015 (2009) [arXiv:0907.1084 [hep-ph]].

[104] S. J. Brodsky and G. F. de Teramond, Phys. Rev. D **78**, 025032 (2008) [arXiv:0804.0452 [hep-ph]].

[105] W. Broniowski and E. R. Arriola, Phys. Rev. D **78**, 094011 (2008) [arXiv:0809.1744 [hep-ph]].

[106] S. J. Brodsky, D. S. Hwang, B. -Q. Ma and I. Schmidt, Nucl. Phys. B **593**, 311 (2001) [hep-th/0003082].

[107] A. V. Belitsky and X. Ji, Phys. Lett. B **538**, 289 (2002) [hep-ph/0203276].

[108] P. .Hagler *et al.* [LHPC Collaboration], Phys. Rev. D **77**, 094502 (2008) [arXiv:0705.4295 [hep-lat]].

[109] R. F. Wagenbrunn, S. Boffi, W. Klink, W. Plessas and M. Radici, Phys. Lett. B **511**, 33 (2001) [nucl-th/0010048].

[110] L. Y. Glozman, M. Radici, R. F. Wagenbrunn, S. Boffi, W. Klink and W. Plessas, Phys. Lett. B **516**, 183 (2001) [nucl-th/0105028].

[111] R. F. Wagenbrunn, S. Boffi, L. Y. .Glozman, W. Klink, W. Plessas and M. Radici, Few Body Syst. Suppl. **14**, 411 (2003) [hep-ph/0212190].

[112] B. Sengl, T. Melde and W. Plessas, Phys. Rev. D **76**, 054008 (2007) [arXiv:0705.1642 [nucl-th]].

[113] T. Melde, K. Berger, L. Canton, W. Plessas and R. F. Wagenbrunn, Phys. Rev. D **76**, 074020 (2007).

[114] T. Melde, L. Canton, W. Plessas, and R. F. Wagenbrunn, Eur. Phys. J. A **25**, 97 (2005).

[115] H. Pagels, Phys. Rev. **144**, 1250 (1966).

[116] X. -D. Ji, Phys. Rev. Lett. **74**, 1071 (1995) [hep-ph/9410274].

[117] X. -D. Ji, Phys. Rev. D **55**, 7114 (1997) [hep-ph/9609381].

[118] O. V. Teryaev, [hep-ph/9904376].

[119] J. M. Maldacena, Adv. Theor. Math. Phys. **2**, 231 (1998) [hep-th/9711200].

[120] J. D. Bekenstein, Phys. Rev. D **7**, 2333 (1973).

[121] K. Becker, M. Becker, J. H. Schwarz and , Cambridge, UK: Cambridge Univ. Pr. (2007) 739 p

[122] J. Polchinski, Phys. Rev. Lett. **75**, 4724 (1995) [hep-th/9510017].

[123] Y. Kim and D. Yi, Adv. High Energy Phys. **2011**, 259025 (2011) [arXiv:1107.0155 [hep-ph]].

[124] E. Witten, Adv. Theor. Math. Phys. **2**, 505 (1998) [hep-th/9803131].

[125] T. Sakai and S. Sugimoto, Prog. Theor. Phys. **113**, 843 (2005) [hep-th/0412141].

[126] T. Sakai and S. Sugimoto, Prog. Theor. Phys. **114**, 1083 (2005) [hep-th/0507073].

[127] H. Hata, T. Sakai, S. Sugimoto and S. Yamato, Prog. Theor. Phys. **117**, 1157 (2007) [hep-th/0701280 [HEP-TH]].

[128] T. Imoto, T. Sakai and S. Sugimoto, Prog. Theor. Phys. **124**, 263 (2010) [arXiv:1005.0655 [hep-th]].

[129] G. Parisi, Phys. Lett. B **39**, 643 (1972).

[130] J. Polchinski and M. J. Strassler, Phys. Rev. Lett. **88**, 031601 (2002) [hep-th/0109174].

[131] J. Polchinski and M. J. Strassler, JHEP **0305**, 012 (2003) [hep-th/0209211].

[132] A. Chodos, R. L. Jaffe, K. Johnson, C. B. Thorn and V. F. Weisskopf, Phys. Rev. D **9**, 3471 (1974).

[133] G. F. de Teramond and S. J. Brodsky, Phys. Rev. Lett. **94**, 201601 (2005) [hep-th/0501022].

[134] G. F. de Teramond and S. J. Brodsky, arXiv:1203.4025 [hep-ph].

[135] A. Karch, E. Katz, D. T. Son and M. A. Stephanov, Phys. Rev. D **74**, 015005 (2006) [hep-ph/0602229].

[136] I. R. Klebanov and J. M. Maldacena, Phys. Today **62**, 28 (2009).

[137] I. Kirsch, JHEP **0609**, 052 (2006) [hep-th/0607205].

[138] J. Polchinski and M. J. Strassler, JHEP **0305**, 012 (2003) [hep-th/0209211].

[139] D. E. Soper, Phys. Rev. D **15**, 1141 (1977).

[140] M. E. Peskin and D. V. Schroeder, Reading, USA: Addison-Wesley (1995) 842 p

[141] S. J. Brodsky and G. F. de Teramond, PoS QCD **-TNT-II**, 008 (2011) [arXiv:1112.4212 [hep-th]].

[142] S. J. Brodsky and G. F. de Teramond, arXiv:1301.2733 [hep-ph].

[143] R. Baldini *et al.*, Eur. Phys. J. C **11**, 709 (1999).

[144] V. Tadevosyan *et al.*, Phys. Rev. C **75**, 055205 (2007) [arXiv:nucl-ex/0607007];

[145] B. Aubert *et al.* Phys. Rev. Lett. **103**, 231801 (2009) [arXiv:0908.3589 [hep-ex]].

[146] K. K. Seth, S. Dobbs, *et al.*, arXiv:1210.1596 [hep-ex].

[147] T. Branz, T. Gutsche, V. E. Lyubovitskij, I. Schmidt and A. Vega, Phys. Rev. D **82**, 074022 (2010) [arXiv:1008.0268 [hep-ph]].

[148] F. Stancu; *Group theory in subnuclear physics*, Oxford Stud. Nucl. Phys. **19**, 1 (1996).

[149] H. Georgi; '*Lie algebras in particle physics*, Westview Press, 2nd edition 1999.

[150] F. E. Close; *An Introduction to Quarks and Partons*,' Academic Press, London 1979.

[151] G. P. Lepage and S. J. Brodsky, Phys. Rev. D **22**, 2157 (1980).

[152] S. J. Brodsky, T. Huang and G. P. Lepage, SLAC-PUB-2540.

[153] S. J. Brodsky, T. Huang and G. P. Lepage, In *Stanford 1981, Proceedings, The Strong Interactions*, 87-140

[154] Y. V. Kovchegov and E. Levin; *Quantum chromodynamics at high energy*, Cambridge University Press, 2012.